

SYNTHESIS OF FUNCTIONALIZED

MESOPOROUS TITANIA FOR

(PHOTO)CATALYSIS

Mieke Meire

Supervisors:

Prof. Dr. Isabel Van Driessche

Prof. Dr. Pascal Van Der Voort

Submitted to the Faculty of Sciences of Ghent University, in Fulfillment of the Requirements for the Degree of Doctor in Sciences.

Academic year: 2016-2017





Universiteit Gent
Faculteit Wetenschappen
Vakgroep Anorganische en Fysische Chemie

Promotoren: Prof. Dr. Isabel Van Driessche
Prof. Dr. Pascal Van Der Voort

Universiteit Gent
Faculteit Wetenschappen

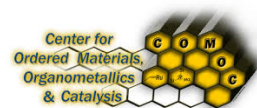
Vakgroep Anorganische en Fysische Chemie
Krijgslaan 281 S3, B-9000 Gent, België

Tel.: +32-9-264.44.49
Fax.: +32-9-264.49.83

Dit werk kwam tot stand in het kader van een aspirantenmandaat van het FWO
(Fonds Wetenschappelijk Onderzoek - Vlaanderen).



Proefschrift tot het behalen van de graad van
Doctor in de Wetenschappen:
Chemie
Academiejaar 2016-2017



Dankwoord

De bladzijden zijn geschreven, de boekjes zijn gedrukt. Na vijf jaar komt er een einde aan dit hoofdstuk. Zonder de hulp van veel mensen, zou ik niet staan waar ik nu sta.

Eerst en vooral wil ik mijn promotoren prof. Isabel Van Driessche en prof. Pascal Van Der Voort bedanken om een gezamenlijk doctoraat in jullie twee fantastische onderzoeksgroepen voor te stellen. De mensen, kennis en ervaringen zullen me mijn hele leven bij blijven.

Daarnaast wil ik graag mijn juryleden prof. De Buysser, prof. Demeestere, prof. Lambert, prof. Smet, prof. Verbruggen en prof. Vincze bedanken. Bedankt voor jullie opmerkingen en correcties. Dankzij jullie inzichten is het mogelijk geweest om dit doctoraat naar een hoger niveau te tillen.

Ik wil zeker en vast het technisch personeel bedanken. Pierre, Kathleen, Bart, Tom, Pat, Funda, Ilse, Bernard, Philip en Els, maar ook Claudine en Danny, zonder jullie zou de vakgroep niet zijn wat ze is. Jullie staan altijd klaar met hulp, een praatje en een onuitputbare hoeveelheid grapjes. Door jullie loopt hier alles op wielmpjes!

Ook de huidige en vroegere collega's van SCRiPTS en COMOC wil ik bedanken. Door jullie heb ik hier 5 fantastische jaren beleefd. Bedankt voor jullie babbels, kennis en vriendschap! Ik wil ook nog een aantal mensen in het bijzonder bedanken. Klaartje, bedankt voor al je steun en kennis. Je stond altijd klaar voor elk klein of groot probleem, wetenschappelijk of persoonlijk en daar ben ik je heel erg dankbaar voor! Joni en Jonas, mijn titania kameraden, we hebben het niet altijd gemakkelijk gehad, maar het onderzoek, titanium dioxide en de omstandigheden hebben ons niet klein gekregen! We zijn er betere mensen door geworden. Nog veel succes met jullie verdere projecten en het ga jullie goed. Hannes, Het was heel fijn om je als collega te hebben, bedankt voor je interesse en de fijne babbels. Nog even volhouden en je bent er ook. Petra, je bent al even weg, maar je bent nog niet vergeten. Bedankt voor alle hulp en voor het goed op weg zetten van dit doctoraat.

Een extra dankbare dank u is er weggelegd voor Els en Katrien. Els, het was heel erg fijn om je te leren kennen! Je staat altijd voor iedereen klaar met persoonlijke en wetenschappelijk raad. Ik ben zeer blij dat ik altijd op je kon rekenen en heb heel erg genoten van de momenten samen met als hoogtepunt een jaar lang lekker eten. Katrien, je begon als de begeleidster van mijn thesis, maar al snel ben je uitgroeid tot een echte vriendin. Het was super om je als bureaugenootje te hebben en vele gesprekken te kunnen voeren. Je staat er altijd met raad en daad

en ik ga je zeker en vast missen, maar ik hoop dat je een vriendin blijft voor het leven.

Natuurlijk draait het niet allemaal om werk en heb je daarnaast ook heel wat mensen nodig om te ontspannen, gedachten te verzetten en het leven nog mooier te maken. Ook hier zijn er heel wat mensen om te bedanken. Heleen en Loes, het was de beste beslissing ooit om in België te komen studeren. Zo kregen we de kans om elkaar te ontmoeten en heel erg veel mooie momenten te beleven. Wat ben ik blij dat we besloten hebben om op woensdag nog steeds samen te komen. Jullie vriendschap heeft me al heel veel fantastische momenten opgebracht, maar ook veel steun gegeven om door te gaan op moeilijke momenten. Jullie zijn van onschatbare waarde!

Uiteindelijk wil ik nog de belangrijkste groep van mensen bedanken: mijn familie. Mama en papa, bedankt om me vrij te laten om te kiezen wat ik wou doen en vertrouwen te hebben dat het allemaal goed ging komen, maar me toch ook altijd steun te bieden. Ik kan altijd op jullie rekenen om in te springen waar nodig, een helpende hand te bieden en goede raad te geven. Joke en Tom, jullie zijn een fantastische zus en broer en een nog betere meter en nonkel. Het was fijn om met jullie op te groeien en vooral om jullie nu samen met alle kindjes te zien. Ook jullie wil ik bedanken om er altijd te zijn! Ook mijn schoonouders ben ik dankbaar om me direct in hun hart te sluiten en altijd geïnteresseerd te zijn in alles wat ik doe.

Lieve kleine Febe, wat is het toch fantastisch om je mama te zijn! Je bent zo'n vrolijke, lieve meid en je maakt van elke dag een prachtige dag. Ik kan al niet wachten om je te zien opgroeien tot de fantastische vrouw die je vast en zeker zal worden!

De aller-allerbelangrijkste persoon wordt altijd tot laatst gehouden. Pieter, mijn liefste, mijn man, mijn vriend en de papa van ons lieve dochter. Zonder jou was dit doctoraat niet tot stand gekomen, maar nog belangrijker, zonder jou zou ik niet zijn wie ik ben. Bedankt om er altijd voor me te zijn, me te steunen waar nodig, me een zetje te geven wanneer ik het kan gebruiken, me uit te dagen en me vooral altijd lief te hebben. Bedankt om te zijn wie je bent!

Gent, augustus 2017
Mieke Meire

Table of Contents

Dankwoord	i
Table of Contents	v
List of Figures	ix
List of Tables	xiii
List of acronyms	xv
Nederlandstalige samenvatting	xvii
English summary	xxi
Preface	1
1 Introduction	1-1
1.1 Titanium dioxide	1-1
1.1.1 Properties	1-1
1.1.2 Photocatalysis	1-2
1.1.3 Specialized applications	1-3
1.1.3.1 Dye sensitized solar cell (DSSC)	1-4
1.1.3.2 Electrochromic devices	1-5
1.1.3.3 Sensors	1-5
1.1.3.4 Photocatalytic water and air purification	1-5
1.1.3.5 Photocatalytic water splitting	1-5
1.2 A brief history on porous materials	1-6
1.3 Mesoporous titania	1-7
1.3.1 General principal	1-7
1.3.2 Synthesis methods	1-9
1.3.2.1 Soft templating	1-9
1.3.2.2 Hard templating	1-10
1.4 Soft templated mesoporous titania	1-10
1.4.1 Precipitation synthesis	1-10
1.4.2 Hydrothermal synthesis	1-11
1.4.3 Evaporation induced self assembly	1-11

1.5	Aim of the research	1-12
References		1-15
2	Microwave assisted synthesis of mesoporous titania	2-1
2.1	Introduction	2-2
2.2	Experimental section	2-3
2.2.1	Synthesis of titania powders	2-3
2.2.2	Characterisation	2-4
2.2.2.1	Surface Photovoltage (SPV) measurements	2-4
2.2.2.2	Photocatalytic degradation	2-5
2.3	Material properties	2-7
2.3.1	Specific surface area and crystallinity	2-7
2.3.2	Electronic properties	2-9
2.4	Photocatalysis	2-10
2.4.1	Aqueous phase	2-10
2.4.2	Gaseous phase	2-12
2.4.3	Comparison of aqueous and gaseous photocatalysis	2-13
2.5	Conclusions	2-14
References		2-15
3	Synthesis of gold nanoparticles	3-1
3.1	Introduction	3-2
3.2	Experimental section	3-4
3.2.1	Synthesis of gold nanoparticles	3-4
3.2.2	Synthesis of Au/TiO ₂ materials	3-5
3.2.3	Characterization	3-6
3.3	Aqueous synthesis of gold nanoparticles	3-6
3.3.1	Turkevich-Frens Method	3-7
3.3.2	Carboxylate capped gold particles	3-8
3.3.3	Gold nanorods	3-8
3.3.4	Incorporation in mesoporous titania matrix	3-9
3.4	Non-Aqueous synthesis of gold nanoparticles	3-10
3.4.1	Brust synthesis	3-10
3.4.2	Phosphine stabilized gold nanoparticles	3-11
3.4.3	Incorporation in mesoporous titania matrix	3-12
3.5	Adsorption of gold nanoparticle on the titania matrix	3-13
3.6	Conclusions	3-13
References		3-15

4	Gold/titania composites: Synthesis and Characterisation	4-1
4.1	Introduction	4-2
4.2	Experimental section	4-3
4.2.1	Synthesis	4-3
4.2.2	Characterization	4-4
4.2.2.1	Photocatalytic degradation	4-5
4.3	Material properties	4-6
4.4	Oxidation state	4-8
4.5	Photocatalysis	4-12
4.6	Conclusions	4-13
	References	4-15
5	Gold/titania composites: carbonylation of glycerol with urea	5-1
5.1	Introduction	5-2
5.2	Experimental section	5-3
5.2.1	Characterisation	5-3
5.2.2	Carbonylation of glycerol with urea	5-4
5.3	Material properties	5-5
5.4	Catalysis	5-5
5.5	Conclusions	5-12
	References	5-15
6	Platinum/titania composites: synthesis and characterisation	6-1
6.1	Introduction	6-2
6.2	Experimental section	6-2
6.2.1	Synthesis	6-2
6.2.2	Characterization	6-3
6.2.3	Photocatalytic degradation	6-3
6.3	Material properties	6-4
6.4	Photocatalysis	6-5
6.5	Conclusions	6-7
	References	6-9
7	General conclusion and future perspectives	7-1
7.1	General summary	7-1
7.2	Microwave assisted synthesis	7-1
7.3	Functionalization with noble metal nanoparticles	7-2
7.3.1	Gold nanoparticles	7-2
7.3.2	Platinum nanoparticles	7-3
7.4	Future perspectives	7-4

A	Supporting information	A-1
A.1	Chapter 2	A-1
	A.1.1 X-ray diffraction	A-1
	A.1.2 Rietveld analysis	A-2
	A.1.3 Nitrogen sorption isotherms of mesoporous titania	A-3
	A.1.4 Differential pore size distributions mesoporous titania	A-4
A.2	Chapter 4	A-5
	A.2.1 Nitrogen sorption isotherms of gold functionalized mesoporous titania	A-5
	A.2.2 Differential pore size distributions of gold functionalized mesoporous titania	A-6
A.3	Chapter 5	A-7
	A.3.1 Nitrogen sorption isotherms of gold functionalized mesoporous titania	A-7
	A.3.2 Differential pore size distributions of gold functionalized mesoporous titania before catalysis	A-8
	A.3.3 Differential pore size distributions of gold functionalized mesoporous titania after catalysis	A-9
B	Scientific disseminations	B-1
B.1	A1 publicatons	B-1
B.2	Conference contributions: oral presentations	B-2
B.3	Conference contributions: poster presentations	B-2

List of Figures

1.1	Most common crystal structures of titania cf. A) rutile B) anatase and C) brookite ¹	1-1
1.2	Difference in band gap of a metal, a semiconductor and an insulator	1-2
1.3	Overview of the photocatalytic process in a titania particle ⁹	1-4
1.4	Schematic of a dye sensitized solar cell	1-4
1.5	Energy diagram of the photocatalytic water splitting reaction with titanium dioxide ³²	1-6
1.6	A) Axel Fredrik Cronstedt and B) the first zeolite, stilbite, which he discovered.	1-6
1.7	Increasing the surface area by reducing the particle size or by introducing pores.	1-8
1.8	A) Soft template synthesis and B) hard template synthesis	1-9
2.1	Microwave heating versus conventional heating. ⁷	2-2
2.2	Flow chart of the synthesis of mesoporous titania, with indications of the additional microwave irradiation steps.	2-4
2.3	Schematic of aqueous photocatalytic test set-up.	2-5
2.4	Schematic of gaseous photocatalytic test set-up. MFC: Mass Flow Controller. ¹⁶	2-6
2.5	TEM images of the titania samples EISA (a, b), MW 1 (c, d), MW 2 (e, f) and MW 3 (g, h).	2-8
2.6	Plots of $[F(R)E]^{1/2}$ in function of E (eV).	2-9
2.7	Surface photovoltage signals under UVA illumination. The error bars represent the standard deviation calculated from four independent measurements.	2-10
2.8	Photocatalytic degradation of aqueous A) methylene blue and B) isoproturon solutions as a function of time.	2-11
2.9	Photocatalytic steady state CO ₂ formation during acetaldehyde degradation under UVA illumination.	2-12
2.10	Area based photocatalytic activity during acetaldehyde degradation (left axis) and anatase fractions (right axis) of the samples. . .	2-13
3.1	The energy levels of a noble metal and a semiconductor not in contact (left) or in contact (right).	3-2

3.2	The different schemes to prepare A) pure mesoporous titania and B) and C) gold functionalized mesoporous titania.	3-6
3.3	TEM images of gold nanoparticles synthesized according to the Turkevich-Frens method.	3-7
3.4	TEM images of gold nanoparticles produced using the modified citrate route.	3-8
3.5	TEM images of carboxylate capped gold nanoparticles.	3-8
3.6	UV-Vis spectra of the gold seeds and gold rods.	3-9
3.7	TEM images of the gold nanoparticles in toluene synthesized according to the two-phases method of Brust.	3-11
3.8	TEM images of gold nanoparticles synthesized according to the Weare method before (left figure) and after ligand exchange (middle and right figure).	3-12
3.9	TEM images of the gold composite materials formed by adsorbing Brust gold nanoparticles onto a mesoporous titania matrix.	3-13
4.1	Schematic of aqueous photocatalytic test set-up.	4-5
4.2	HAADF STEM images of the Au/TiO ₂ composite materials using the A) UV, B) MW, C) H ₂ and D) NaBH ₄ reduction. Some of the gold nanoparticles are encircled.	4-7
4.3	Particle size distribution of the gold nanoparticles obtained by A) UV, B) MW, C) H ₂ and D) NaBH ₄ reduction.	4-8
4.4	Au-L ₃ XANES spectra of the different Au/TiO ₂ materials.	4-9
4.5	Au-L ₃ XANES spectra of A) the unreduced sample and B) the microwave reduced sample as a function of irradiation time.	4-10
4.6	High resolution Au-L ₃ XANES of the microwave and UV reduced sample. The Au foil spectrum is used as reference.	4-10
4.7	Photocatalytic degradation of phenol under UV illumination using Au/TiO ₂ catalysts and unfunctionalized TiO ₂ as reference.	4-12
4.8	Photocatalytic degradation of phenol under UV illumination using Au/P25 catalysts and unfunctionalized Evonik P25 (left) and Au/Hombikat and unfunctionalized Hombikat UV100 (right).	4-13
5.1	Reaction scheme for the synthesis of glycerol carbonate from glycerol and urea as CO ₂ donor. ¹²	5-2
5.2	HAADF STEM images of the UV (A, E), thermally (B, F), microwave (C, G) and NaBH ₄ (D, H) reduced samples before (A-D) and after (E-H) catalysis.	5-6
5.3	Gold particle size distributions of the UV (A), thermally (B) microwave (C) and NaBH ₄ (D) reduced samples before catalysis.	5-7
5.4	Possible reaction pathways for the reaction between glycerol and urea. ¹⁶	5-9
5.5	NH ₃ -TPD profiles of the studied materials.	5-9
5.6	Gold particle size distributions of the UV (A), thermally (B) microwave (C) and NaBH ₄ (D) reduced samples after catalysis.	5-10

5.7	The selectivity towards glycerol carbonate for three runs of the different gold/titania catalysts.	5-12
5.8	XAS spectra of the UV reduced sample before and after catalysis and the metallic foil reference.	5-13
6.1	HAADF STEM images of the Pt/TiO ₂ composite materials using the A) UV, B) MW, C) H ₂ and D) NaBH ₄ reduction.	6-5
6.2	Photocatalytic degradation of an isoproturon solution as a function of time.	6-6
A.1	XRD spectra of the EISA, MW 1, MW 2 and MW 3. The sharp peaks are generated from ZnO with is present to determine the degree of crystallinity.	A-1
A.2	XRD spectra and Rietveld convolutions of MW 1 (above) en MW 2 (below).	A-2
A.3	Nitrogen sorption isotherms of A) EISA, B) MW 1, C) MW 2 and D) MW 3.	A-3
A.4	Differential pore size distributions of A) EISA, B) MW 1, C) MW 2 and D) MW 3.	A-4
A.5	Nitrogen sorption isotherms of the pure and gold functionalized mesoporous titania samples.	A-5
A.6	Differential pore size distributions of A) TiO ₂ , B) TiO ₂ + HauCl ₄ , C) Au/TiO ₂ UV, D) Au/TiO ₂ MW, E) Au/TiO ₂ H ₂ and F) Au/TiO ₂ NaBH ₄	A-6
A.7	Nitrogen sorption isotherms of the pure and gold functionalized mesoporous titania samples A) before and B) after catalysis.	A-7
A.8	Differential pore size distributions of the A) UV, B) thermally, C) microwave and D) NaBH ₄ reduced gold/titania materials before catalysis.	A-8
A.9	Differential pore size distributions of the A) UV, B) thermally, C) microwave and D) NaBH ₄ reduced gold/titania materials after catalysis.	A-9

List of Tables

2.1	Crystal fractions and specific surface areas of the titania samples. .	2-7
2.2	Amount of methylene blue adsorbed before catalysis and rate constants of the discolouration of methylene blue and isoproturon degradation.	2-11
4.1	Properties of the mesoporous titania host and the different Au/TiO ₂ composite materials.	4-6
4.2	Rate constants of the degradation of phenol for pure TiO ₂ and the different Au/TiO ₂ composite materials.	4-12
5.1	Material properties of all gold/titania catalysts before and after one catalytic run. A standard deviation was calculated for the gold particles sizes.	5-6
5.2	Results of the first catalytic conversion of glycerol to glycerol carbonate using gold/titania catalysts and pure titania and commercial ZnO as references.	5-8
5.3	Ammonia uptake calculated from the NH ₃ -TPD profiles, from 50 to 550 °C.	5-8
6.1	Properties of the mesoporous titania host and the different Pt/TiO ₂ composite materials.	6-5
6.2	Isoproturon degradation rate constants derived from the $\ln(C/C_0)=kt$ graph.	6-6

List of acronyms

BET: Brunauer - Emmett - Teller
CTAB: N-cetyl-N,N,N-trimethylammonium bromide
EDX: Energy-dispersive X-ray
EISA: Evaporation induced self assembly
HAADF STEM: High-angle annular dark-field scanning transmission electron microscopy
ESRF: European Synchrotron Radiation Facility
FTIR: Fourier transform infra-red
GC: Gas chromatography
HPLC: High-performance liquid chromatography
ICP MS: Inductively coupled plasma mass spectrometry
ISO: International Organization for Standardization
ITO: Indium titanium oxide
IUPAC: International Union of Pure and Applied Chemistry
MW: Microwave
rpm: revolutions per minute
SNBL: Swiss-Norwegian beam line
SPV: Surface photo voltage
STEM: Scanning transmission electron microscopy
TEM : Transmission electron microscopy
TPD: Temperature programmed desorption
UV: Ultraviolet
UVA: Ultraviolet A
UV-Vis: Ultraviolet - visible
XANES: X-ray absorption near edge structure
XAS: X-ray absorption spectroscopy
XPS: X-ray photoelectron spectroscopy
XRD: X-ray diffraction
XRF: X-ray fluorescence

Nederlandstalige samenvatting

Onze samenleving creëert veel afval. Een deel hiervan, o. a. plastic, CO₂ en organische vervuiling (pesticiden, herbiciden, medicatie, etc.) worden in het milieu geloosd. Dit heeft niet alleen een schadelijk effect op flora en fauna, maar het heeft ook een negatief effect op de menselijke gezondheid. Het is daarom nodig om een efficiënt en robuust zuiveringssysteem te ontwikkelen. Daarnaast is het omzetten van schadelijke stoffen, zoals CO₂, naar nuttige, minder kwalijke stoffen een goede zaak voor de natuur.

In dit opzicht is titanium dioxide (TiO₂, titania) een zeer interessant materiaal aangezien het fotokatalytisch actief is. Dit wil zeggen dat onder invloed van zonlicht (UV straling) elektronen geëxciteerd worden van de valentieband naar de conductieband, waardoor er vrije elektronen en gaten ontstaan. Wanneer deze migreren naar het oppervlak kunnen ze reageren met zuurstofgas en water om radicalaire species te vormen. Deze species zijn zeer reactief en kunnen organische moleculen degraderen tot CO₂ en H₂O. Om deze vervuiling te kunnen afbreken, moeten de organische moleculen zich op, of op zijn minst heel dicht bij, het oppervlak van de titanium dioxide katalysator bevinden. Het verhogen van het specifieke oppervlak is daarom een goede manier om de fotokatalytische activiteit van titania te verbeteren. Daarnaast is ook belangrijk dat titaan dioxide zeer kristallijn is, aangezien enkel de kristallijne fase fotokatalytisch actief is. Het is echter zeer moeilijk om een materiaal te verkrijgen met zowel een hoog specifiek oppervlak als een hoge kristalliniteitsgraad. Er is namelijk een hoge temperatuur (> 400 °C) nodig om titania te kristalliseren. De organische moleculen die gebruikt worden om de poriën te vormen, zijn bij deze temperaturen echter reeds gedegradéerd. Dit heeft als gevolg dat de poriën instorten en er een laag specifiek oppervlak verkregen wordt.

Om een hoge kristalliniteitsgraad en een groot specifiek oppervlak te verkrijgen, is een microgolf behandeling toegevoegd aan de *evaporation induced self assembly* synthese van mesoporeus titania. In het geval van nanokristal synthese is er al bewezen dat een microgolf behandeling de synthesesettemperatuur met succes kan verlagen tot 120 °C. Bij deze, lagere, temperaturen zijn de organische poriënvormende moleculen nog niet gedegradéerd, waardoor het via deze methode mogelijk zou moeten zijn om hoog poreus, kristallijn titanium dioxide te produceren. Wanneer de microgolf behandeling uitgevoerd wordt op de titania precursor of net voor de calcinatie stap, is het inderdaad mogelijk om mesoporeus titania te verkrijgen met een hogere kristalliniteitsgraad zonder dat het specifiek oppervlak verkleind wordt in vergelijking met het niet behandelde titanium dioxide poeder.

De fotokatalytische activiteit van de materialen werd getest in waterige en gasvormige omstandigheden. In beide omstandigheden hebben de microgolf behandelde materialen een verhoogde activiteit. In de waterige fase is dit enkel het geval voor het materiaal met het hoogste specifiek oppervlak. In de gasfase is dit echter het geval voor alle microgolf behandelde stalen. Naargelang de gewenste toepassing, kan het materiaal met de gewenste eigenschappen gekozen worden.

Een tweede manier om de fotokatalytische activiteit van titania te verhogen is het toevoegen van edelmetalen nanodeeltjes. Aan de overgang van het edelmetaal met titania wordt een Schottky barrière gecreëerd. Dit heeft als resultaat dat de foton gegenereerde elektronen en gaten fysisch gescheiden worden. Bijgevolg zijn er minder elektronen en gaten die zullen recombineren.

Er zijn verschillende mogelijkheden om composiet materialen te synthetiseren. Dit onderzoek focust op twee verschillende routes om Au/TiO₂ materialen te maken. De eerste methode start van voordien gesynthesiseerde goud nanodeeltjes die toegevoegd worden aan de titania precursor waarna het gebruikelijke mesoporeus titania recept gevolgd wordt. De tweede methode is gebaseerd op het voordien geproduceerd mesoporeus titania poeder dat geïmpregneerd wordt met een goud zout. In een daaropvolgende stap wordt het zout gereduceerd om nanodeeltjes te vormen.

Goud nanodeeltjes kunnen zowel in polaire als apolaire media geproduceerd worden. De titania precursor bestaat echter voornamelijk uit ethanol, een beetje water en een beetje isopropanol, wat er voor zorgt dat de titania precursor een polaire oplossing is. Het is daarom noodzakelijk dat de goud nanodeeltjes dispergeerbaar zijn in een polair medium. Anders zal er geen homogeen poeder verkregen worden. Vandaar dat waterige syntheses geprefereerd worden. Jammer genoeg resulteren de polaire syntheses in grote geagglomereerde goud deeltjes die niet geschikt zijn voor de synthese van composiet materialen. De apolaire syntheses hebben als nadeel dat er nanodeeltjes verkregen worden die dispergeerbaar zijn in apolaire solventen, maar niet in polaire solventen. Er moet dus nog een bijkomende liganduitwisselingsstap uitgevoerd worden voordat de goud nanodeeltjes dispergeerbaar zijn in polaire solventen.

Wanneer het Brust recept gevolgd wordt, worden er kleine (1-3 nm), uniforme nanodeeltjes in toluen verkregen. Het was echter niet mogelijk om de dodecaanthiol liganden te vervangen door meer polaire liganden. Dit komt doordat dodecaanthiol te stevig gebonden is aan het goud deeltje. De Brust synthese werd aangepast door fosfine liganden te gebruiken die minder sterke interacties met goud vertonen. De verkregen nanodeeltjes waren, zoals gewenst, opnieuw klein en uniform. Door het gebruik van de fosfine liganden was het wel mogelijk om de liganden te vervangen door mercaptopropionzuur. Dit leverde goud deeltjes op die dispergeerbaar zijn zowel in water als in ethanol. Desondanks was het niet mogelijk om mesoporeus titania gedopeerd met goud nanodeeltjes te produceren, omdat de goud nanodeeltjes de sterk zure condities van de titania precursor niet kunnen weerstaan.

Voor de tweede synthese route van Au/TiO₂ materialen worden vier verschillende reductiemethoden (thermisch, microgolf, chemische, UV straling) van het

goud zout vergeleken. De impregnatie en reductie van het goud zout verandert het specifiek oppervlak van de katalysatoren niet. Alle methoden leveren ongeveer dezelfde belading op. De oxidatie toestand van de goud atomen werd geanalyseerd door middel van XANES. Alle reductie methoden reduceren de goud species volledig, behalve de UV reductie. Bij deze laatste reductiemethode worden er partieel positieve goud nanodeeltjes geproduceerd op het titania oppervlak. Dit zou een belangrijk effect kunnen hebben op de fotokatalytische activiteit van het composiet materiaal. Jammer genoeg levert de toevoeging van de goud nanodeeltjes geen verhoging van de fotokatalytische activiteit op. Daardoor is het ook onmogelijk om het effect van de positieve lading op de fotokatalytische activiteit van mesoporeus titania te bestuderen.

Om het effect van de positieve lading toch te kunnen onderzoeken wordt de katalytische omzetting van glycerol naar glycerol carbonaat gevolgd. Deze reactie wordt door goud partikels gekatalyseerd. In een eerste katalytische test heeft de UV gereduceerde katalysator een lage selectiviteit, maar een hoge conversiegraad in vergelijking met de andere, volledige neutrale, Au/TiO₂ katalysatoren. De positieve lading en de corresponderende zure plaatsen, kunnen urea activeren waardoor een hoge conversiegraad bereikt wordt. Langs de andere kant is de negatieve lading nefast voor de ringsluitingsstap van de glycerol carbonaat vorming, waardoor een lage opbrengst van het gewenste product verkregen wordt. De selectiviteit van de neutrale katalysatoren blijft gelijk bij een tweede en derde gebruik. In het geval van de UV gereduceerde katalysator verhoogt de selectiviteit omdat de positieve lading tijdens of na het eerste gebruik verdwijnt.

Om te onderzoeken of andere edelmetalen wel in staat zijn om de fotokatalytische activiteit van titania te verhogen, wordt titania geïmpregneerd met een platinum zout dat daarna gereduceerd wordt. De reductie van H₂PtCl₆ is echter moeilijker dan die van HAuCl₄ doordat het Pt zout een lager reductiepotentiaal heeft. Daarom leiden niet alle reductiemethoden tot de vorming van nanodeeltjes. Wanneer er wel Pt partikels gevormd worden zijn deze niet klein en uniform, maar groot en grillig van vorm. Desondanks is de fotokatalytische activiteit van de Pt/TiO₂ composiet materialen wel verhoogd ten opzichte van puur mesoporeus titania. De toevoeging van bepaalde edelmetalen kan dus wel degelijk een positieve invloed hebben op de fotokatalytische activiteit van mesoporeus titania.

English summary

Our society releases a lot of waste in the environment. Next to CO₂ and plastics, organic molecules (pesticides, herbicides, pharmaceuticals, etc.) have a harmful effect on flora and fauna, and subsequently on human life. An efficient and robust system to remove pollution is therefore necessary. Next to the elimination of harmful products, the conversion of for example CO₂ into useful and/or less detrimental products can be very beneficial for the environment.

In the light of this problem, titanium dioxide (TiO₂, titania) is a very interesting material as it is photocatalytically active, meaning it can use solar (UV) light to degrade organic molecules, both in air and in water, into CO₂ and H₂O. To be able to degrade pollutants, the contaminants have to be adsorbed on, or at least be near the surface of the photocatalyst. Hence, an effective way to enhance the photocatalytic activity of titania is increasing its specific surface area. In addition, a high crystallinity is also very important, as only the crystalline phase is photocatalytically active. However, the combination of a high specific surface area with a high crystallinity is very difficult to achieve as high temperatures are needed to obtain a crystalline material. At those temperatures, the organic pore forming molecules have already been degraded, leading to collapsing of the pores and low specific surface areas.

In order to achieve a high degree of crystallinity and a high specific surface area, microwave irradiation was incorporated into the evaporation induced self assembly synthesis of mesoporous titania. In nanocrystal synthesis, it has already been proven that microwave irradiation can successfully lower the synthesis temperature of titania nanoparticles to 120 °C. At this temperature, the organic templating molecules, used as pore forming agents, are still stable. Therefore, it should be possible to obtain highly porous, crystalline titanium dioxide using microwave irradiation.

When the microwave irradiation step is performed on the titania precursor or just before the calcination step, it is indeed possible to obtain mesoporous titania powders with an increased crystallinity degree (up to 81% crystallinity) without decreasing the specific surface area compared to non microwave treated mesoporous titania (35 % crystallinity). The photocatalytic activity of the materials is tested in aqueous and gaseous media. The microwave treatment leads in both cases to an increased photocatalytic activity. In aqueous media this is only the case for the sample with the highest specific surface area, but in gaseous media all microwave treated samples have an increased activity. Depending on the desired application, the material with the appropriate characteristics can be chosen.

A second way to improve the photocatalytic activity of titania is the incorporation of noble metal nanoparticles. At the junction of the noble metal and titania a Schottky barrier is created, resulting in the physical separation of the photogenerated electron and holes, diminishing the recombination rate. There are different possibilities to synthesize the composite materials, but this research focussed on two. The first is the incorporation of pre-synthesized gold nanoparticles in the titania precursor and subsequent synthesis of the hybrid Au/TiO₂ material by following the mesoporous titania recipe. The second synthesis route starts from a pre-synthesized mesoporous titania powder, which is impregnated with a metal salt. In a following step the salt is reduced to form nanoparticles.

Gold nanoparticles can be synthesized both in polar and apolar media. However, the titania precursor contains mainly ethanol, a small amount of water and titanium isopropoxide, resulting in a relatively polar precursor. Hence, the gold nanoparticles should be dispersible in polar media as otherwise no homogeneous powders can be obtained. As a result, aqueous syntheses of gold nanoparticles are preferred. Unfortunately, the polar syntheses resulted in large, agglomerated particles, unsuitable for the synthesis of composite materials. The apolar synthesis routes have the disadvantage that the synthesized particles are only dispersible in apolar media. An additional ligand exchange step has to be performed in order to produce nanoparticles that are dispersible in polar media. Using the Brust synthesis it was possible to produce small (1-3 nm), uniform gold nanoparticles. However, it was not possible to exchange the dodecanethiol ligands for more polar ones, as dodecanethiol was too tightly bound to the gold nanoparticle. Adapting the Brust synthesis by using phosphine ligands instead of thiol ligands, also produces small gold nanoparticles. It was possible to exchange the phosphine ligands with mercaptopropionic acid, producing particles dispersible in both water and ethanol. Nevertheless, it was not possible to produce mesoporous titania functionalized with gold nanoparticles as the gold nanoparticles dissolve in the harsh acidic conditions of the titania precursor.

The second synthesis route of Au/TiO₂ materials compares four reduction methods (thermal, microwave, chemical and UV) of the gold salt. The synthesis of the composite materials did not diminish their specific surface areas and approximately the same gold loading was achieved for all samples. The oxidation state of the gold atoms was analysed using XANES. All reduction methods resulted in completely reduced gold species except for the UV reduction. This reduction method results in partially positively charged gold nanoparticles on mesoporous titania. This could have an important effect on the photocatalytic activity of the materials. Unfortunately, the addition of gold nanoparticles did not lead to an improvement of the photocatalytic activity, making it impossible to investigate the effect of the positive charge on the photocatalytic activity of mesoporous titania.

In order to research the effect of the positive charge present on the gold atoms, the catalytic conversion of glycerol to glycerol carbonate using urea is followed. This reaction is catalysed by gold particles. In a first run, the UV reduced samples has a low selectivity, but a high conversion, compared to samples containing completely reduced, neutral gold nanoparticles. The positive charge and corresponding

acid sites can activate urea, leading to a high conversion rate. On the other hand, the positive charge is not favourable for the ring closure step in the formation of glycerol carbonate, leading to a low yield of the desired product. The selectivity of the neutral catalysts remains constant in a second and third run. In the case of the UV reduced catalyst the selectivity increases as the positive charge disappears during/after the first run.

To investigate if other noble metal nanoparticles can improve the photocatalytic activity of titanium dioxide, a platinum salt is added and subsequently reduced. The reduction of H_2PtCl_6 is more difficult compared to HAuCl_4 due to the smaller reduction potential of the platinum salt. Hence, not all reduction methods lead to the formation of nanoparticles. Furthermore, the other reduction methods (thermal and chemical) did not produce small, uniform nanoparticles. However, an improvement of the photocatalytic activity is observed. The fact that gold nanoparticles do not improve the photocatalytic activity in our case, is therefore not inherent to the used reduction methods.

Preface

As a society, we release all kinds of waste in our environment: CO₂ from energy production and transport, herbicides and pesticides to improve food production, pharmaceuticals from urine, plastics from packaging, waste produced in industry and so much more. Many of these molecules have a significant impact on the environment as they pollute the water streams, which has a big influence on wild life but could also have a substantial impact on our health, contribute to global warming, ozone depletion or create smog. It is the duty of mankind to produce as less waste as possible and even to decrease the waste mountain, but especially for me as a chemist. Therefore, the aim of this PhD is the development of materials to remove pollutants from water and air streams and the upgrading of waste molecules to value added chemicals.

When looking for suitable materials, the semi-conductor titanium dioxide (TiO₂, titania) is very attractive as it is abundant, cheap, non-toxic, bio-compatible, chemically stable in a wide pH range and it exhibits promising (photo)catalytic properties. Especially as a photocatalyst, titania is very interesting for green chemistry as it can degrade organic molecules to CO₂ and water under solar irradiation.

Degradation reactions, similar to other catalytic reactions, proceed on the surface of the catalyst. Increasing the specific surface area therefore increases the activity of the material as more surface is available for the reaction to take place. Increasing the surface area of a powder can be carried out in two ways: decreasing the particle size of individual particles or creating a porosity. Small particles have the disadvantage that it is not always straightforward to obtain a suspension of individual, separate particles and it is not easy to regenerate the particles for reuseability, especially when working on large scale. On large scale, big, porous materials are much easier to separate from dispersions than small particles. Because of the advantage of regeneration, we choose to focus on mesoporous titania to obtain a large surface area.

Titanium dioxide has two major drawbacks as a catalyst: Its high recombination rate (90%) resulting in less electrons that can participate in the reactions and thus less activity and its wide bandgap (3.2 eV). The high recombination rate is inherent to the material, but is enhanced when amorphous material is present. The wide bandgap implies that only UV light (4% of the solar spectrum) can be used to excite electrons from the valence to the conduction band while the visible part of the

sunlight ($\pm 50\%$ of the solar spectrum) remains unused. During this PhD project we primarily focussed on the reduction of the recombination rate. Two routes were followed to mitigate the problem: 1) increasing the degree of crystallinity of mesoporous titania and 2) functionalization of mesoporous titania with noble metal particles.

The materials were used for the degradation of methylene blue, a common pollutant from the textile industry, and isoproturon, a herbicides commonly found in the environment. The gold/titania composite materials were also applied in the reassessment of glycerol, a cheap by-product from the production of biofuels, to glycerol carbonate, a value added product which is used in fine chemical synthesis, polymer industry and as electrolyte in lithium ion batteries.

This research brings us closer to better air and water refinement facilities and shows the ability of gold/titania materials to obtain value added chemicals from waste.

1

Introduction

1.1 Titanium dioxide

1.1.1 Properties

Titanium dioxide, titania or TiO_2 is a naturally occurring transition metal oxide. It is abundant, cheap, environmentally benign and chemically stable. The most common crystalline structures of titanium dioxide are rutile, anatase and brookite (Figure 1.1), but many more crystal phases are known. Rutile is thermodynamically the most stable crystal structure, while both anatase and brookite are metastable structures. However, the stability also depends on the particle size as the surface energy of the three polymorphs are rather close. For particles smaller than 11 nm, anatase is the most stable structure. Brookite is the most favourable phase for par-

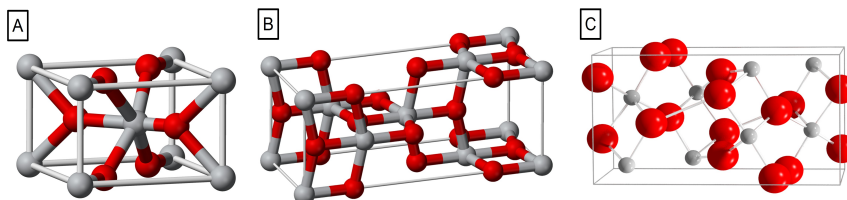


Figure 1.1: Most common crystal structures of titania cf. A) rutile B) anatase and C) brookite¹

ticles with a size between 11 nm and 35 nm and for particles bigger than 35 nm rutile has the lowest energy.² When synthesizing titania, an amorphous phase is almost always obtained at temperatures below 300 °C.³⁻⁵ When the temperature is increased, crystallization of anatase titania particles starts. These particles will grow and eventually recrystallize in the rutile phase, which is generally observed from 600 °C.^{6,7}

Titania has a white color and a very high refractive index (2.49 for anatase and 2.90 for rutile), leading to its most common application as white pigment in paint, paper, cosmetics and even in food (with number E171). Another common application is in sunscreens as it reflects UV light. A minor part of its consumption can be found in more specialized applications. These are based on the semiconducting properties of titania.

1.1.2 Photocatalysis

A material is catalogued as a conductor, semiconductor or insulator, depending on its band gap energy, the energy necessary to excite an electron from the valence to the conduction band (Figure 1.2).

In the case of a conductor, for example a metal, there is an overlap between the conduction band and the valence band, therefore there is no band gap. In the case of a semiconductor, like titania, the gap between the valence band and the conduction band is small enough for electrons to get excited from the valence band to the conduction band when enough energy is added. The band gap of an insulator, for example glass, is too big for the electrons to get excited to the conduction band as a result, these materials cannot conduct electrons.

The band gap of anatase is 3.2 eV. This means that a photon with a wavelength smaller than 388 nm, i.e. in the UV part of the solar spectrum, is able to excite an electron from the valence to the conduction band. This process creates a negatively charged electron in the conduction band and a positively charged hole in the

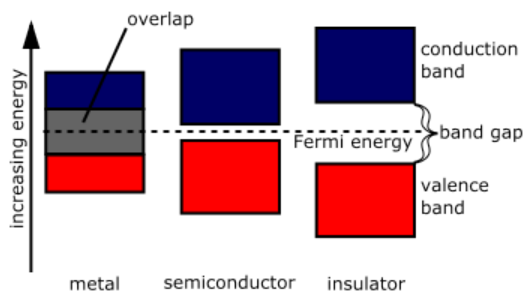
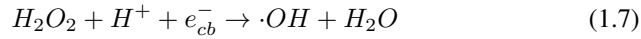
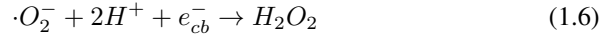
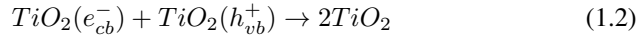
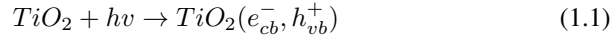


Figure 1.2: Difference in band gap of a metal, a semiconductor and an insulator

valence band (equation 1.1). The electron hole pair is also called an exciton.

An exciton can undergo different processes: the electron and hole can move to the surface of the material or they can recombine (equation 1.2). On the surface of titania, hydroxyl groups are present, but also water and oxygen molecules can be adsorbed. The electron and holes that reach the surface will react with these groups/molecules to form radical species (equations 1.3 - 1.7). These radical species will degrade pollutants, which are present on the surface of titania. The electrons and holes can also directly react with pollutant molecules that are adsorbed onto the surface (equation 1.8 - 1.9).



In titania, the recombination process occurs at a high rate and as a result 90% of the electron-hole pairs recombine before they reach the surface. This means that the largest fraction of the electron and holes cannot be used in a photocatalytic process. This is one of the major drawbacks of titania as a photocatalyst.⁸ An overview of the photocatalytic process is summarized in figure 1.3.

1.1.3 Specialized applications

In 1972, Fujishima and Honda described the photocatalytic water splitting at a TiO_2 anode and a platinum cathode.¹⁰ Since then, there is an increasingly amount of research devoted to titania, resulting in many applications in a wide range of research fields. A few of the most important applications are described below.

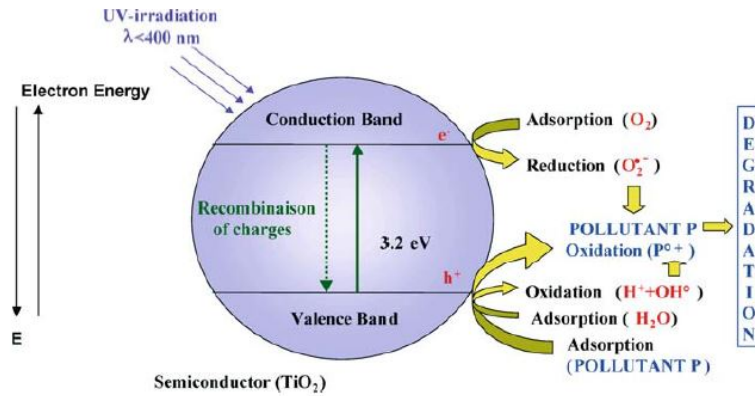


Figure 1.3: Overview of the photocatalytic process in a titania particle⁹

1.1.3.1 Dye sensitized solar cell (DSSC)

A dye sensitized solar cell is a thin film solar cell. It is based on a crystalline titania film with a charge transfer dye adsorbed onto the surface. This is placed into contact with a redox electrolyte and a counter electrode.¹¹ Upon irradiation, the dye is excited and injects an electron in the conduction band of TiO₂. The electron can be conducted to the outer circuit to generate power. A redox couple, generally iodide/triiodide, is used to restore the dye to its original form, resulting in a system that generates power from light without permanent chemical transformations (figure 1.4).¹²⁻¹⁴

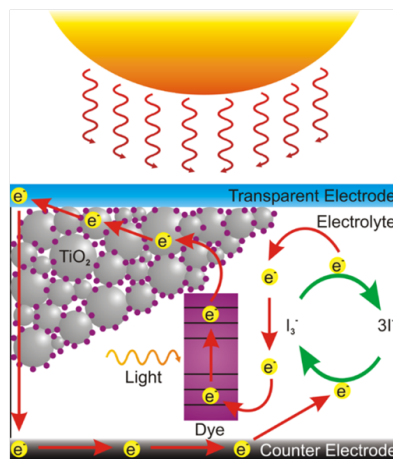


Figure 1.4: Schematic of a dye sensitized solar cell

1.1.3.2 Electrochromic devices

Electrochromism is the phenomenon that a material changes color upon an electrochemical reaction. The oxidation/reduction reaction is reversible and the transmittance/refraction change is visibly detectable. In most cases there is a transparent and a colored state, but different colored states are also possible. Generally, a small voltage is applied to darken the device. Reversing the voltage will lighten it again.^{11, 15} Titania is used in two types of electrochromic devices. The first type is based on the reversible incorporation of Li^+ in an anatase lattice.^{16, 17} The second device consists of titania electrodes modified with electrochromophores (typically viologens), where the color change is induced by the reduction/oxidation of the electrochromic groups. In this case the titania matrix acts as an electron conductor.^{18, 19} Electrochromic devices are used for smart windows and electronic displays among other things.

1.1.3.3 Sensors

TiO_2 can be applied as sensor for various gases, as differences in electrical resistance are observed dependent on the molecule adsorbed on titania. Titania materials are investigated as sensor for H_2 ,²⁰⁻²² CO ,^{23, 24} methanol^{25, 26} and ethanol.^{25, 27}

1.1.3.4 Photocatalytic water and air purification

One of the most investigated high end applications of titania is the decontamination of air and water stream. As described above, titania generates radicals upon irradiation with UV light. These radicals can degrade organic molecules that are adsorbed onto the surface to CO_2 and H_2O .

There are already some commercially available applications of titania as air purifier. Titania is already used in walls of tunnels, on building facades and in air circulators.^{9, 28-30} In Japan and Westminster, paving stones coated with titanium dioxide can be found to reduce volatile organic molecules and smog.

In the case of water remediation, titania is very promising, but applications are, not yet, commercially available.

Air and especially water remediation is the application that we will focus on.

1.1.3.5 Photocatalytic water splitting

As green energy becomes more and more important, the production of clean fuels in an environmentally friendly way is very significant. The photocatalytic water splitting reaction, that produces H_2 and O_2 from water using light energy could be a solution to the energy problem.³¹ Figure 1.5 shows the energy potentials of the water splitting reaction and the band edge position of titania. The holes that are generated in the valence band have enough energy to oxidise water to oxygen and

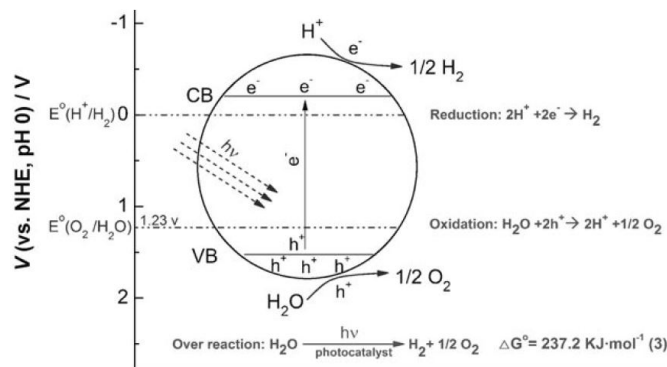


Figure 1.5: Energy diagram of the photocatalytic water splitting reaction with titanium dioxide³²

protons, whereas the electrons are low enough in energy to reduce the protons to hydrogen gas. Therefore the overall reaction converts photon energy into chemical energy.^{32–35} Titanium dioxide however, has a large overpotential, making it not very efficient. Noble metals nanoparticles (Pt, Au, etc.) can be deposited on the surface to make the photocatalytic water splitting reaction much more efficient.³⁶

1.2 A brief history on porous materials

In 1756, the Swedish mineralogist Axel Fredrik Cronstedt discovered an unidentified silicate mineral, stilbite.³⁷ When the mineral was rapidly heated, steam was produced, causing Cronstedt to call the mineral "zeolite" derived from the Greek words $\zeta\epsilon\omega$ (to boil) and $\lambda\iota\theta\omicron\varsigma$ (stone). From there on, research was performed on several types of zeolites, resulting in the discovery of properties ranging from absorption to dehydration and ion exchangability. Several syntheses were described

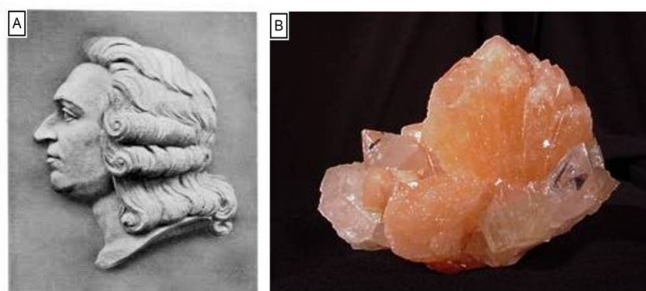


Figure 1.6: A) Axel Fredrik Cronstedt and B) the first zeolite, stilbite, which he discovered.

but these lacked reproducibility.³⁸ In the 1940's, Richard Barrer was the first to classify the until then known zeolites and to describe reproducible syntheses for zeolites.³⁹⁻⁴¹ His work inspired companies like Union Carbide and Mobil Oil Corporation to initiate research on zeolites, leading to the patents of zeolite A, X and Y. These were first used for separation and purification applications, but quickly found their use as a catalyst for isomerization reactions, hydrocarbon cracking reactions and shape selective catalysis.

Nowadays, 201 crystalline and 22 amorphous zeolites are known.⁴² Despite their large number, all zeolites exhibit rather small pore sizes (0.3 nm - 1.5 nm). In case of the separation of gases this is very interesting, because gas molecules are very small and the pores of zeolites are small enough to separate gas molecules on the basis of their sizes, whereby one gas can penetrate the pores, while another cannot. However, in the synthesis and separation of larger molecules, the porosity of zeolites is not useful anymore, because the molecules cannot enter the pores. In a quest to obtain materials with larger pore sizes, templating molecules were used to enlarge the pores. The most important milestone for this research is the Mobil Patent of the M41S family of materials in 1992.⁴³ This patent describes the use of quaternary alkylammonium surfactants to synthesize a family of ordered mesoporous silicate and aluminasilicate materials. Depending on the surfactant that is used, different pore structures are obtained (*e.g.* hexagonal, cubic,...). Some examples of silica materials using cetyltrimethylammonium bromide as surfactant are MCM-41 with a hexagonal pore structure, MCM-48 with a cubic pore structure and MCM-50 with a lamellar structure.^{44,45} Soon after the discovery of these silica materials, these syntheses were adapted to other transition metal oxides like vanadium oxide,⁴⁶ niobium oxide,⁴⁷ tantalum oxide,⁴⁸ zirconium oxide⁴⁹ and titanium dioxide.⁵⁰

1.3 Mesoporous titania

1.3.1 General principal

As many of the above described applications depend on the surface of titania, increasing its specific surface area should be beneficial for these applications. There are two main approaches, namely 1) creating smaller particles or 2) introducing pores in larger particles (Figure 1.7).

In the case of spherical particles the surface area and volume are linked according to: $S = 3 V / r$. This means that when the particle size decreases, the volume increases relatively faster than the surface area. However, small nanoparticles are difficult to separate from a reaction mixture. Standard filtration or centrifugation methods will not work. One needs to add an additional non-solvent to precipitate the particles before they can be separated from the reaction mixture with a stan-

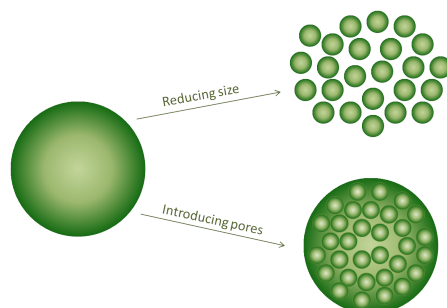


Figure 1.7: Increasing the surface area by reducing the particle size or by introducing pores.

dard method. This additional step takes time, solvent and thus money, which is not encouraged in the industry. Another disadvantage of nanoparticles is that they can cause health issues when taking in through the respiratory system. A way to circumvent these problems would be to immobilise the particles on a matrix, but this again costs a lot of addition time, material and results in a small loss of specific surface area.

The second approach to increase the specific surface area of a material is by inducing pores in larger particles. The surface of the materials now not only consists of the outer surface of the particles, but also the walls of the pores add to the surface, increasing the total specific surface area of the material. For the pores to be accessible to organic molecules, the pores cannot be too small ($> 2\text{nm}$), otherwise the molecule cannot enter the pores. IUPAC defines three regions in the case of cylindrical pores: Microporous materials have pores with a diameter smaller than 2 nm, mesoporous materials consist of pores with a size between 2 nm and 50 nm and the pore size of macroporous materials is larger than 50 nm. As porous materials generally consist of large particles, the separation of the powder from a reaction mixture is much more straightforward than in the case of nanoparticles. However, one has to take into account that the light has to penetrate the complete material, otherwise not all available surface will be activated. The porous structures should therefore be smaller than $0.5\ \mu\text{m}$.

In the case of gaseous application, nanoparticles cannot be used as they have to be dispersed in solution or they will agglomerate and lose their high specific surface area, while this is not the case for porous materials. As this research will focus on the remediation of gas and water streams, we will focus on the synthesis of porous materials. Since micropores are generally too small for organic pollutants to enter, especially in aqueous solutions, we aimed for mesoporous titanium dioxide.

1.3.2 Synthesis methods

There are two major routes to obtain ordered mesoporous materials, namely the hard templating and the soft templating route. In a templating synthesis, a design is used in/around which the material is produced. The template designs the shape of the pores as it has to be removed to create the pores.

1.3.2.1 Soft templating

In the case of a soft template synthesis, polymer molecules are used as a template (Figure 1.8A). The polymers have a polar and a apolar part. Due to the interaction with the solvent, micelles will be formed: one part will be attracted to the solvent and form outside of the micelle. The other part will be repulsed by the solvent and attracted by other polymer parts with the same polarity. These will form the inside of the micelles. At a critical concentration the micelles will order themselves into liquid crystals. The titania precursor hydrolyses around these crystals, forming a porous material in which the pores are filled with polymers. Afterwards, the amorphous titanium dioxide phase is crystallized and the polymer template removed at the same time at high temperatures. The advantage of this method is the simplicity and few synthesis steps, but the disadvantage is the instability of the template molecules at the temperatures that are needed to crystallize titania. There is always a compromise between crystallinity and specific surface area as titania needs relatively high temperatures ($> 400\text{ }^{\circ}\text{C}$) to crystallize, but most polymers are degraded at these temperatures, resulting in the collapsing of the pores during the final thermal treatment and a lower specific surface area.^{5, 51–55}

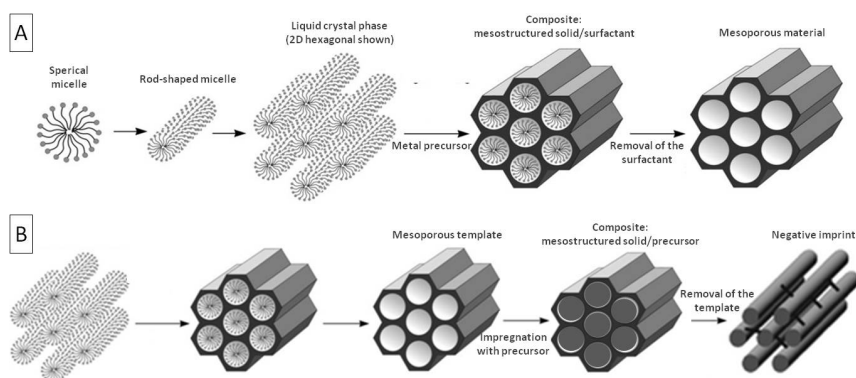


Figure 1.8: A) Soft template synthesis and B) hard template synthesis

1.3.2.2 Hard templating

In a hard templating synthesis, a solid porous material like a silica (SBA-15, MCM-41, MCM-48) or carbon (KIT-6, CMK-8) is used as a template (Figure 1.8B). This template is impregnated with a titania precursor, the precursor is transformed to crystalline titanium dioxide at higher temperatures leaving the hard template unaffected. In an additional step, the template is removed, resulting in the negative imprint of the hard template. The advantage of this method is that the template is stable at high temperatures, so the crystallization of titania can be completed inside the pores, before the template is removed. The disadvantages are that more steps are needed to complete the synthesis (*e.g.* synthesizing the template and removing the template in an additional step), making this route more expensive. It is also very difficult to obtain a complete and uniform filling of the pores. When only parts of the template are filled, the structure will not be stable and it will not be possible to obtain a full negative imprint of the template. As a consequence, the material will have a low specific surface area.

In general, it is easier to obtain a stable material with a high specific surface area when using a soft template synthesis, compared to a hard template method, due to the very difficult impregnation step of the hard templating synthesis. Therefore, the focus of this research is the soft template synthesis of mesoporous titania.

It is however, not straightforward to obtain an ordered mesoporous titanium dioxide material as titanium precursors have the tendency to form particles, rather than polymeric structures.⁵⁶ Most often, agglomerates of particles are formed using the soft templating synthesis, instead of uniformly ordered porous materials.^{51, 57} Materials with uniform pores have the advantage that the diffusion inside the pores is easier. They can also be used for shape selective catalysis, which is not the case of materials with irregular pores. In the case of adsorption and (photo)catalysis, this is not that important. The titania materials synthesized during this research were not ordered, but this is not necessary for the applications that are used.

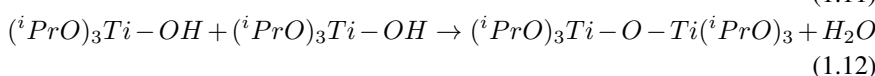
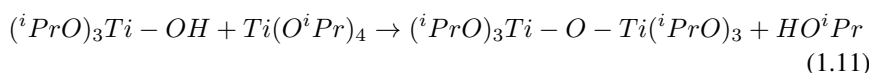
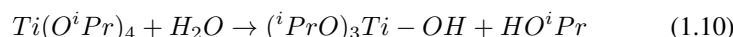
1.4 Soft templated mesoporous titania

In general, three types of soft templated synthesis methods are used to produce mesoporous titania: precipitation syntheses, hydrothermal syntheses and evaporation induced self assembly methods.⁵⁸

1.4.1 Precipitation synthesis

In a typical precipitation synthesis the template (amines, phosphines, blockcopolymers,...) is dissolved in an alcohol, usually ethanol. The titania precursor, often $\text{Ti}(\text{O}^i\text{Pr})_4$, and water are added. After some time a precipitation is formed due

to hydrolysis and condensation reactions (Equations 1.10-1.12). The precipitation is separated from the liquid phase. The obtained powder is calcined to remove the template and to crystallize the material. Using this synthesis method, titanium dioxide with a specific surface area of 40 - 180 m²/g are generally produced.⁵⁹⁻⁶³



1.4.2 Hydrothermal synthesis

Generally, a hydrothermal synthesis consists of following steps: The template is dissolved in water and mostly some acid is added. The acid is produce crystalline material. Depending on the acid used, crystalline of amorphous phases are obtained. Hydrochloric acid and nitric acid are know to induce crystallinity, while the use acetic acid and sulphuric acid result in amorphous powders. The latter have stronger interactions with the titanium ions inhibiting the structural arrangement of crystalline titanium dioxide.⁶⁴ In a separate vial, the titania precursor is mixed with a stabilizer (acetylaceton) to prevent the direct hydrolysatation of the titania precursors when mixed with the aqueous phase. The titania precursor is slowly added to the template solution and the resulting solution is transferred to an autoclave. The hydrothermal treatment is carried out in a muffle oven at a temperature between 90 °C and 190 °C for 1 hour to 3 days. Afterwards a calcination step is performed to remove the template. Specific surface areas between 40 - 400 m²/g are obtained using this method.^{5, 51, 57, 65-67} This method has the advantage that higher specific surface areas can be obtained, but the disadvantage is the longer reaction time.

1.4.3 Evaporation induced self assembly

The third typical synthesis method for titania is the evaporation induced self assembly (EISA).⁶⁸ The template, a titania precursor and an acid are dissolved in a solvent with a low boiling point, usually an alcohol and some water is added. The solution is placed in a Petri dish at low temperatures (< 100 °C) to evaporate the solvent. At the beginning of the synthesis the concentrations of the template molecules are below the critical micelle concentration, therefore no superstructures are present. As more and more solvent evaporates, the concentration increases and micelles and superstructures are formed. The titania precursor hydrolyses around these superstructures to form an amorphous mesoporous titanium dioxide network. The evaporation step takes place in 1 to 7 days. The dry powdery

film can be treated with a base (ammonia or NaOH) to increase the crystallinity of the powder.^{3, 69, 70} The last step is again the calcination to remove the template molecules and to crystallize the powder. Specific surface areas of 40 - 570 m²/g are reached.^{3, 53, 68-75} This synthesis methods results in the highest specific surface areas, but is also the most time consuming.

1.5 Aim of the research

As photocatalyst, titanium dioxide has two major drawbacks: 1) Only photons with a wavelength shorter than 388 nm (UV light) can be used to excite electrons to the conduction band due to it's wide band gap. Therefore, a large part of the solar spectrum (~95%) cannot be used as illumination source. 2) Titanium dioxide has a high recombination rate. Only 10% of the photogenerated electrons reach the surface where they can participate in reactions.

The band gap of titania can be diminished by doping the material with non-metals like N, C, P and S or with transition metals.⁷⁶⁻⁸² By changing the width of the band gap, the electronic levels of the materials also change and they become active in the visible part of the solar spectrum. Doping with non-metals create acceptor states above the valence band, while doping with transition metal species create donor states below the conduction band.⁸³ However, the change in electronic levels can result in materials that are less active for certain reactions, for example for the formation of very reactive hydroxyl radicals. These materials are active under visible light irradiation, which is not the case for undoped titania, but when one looks at the total activity under solar irradiation, these materials are less active than their undoped counterparts.^{84, 85}

The diminishing of the electron and hole recombination can be achieved in different ways: increasing the crystallinity, addition of noble metal nanoparticles, decreasing the crystallite size, coupling with another semiconductor and doping with transition metal species.⁸⁶ We focussed on the first two approaches: increasing the crystallinity and the addition of noble metal nanoparticles.

Amorphous phases present in titania enhance the electron-hole recombination rate, accordingly increasing the crystallinity (and thus decreasing the amorphous fraction) ameliorates the rate of electrons and holes that reach the surface. To enhance the amount of electrons and holes that reach the surface even more, the specific surface area of titania is increased by synthesising a mesoporous material. Enlarging the specific surface area is however not straightforward for titania as there is a compromise between a high specific surface area and the degree of crystallinity as described above. There is already a lot of literature available on the synthesis of mesoporous titania, but there is no clear reason why some syntheses result in materials with a high specific surface area and others in materials with very small specific surface areas. Only a limited amount of papers investigates the

degree of crystallinity, while this is a very important factor for the photocatalytic activity.⁸⁷ This research aims for a reproducible synthesis of highly porous titania with an increased degree of crystallinity.

In chapter 2 we explored the use of microwave irradiation to increase the crystallinity of mesoporous titania. In case of titania nanoparticles synthesized through hydrothermal methods, it has been shown earlier that microwave irradiation improves the crystallinity of the nanoparticles and allows reducing synthesis temperature and time.⁸⁸⁻⁹¹ Only a few articles discuss the synthesis of mesoporous titania with microwave irradiation, but the amount of amorphous material in the samples is not quantified and no comparisons are made with conventional methods.^{19, 92-95}

When noble metal nanoparticles are deposited onto the surface of titania, a Schottky barrier is obtained, causing the photogenerated electrons to move to the metal particle.^{72, 86, 96, 97} This process results in a physical separation of the electron and holes, reducing the recombination rate. This can lead to rate constants three times higher in the case of Au/TiO₂ materials compared to bare titanium dioxide.⁹⁸⁻¹⁰⁰ In this research we investigated the effect of the addition of gold and platinum nanoparticles to mesoporous titania on photocatalytic degradation reactions. The synthesis of gold nanoparticles and their addition to a titania matrix is described in chapter 3. Chapter 4 discusses the in-situ synthesis of gold/titania composite materials and their characterisation, whereas chapter 5 addresses their (photo)catalytic activity.

References

- [1] Robert H. Austin, S.-f. L. Introductory perspective: The sackler colloquium on promises and perils in nanotechnology for medicine. *Proceedings of the National Academy of Sciences of the United States of America* **105**, 17217–17221 (2008).
- [2] Zhang, H. & Banfield, J. F. Understanding polymorphic phase transformation behavior during growth of nanocrystalline aggregates: insights from TiO₂. *The Journal of Physical Chemistry B* **104**, 3481–3487 (2000).
- [3] Zimny, K., Ghanbaja, J., Carteret, C., Stebe, M.-J. & Blin, J.-L. Highly ordered mesoporous titania with semi crystalline framework templated by large or small nonionic surfactants. *New Journal of Chemistry* **34**, 2113–2117 (2010).
- [4] Robben, L. *et al.* Facile synthesis of highly ordered mesoporous and well crystalline TiO₂: Impact of different gas atmosphere and calcination temperatures on structural properties. *Chemistry of Materials* **24**, 1268–1275 (2012).
- [5] Kim, D. S., Han, S. J. & Kwak, S.-Y. Synthesis and photocatalytic activity of mesoporous TiO₂ with the surface area, crystallite size, and pore size. *J. Colloid Interface Sci.* **316**, 85–91 (2007).
- [6] Zhang, Q. H., Gao, L. & Guo, J. K. Effects of calcination on the photocatalytic properties of nanosized TiO₂ powders prepared by TiCl₄ hydrolysis. *Applied Catalysis B-Environmental* **26**, 207–215 (2000).
- [7] Ovenstone, J. & Yanagisawa, K. Effect of hydrothermal treatment of amorphous titania on the phase change from anatase to rutile during calcination. *Chemistry of Materials* **11**, 2770–2774 (1999).
- [8] Titania based nanocomposites as a photocatalyst: A review. *AIMS Materials Science* **3**.
- [9] Herrmann, J. M. Heterogeneous photocatalysis: State of the art and present applications. *Top. Catal.* **34**, 49–65 (2005).

- [10] Fujishima, A. & Honda, K. Electrochemical photolysis of water at a semiconductor electrode. *Nature* **238**, 37–38 (1972).
- [11] Chen, X. & Mao, S. S. Titanium dioxide nanomaterials: Synthesis, properties, modifications, and applications. *Chem. Rev.* **107**, 2891–2959 (2007).
- [12] Gratzel, M. Photoelectrochemical cells. *Nature* **414**, 338–344 (2001).
- [13] Gratzel, M. Dye-sensitized solar cells. *Journal of Photochemistry and Photobiology C-Photochemistry Reviews* **4**, 145–153 (2003).
- [14] Li, Z.-Q. *et al.* One-Pot Synthesis of Mesoporous TiO₂ Microspheres and Its Application for High-Efficiency Dye-Sensitized Solar Cells. *ACS Applied Materials & Interfaces* **7**, 10928–10934 (2015).
- [15] Somani, P. R. & Radhakrishnan, S. Electrochromic materials and devices: present and future. *Materials Chemistry and Physics* **77**, 117–133 (2003).
- [16] Ottaviani, M., Panero, S., Morzilli, S., Scrosati, B. & Lazzari, M. The electrochromic characteristics of titanium-oxide thin-film electrodes. *Solid State Ionics* **20**, 197–202 (1986).
- [17] Hagfeldt, A., Vlachopoulos, N. & Gratzel, M. Fast electrochromic switching with nanocrystalline oxide semiconductor-films. *Journal of the Electrochemical Society* **141**, L82–L84 (1994).
- [18] Bach, U., Corr, D., Lupo, D., Pichot, F. & Ryan, M. Nanomaterials-based electrochromics for paper-quality displays. *Advanced Materials* **14**, 845–848 (2002).
- [19] Periyat, P. *et al.* Rapid microwave synthesis of mesoporous TiO₂ for electrochromic displays. *J. Mater. Chem.* **20**, 3650–3655 (2010).
- [20] Varghese, O. K., Gong, D. W., Paulose, M., Ong, K. G. & Grimes, C. A. Hydrogen sensing using titania nanotubes. *Sensors and Actuators B-Chemical* **93**, 338–344 (2003).
- [21] Varghese, O. K. *et al.* Extreme changes in the electrical resistance of titania nanotubes with hydrogen exposure. *Advanced Materials* **15**, 624–627 (2003).
- [22] Birkefeld, L. D., Azad, A. M. & Akbar, S. A. Carbon-monoxide and hydrogen detection by anatase modification of titanium-dioxide. *Journal of the American Ceramic Society* **75**, 2964–2968 (1992).

- [23] Ruiz, A. M., Cornet, A., Shimanoe, K., Morante, J. R. & Yamazoe, N. Transition metals (Co, Cu) as additives on hydrothermally treated TiO₂ for gas sensing. *Sensors and Actuators B-Chemical* **109**, 7–12 (2005).
- [24] Ferroni, M. *et al.* Preparation and characterization of nanosized titania sensing film. *Sensors and Actuators B-Chemical* **77**, 163–166 (2001).
- [25] Comini, E. *et al.* Sensitivity enhancement towards ethanol and methanol of TiO₂ films doped with pt and nb. *Sensors and Actuators B-Chemical* **64**, 169–174 (2000).
- [26] Benkstein, K. D. & Semancik, S. Mesoporous nanoparticle TiO₂ thin films for conductometric gas sensing on microhotplate platforms. *Sensors and Actuators B-Chemical* **113**, 445–453 (2006).
- [27] Ruiz, A. M., Cornet, A. & Morante, J. R. Performances of La-TiO₂ nanoparticles as gas sensing material. *Sensors and Actuators B-Chemical* **111**, 7–12 (2005).
- [28] Gaya, U. I. & Abdullah, A. H. Heterogeneous photocatalytic degradation of organic contaminants over titanium dioxide: A review of fundamentals, progress and problems. *Journal of Photochemistry and Photobiology C: Photochemistry Reviews* **9**, 1–12 (2008).
- [29] Hsken, G., Hunger, M. & Brouwers, H. J. H. Experimental study of photocatalytic concrete products for air purification. *Building and Environment* **44**, 2463–2474 (2009).
- [30] Zhao, J. & Yang, X. Photocatalytic oxidation for indoor air purification: a literature review. *Building and Environment* **38**, 645–654 (2003).
- [31] Ismail, A. A. & Bahnemann, D. W. Photochemical splitting of water for hydrogen production by photocatalysis: A review. *Solar Energy Materials and Solar Cells* **128**, 85 – 101 (2014).
- [32] Leung, D. Y. C. *et al.* Hydrogen production over titania-based photocatalysts. *Chemsuschem* **3**, 681–694 (2010).
- [33] Yi, H. *et al.* Photocatalytic H₂ production from methanol aqueous solution over titania nanoparticles with mesostructures. *Int. J. Hydrogen Energy* **33**, 672–678 (2008).
- [34] Yu, J., Qi, L. & Jaroniec, M. Hydrogen production by photocatalytic water splitting over Pt/TiO₂ nanosheets with exposed (001) facets. *J. Phys. Chem. C* **114**, 13118–13125 (2010).

- [35] Yan, K., Wu, G. S., Jarvis, C., Wen, J. L. & Chen, A. C. Facile synthesis of porous microspheres composed of TiO₂ nanorods with high photocatalytic activity for hydrogen production. *Applied Catalysis B-Environmental* **148**, 281–287 (2014).
- [36] Ma, Y. *et al.* Titanium Dioxide-Based Nanomaterials for Photocatalytic Fuel Generations. *Chem. Rev.* **114**, 9987–10043 (2014).
- [37] Cronstedt, A. F. Ron ochbeskrifning om en obekant bergart, som kallas zeolites. *Akad. Handl. Stockholm* **18**, 120–130 (1756).
- [38] Flanigen, E. M., Broach, R. W. & Wilson, S. T. *Zeolites in Industrial Separation and Catalysis*, chap. Chapter 1, introduction, 1–26 (Wiley-VCH, 2010).
- [39] Barrer, R. M. Separation of mixtures using zeolites as molecular sieves. i. three classes of molecular - sieve zeolite. *J. Soc. Chem. Ind.* **64**, 130 (1945).
- [40] Barrer, R. M. Synthesis and reactions of mordenite. *J. Soc. Chem.* 2158 (1948).
- [41] Barrer, R. M. Synthesis of a zeolitic mineral with chabazite - like sorptive properties. *J. Soc. Chem.* 127 (1948).
- [42] Perego, C. & Millini, R. Porous materials in catalysis: challenges for mesoporous materials. *Chem. Soc. Rev.* **42**, 3956–3976 (2013).
- [43] Kresge, C., Leonowicz, M., Roth, W., Schmitt, K. & Vartuli, J. Synthetic mesoporous crystalline material (1993). US Patent 5,198,203.
- [44] Kresge, C. T., Leonowicz, M. E., Roth, W. J., Vartuli, J. C. & Beck, J. S. Ordered mesoporous molecular sieves synthesized by a liquid-crystal template mechanism. *Nature* **359**, 710–712 (1992).
- [45] Beck, J. S. *et al.* A new family of mesoporous molecular sieves prepared with liquid crystal templates. *Journal of the American Chemical Society* **114**, 10834–10843 (1992).
- [46] Luca, V. & Hook, J. M. Study of the structure and mechanism of formation through self-assembly of mesostructured vanadium oxide. *Chemistry of Materials* **9**, 2731–2744 (1997).
- [47] Antonelli, D. M. & Ying, J. Y. Synthesis of a stable hexagonally packed mesoporous niobium oxide molecular sieve through a novel ligand-assisted templating mechanism. *Angewandte Chemie International Edition in English* **35**, 426–430 (1996).

- [48] Antonelli, D. M., & Ying*, J. Y. Synthesis and characterization of hexagonally packed mesoporous tantalum oxide molecular sieves. *Chemistry of Materials* **8**, 874–881 (1996).
- [49] Knowles, J. A. & Hudson, M. J. Preparation and characterisation of mesoporous, high surface area zirconium(iv) oxides. *J. Chem. Soc., Chem. Commun.* 2083–2084 (1995).
- [50] Antonelli, D. M. & Ying, J. Y. Synthesis of hexagonally packed mesoporous TiO₂ by a modified solgel method. *Angewandte Chemie International Edition in English* **34**, 2014–2017 (1995).
- [51] Kim, D. S. & Kwak, S.-Y. The hydrothermal synthesis of mesoporous TiO₂ with high crystallinity, thermal stability, large surface area, and enhanced photocatalytic activity. *Appl. Catal., A* **323**, 110–118 (2007).
- [52] Ismail, A. A., Bahnemann, D. W., Robben, L., Yarovy, V. & Wark, M. Palladium doped porous titania photocatalysts: Impact of mesoporous order and crystallinity. *Chem. Mater.* **22**, 108–116 (2010).
- [53] Choi, S. Y., Mamak, M., Coombs, N., Chopra, N. & Ozin, G. A. Thermally stable two-dimensional hexagonal mesoporous nanocrystalline anatase, meso-nc-TiO₂: Bulk and crack-free thin film morphologies. *Advanced Functional Materials* **14**, 335–344 (2004).
- [54] Yu, J. C., Wang, X. C. & Fu, X. Z. Pore-wall chemistry and photocatalytic activity of mesoporous titania molecular sieve films. *Chem. Mater.* **16**, 1523–1530 (2004).
- [55] Dong, W. *et al.* Controllable and repeatable synthesis of thermally stable anatase nanocrystal-silica composites with highly ordered hexagonal mesostructures. *J. Am. Chem. Soc.* **129**, 13894–13904 (2007).
- [56] Brinker, C. J. & Scherer, G. W. *Sol-Gel Science: The Physics and Chemistry of Sol-Gel Processing*. (Academic Press, San Diego, 1990).
- [57] Peng, T. Y., Zhao, D., Dai, K., Shi, W. & Hirao, K. Synthesis of titanium dioxide nanoparticles with mesoporous anatase wall and high photocatalytic activity. *Journal of Physical Chemistry B* **109**, 4947–4952 (2005).
- [58] Bagheri, S., Hir, Z. A. M., Yousefi, A. T. & Hamid, S. B. A. Progress on mesoporous titanium dioxide: Synthesis, modification and applications. *Microporous and Mesoporous Materials* **218**, 206 – 222 (2015).
- [59] Kumaresan, L., Prabhu, A., Palanichamy, M. & Murugesan, V. Synthesis of mesoporous TiO₂ in aqueous alcoholic medium and evaluation of its photocatalytic activity. *Materials Chemistry and Physics* **126**, 445–452 (2011).

- [60] Tayade, R. J., Kulkarni, R. G. & Jasra, R. V. Transition metal ion impregnated mesoporous TiO₂ for photocatalytic degradation of organic contaminants in water. *Industrial and Engineering Chemistry Research* **45**, 5231–5238 (2006).
- [61] Antonelli, D. M. Synthesis of phosphorus-free mesoporous titania via templating with amine surfactants. *Microporous and Mesoporous Materials* **30**, 315–319 (1999).
- [62] Wang, Y. Q. *et al.* Sonochemical synthesis of mesoporous titanium oxide with wormhole-like framework structures. *Advanced Materials* **12**, 1183–1186 (2000).
- [63] Ghorai, T. K. Synthesis of spherical mesoporous titania modified iron-niobate nanoclusters for photocatalytic reduction of 4-nitrophenol. *Journal of Materials Research and Technology* **4**, 133 – 143 (2015).
- [64] Zhang, D., Qi, L., Ma, J. & Cheng, H. Formation of crystalline nanosized titania in reverse micelles at room temperature. *J. Mater. Chem.* **12**, 3677–3680 (2002).
- [65] Lu, C.-H., Wu, W.-H. & Kale, R. B. Microemulsion-mediated hydrothermal synthesis of photocatalytic TiO₂ powders. *Journal of Hazardous Materials* **154**, 649–654 (2008).
- [66] Goswami, P. & Ganguli, J. N. Evaluating the potential of a new titania precursor for the synthesis of mesoporous Fe-doped titania with enhanced photocatalytic activity. *Mater. Res. Bull.* **47**, 2077–2084 (2012).
- [67] Chowdhury, I. H., Ghosh, S. & Naskar, M. K. Aqueous-based synthesis of mesoporous TiO₂ and AgTiO₂ nanopowders for efficient photodegradation of methylene blue. *Ceramics International* **42**, 2488 – 2496 (2016).
- [68] Mahoney, L. & Koodali, R. T. Versatility of evaporation-induced self-assembly (EISA) method for preparation of mesoporous TiO₂ for energy and environmental applications. *Materials* **7**, 2697–2746 (2014).
- [69] Cassiers, K. *et al.* Surfactant-directed synthesis of mesoporous titania with nanocrystalline anatase walls and remarkable thermal stability. *Journal of Physical Chemistry B* **108**, 3713–3721 (2004).
- [70] Beyers, E., Cool, P. & Vansant, E. F. Stabilisation of mesoporous TiO₂ by different bases influencing the photocatalytic activity. *Micropor. Mesopor. Mater.* **99**, 112–117 (2007).

- [71] Ismail, A. A. & Bahnemann, D. W. One-step synthesis of mesoporous platinum/titania nanocomposites as photocatalyst with enhanced photocatalytic activity for methanol oxidation. *Green Chemistry* **13**, 428–435 (2011).
- [72] Bannat, I. *et al.* Improving the photocatalytic performance of mesoporous titania films by modification with gold nanostructures. *Chemistry of Materials* **21**, 1645–1653 (2009).
- [73] Dai, Y. *et al.* High-surface-area mesoporous crystalline TiO_2 : Synthesis, characterization, and application as support for making stable Au catalysts. *Journal of Nanoscience and Nanotechnology* **17** (2017).
- [74] Chen, J. E. *et al.* Synthesis of magnetic mesoporous titania colloidal crystals through evaporation induced self-assembly in emulsion as effective and recyclable photocatalysts. *Phys. Chem. Chem. Phys.* **17**, 27653–27657 (2015).
- [75] Aging dependent phase transformation of mesostructured titanium dioxide nanomaterials prepared by evaporation-induced self-assembly process: Implications for solar hydrogen production. *AIMS Materials Science* **2**.
- [76] Thompson, T. L. & Yates, J. T. TiO_2 -based photocatalysis: Surface defects, oxygen and charge transfer. *Topics in Catalysis* **35**, 197–210 (2005).
- [77] Ahmed, S., Rasul, M. G., Martens, W. N., Brown, R. & Hashib, M. A. Heterogeneous photocatalytic degradation of phenols in wastewater: A review on current status and developments. *Desalination* **261**, 3–18 (2010).
- [78] Di Paola, A. *et al.* Preparation of polycrystalline TiO_2 photocatalysts impregnated with various transition metal ions: Characterization and photocatalytic activity for the degradation of 4-nitrophenol. *Journal of Physical Chemistry B* **106**, 637–645 (2002).
- [79] Zaleska, A. Doped- TiO_2 : A review. *Recent Patents on Engineering* **2**, 157–164 (2008).
- [80] Tian, L. & Chen, X. High visible-light photocatalytic activity with mesoporous titanium dioxide. *SPIE* (2016).
- [81] Zou, M. *et al.* Visible light photocatalysts (Fe, N): TiO_2 from ammonothermally processed, solvothermal self-assembly derived Fe- TiO_2 mesoporous microspheres. *Materials Chemistry and Physics* **195**, 259–267 (2017).
- [82] Appavu, B., Kannan, K. & Thiripuranthagan, S. Enhanced visible light photocatalytic activities of template free mesoporous nitrogen doped reduced graphene oxide/titania composite catalysts. *Journal of Industrial and Engineering Chemistry* **36**, 184 – 193 (2016).

- [83] Li, L. *et al.* Sub-10 nm rutile titanium dioxide nanoparticles for efficient visible-light-driven photocatalytic hydrogen production. *Nature Commun.* **6** (2015).
- [84] Pelaez, M. *et al.* A review on the visible light active titanium dioxide photocatalysts for environmental applications. *Applied Catalysis B: Environmental* **125**, 331 – 349 (2012).
- [85] Rengifo-Herrera, J. & Pulgarin, C. Photocatalytic activity of N, S co-doped and N-doped commercial anatase TiO₂ powders towards phenol oxidation and E. coli inactivation under simulated solar light irradiation. *Solar Energy* **84**, 37 – 43 (2010).
- [86] Mohamed, H. H. & Bahnemann, D. W. The role of electron transfer in photocatalysis: Fact and fictions. *Appl. Catal. B-Environ.* **128**, 91–104 (2012).
- [87] Tobaldi, D. M., Tucci, A., kapin, A. S. & Esposito, L. Effects of sio₂ addition on tio₂ crystal structure and photocatalytic activity. *Journal of the European Ceramic Society* **30**, 2481 – 2490 (2010).
- [88] Baghbanzadeh, M., Carbone, L., Cozzoli, P. D. & Kappe, C. O. Microwave-assisted synthesis of colloidal inorganic nanocrystals. *Angew. Chem., Int. Ed.* **50**, 11312–11359 (2011).
- [89] Dufour, F., Cassaignon, S., Durupthy, O., Colbeau-Justin, C. & Chaneac, C. Do TiO₂ nanoparticles really taste better when cooked in a microwave oven? *Eur. J. Inorg. Chem.* 2707–2715 (2012).
- [90] Arin, M. *et al.* Deposition of photocatalytically active TiO₂ films by inkjet printing of TiO₂ nanoparticle suspensions obtained from microwave-assisted hydrothermal synthesis. *Nanotechnology* **23**, 165603 (2012).
- [91] Arin, M. *et al.* Low temperature deposition of TiO₂ layers from nanoparticle containing suspensions synthesized by microwave hydrothermal treatment. *J. Sol-Gel Sci. Technol.* **66**, 100–111 (2013).
- [92] Jena, A., Vinu, R., Shivashankar, S. A. & Madras, G. Microwave assisted synthesis of nanostructured titanium dioxide with high photocatalytic activity. *Ind. Eng. Chem. Res.* **49**, 9636–9643 (2010).
- [93] Suprabha, T., Roy, H. G., Thomas, J., Kumar, K. P. & Mathew, S. Microwave-assisted synthesis of titania nanocubes, nanospheres and nanorods for photocatalytic dye degradation. *Nanoscale Res. Lett.* **4**, 144–152 (2009).

- [94] Qi, L., Cheng, B., Yu, J. & Ho, W. High-surface area mesoporous pt/tio₂ hollow chains for efficient formaldehyde decomposition at ambient temperature. *Journal of Hazardous Materials* **301**, 522 – 530 (2016).
- [95] Wang, H.-W., Kuo, C.-H., Lin, H.-C., Kuo, I.-T. & Cheng, C.-F. Rapid formation of active mesoporous tio₂ photocatalysts via micelle in a microwave hydrothermal process. *Journal of the American Ceramic Society* **89**, 3388–3392 (2006).
- [96] Lin, Z. *et al.* On the role of localized surface plasmon resonance in uv-vis light irradiated Au/TiO₂ photocatalysis systems: pros and cons. *Nanoscale* **7**, 4114–4123 (2015).
- [97] Chen, J., Qiu, F., Xu, W., Cao, S. & Zhu, H. Recent progress in enhancing photocatalytic efficiency of tio₂-based materials. *Applied Catalysis A: General* **495**, 131 – 140 (2015).
- [98] Yu, Y., Wen, W., Qian, X.-Y., Liu, J.-B. & Wu, J.-M. UV and visible light photocatalytic activity of Au/TiO₂ nanoforests with Anatase/Rutile phase junctions and controlled Au locations. *Scientific Reports* **7** (2017).
- [99] Mehta, A., Sharma, M., Kumar, A. & Basu, S. Effect of au content on the enhanced photocatalytic efficiency of mesoporous au/tio₂ nanocomposites in uv and sunlight. *Gold Bulletin* **50**, 33–41 (2017).
- [100] Wei, Z. *et al.* Size-controlled gold nanoparticles on octahedral anatase particles as efficient plasmonic photocatalyst. *Applied Catalysis B-Environmental* **206**, 393–405 (2017).

2

Microwave assisted synthesis of mesoporous titania

In this chapter the synthesis of mesoporous titania is described. Microwave irradiation is used to obtain a high degree of crystallinity while preserving a high specific surface area ($> 360 \text{ m}^2/\text{g}$). The obtained materials are evaluated for their photocatalytic activity in aqueous and gaseous media. The microwave treated samples show an improved performance over the untreated samples.

Adapted from:

Meire, M.; Verbruggen, S. W.; Lenaerts, S.; Lommens, P.; Van Der Voort, P.; Van Driessche, I., Microwave-assisted synthesis of mesoporous titania with increased crystallinity, specific surface area, and photocatalytic activity. Journal of Materials Science 2016, 51 (21), 9822-9829.

2.1 Introduction

The degree of crystallinity of titania is important for many of its applications, but especially for its use as photocatalyst as the defects have a strong influence on the charge recombination rate and therefore also on the photocatalytic activity itself.¹ A soft templating titania synthesis minimally consists of a hydrolysis step, forming an amorphous titania network around the polymer template and a calcination step to form crystalline titania and to remove the template. The major drawback of this route is that one has to compromise between a high crystallinity and a high specific surface area as the organic templates are not stable at the temperatures required for the crystallization of the titania precursor.

In the case of titania nanoparticles synthesized through hydrothermal methods, it has been shown earlier that microwave irradiation improves the crystallinity of the nanoparticles and allows reducing synthesis temperature and time.²⁻⁵ Conventional heating methods, like muffle ovens, are often inefficient because of the temperature gradient that is generated within the vessel. The vessel is heated from the outside, first heating the reaction vessel itself before the reaction mixture gradually can absorb heat (Figure 2.1). After some time a thermal equilibrium will be reached and the temperature gradient will disappear, but this generally takes several hours. Microwave irradiation does not suffer from these disadvantages. The microwaves interact directly with the (solvent)molecules in the reaction mixture, resulting in a fast and more homogeneous temperature increase. The heating does not depend on the thermal conductivity of the reaction vessel, but on the interactivity of the molecules in the reaction mixture with the microwave irradiation.⁶

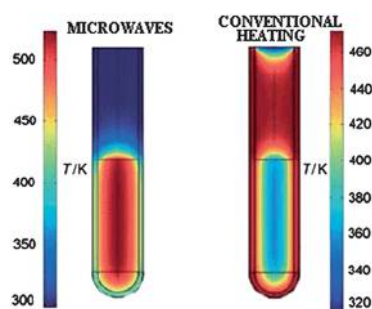


Figure 2.1: Microwave heating versus conventional heating.⁷

Microwave irradiation could also be a solution for the crystallinity/surface area compromise for mesoporous materials as lower temperatures are needed to obtain crystalline materials and the faster heating results in shorter reaction times. As the template molecules have to withstand a lesser time at high temperatures, it could be possible they remain stable during the complete reaction, resulting in higher

specific surface areas. Only a few articles discuss the synthesis of mesoporous titania with microwave irradiation, but the comparison with conventional methods is not made.⁸⁻¹⁰ Another major lack in the literature concerning the synthesis of mesoporous titania is the quantitative analysis of the material composition. The relative composition of the crystal phases is given, but whether or not amorphous material is present is not discussed. However, the presence of an amorphous fraction is important to evaluate the catalytic activity of the materials. To the best of my knowledge, no articles discussing standard mesoporous titania syntheses give a quantitative analysis of the material composition. In this chapter the amorphous fraction of the samples will be analysed using Rietveld analysis with a standard addition method.

In this chapter, the adaptation of an evaporation induced self-assembly (EISA) synthesis with an additional microwave treatment, is discussed. The photocatalytic activity of the resulting powders was tested for both aqueous and gaseous systems. Methylene blue, a common dye in the textile industry and isotroturon, a persistent herbicide were used as test molecules to determine the photocatalytic activity of mesoporous titania in aqueous media. In the case of the air purification application, acetaldehyde, a common pollutant indoors, was used.

2.2 Experimental section

Materials. Titanium(IV) isopropoxide ($\text{Ti}(\text{O}^i\text{Pr})_4$, $\geq 97\%$), methylene blue hydrate ($\geq 95\%$) and isotroturon (PESTANAL®), analytical standard) are purchased from Sigma-Aldrich, hexadecyltrimethylammonium bromide (CTAB, $\geq 98.0\%$) is acquired from Tokyo Chemical Industry (TCI) and ethanol (absolute PA) from Panreac. All chemicals are used as received.

2.2.1 Synthesis of titania powders

The synthesis was adapted from a recipe described by Beyers *et al.*^{11, 12} A clear, colorless ethanolic solution (6 mL) containing CTAB (0.59 g) at 40 °C is mixed with a colorless solution of EtOH (5.7 mL), $\text{Ti}(\text{O}^i\text{Pr})_4$ (3 mL) and HCl (1.2 mL). Distilled water (2.06 mL) is added drop wise while stirring vigorously. The resulting mixture is stirred for 15 minutes and transferred to a Petri Dish with a diameter of 9 cm. This is kept in an oven at 75 °C for 3 days. The obtained yellow solid is subjected to a base treatment consisting of 48 hours refluxing in NaOH solution (50 mL 0.1 M). The white powder is filtered, washed 3 times with distilled water and dried overnight at ambient conditions. The calcination proceeds for 2 hours at 450 °C with a heating rate of 2 °C min⁻¹. A specific surface area of 340 m²/g \pm 27 m²/g is obtained from 15 syntheses.

To investigate the influence of microwave irradiation on the crystallinity, an

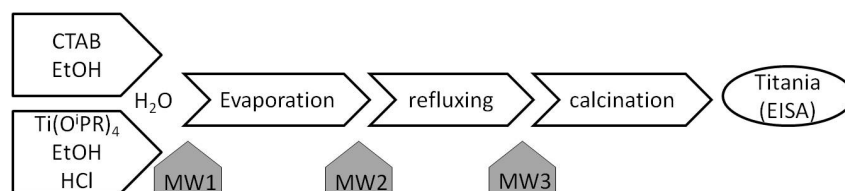


Figure 2.2: Flow chart of the synthesis of mesoporous titania, with indications of the additional microwave irradiation steps.

additional microwave treatment of 1 hour at 120 °C is performed at three different stages of the synthesis. In the first case, this is before the transfer to the Petri Dish and this sample is called MW 1. The MW 2 and MW 3 samples underwent a microwave treatment respectively before and after the NaOH treatment. A flow chart of the synthesis is depicted in Figure 2.2.

2.2.2 Characterisation

Nitrogen sorption experiments are carried out on a TriStar 3000 (Micromeritics) at -196 °C. The specific surface areas are calculated using the Brunauer-Emmett-Teller (BET) method. X-ray diffraction (XRD) diffractograms are recorded on an ARL XTRA Diffractometer (Thermo Scientific) equipped with a Cu-K α tube and a Peltier cooled lithium drifted silicon solid state detector. To calculate the amorphous content of the samples, 10 wt% ZnO is added as an internal standard.¹³ The powders are side loaded onto the sample holder to reduce preferential orientation. The amorphous content is evaluated by quantitative Rietveld refinement using Topas Academic V4.1 software.¹⁴ Total diffusion reflectance UV-Vis measurements on the titania powders are performed on a Varian Cary 500 spectrometer equipped with an integrating sphere coated with BaSO₄. The reflectance is transformed to F(R) using the Kubelka-Munk function. Anatase has an indirect band gap as the maximum energy of the valence band and the minimal energy of the conduction band have different k-vectors. The band gap energy is therefore obtained from the [F(R)E]² versus the energy of the exiting light (E) plot by extrapolating the linear part of the graph, where the intersection with the x-axis represents the band gap energy. For TEM analysis, a copper support TEM grid (200 mesh) was dipped into an aqueous dispersion of the titania powders and air-dried. A JEOL JEM-2200FS transmission electron microscope with Cs corrector and an accelerating voltage of 200 kV was used.

2.2.2.1 Surface Photovoltage (SPV) measurements

The setup is a custom made apparatus as described by Verbruggen *et al.*,¹⁵ in which the powder sample is sandwiched between two ITO electrodes (Sigma Aldrich,

1.2 mm thickness, $8\text{-}12 \Omega \text{ cm}^{-2}$ resistivity), connected to an amplifier (10^6 voltage amplification). No external bias is applied. In order to perform reproducible measurements, a section of $5 \text{ mm} \times 5 \text{ mm}$ is illuminated. $8.5 \pm 0.5 \text{ mg}$ of each catalyst is used to obtain a good contacting layer between both ITO electrodes. The exact SPV value was determined by taking the difference between the voltage readout after 1.5 min of UVA illumination and the steady voltage readout in the dark. For all samples, four independent measurements were performed and averaged. The standard deviation was calculated to give an estimate of the error on the measurements.

2.2.2.2 Photocatalytic degradation

Water purification. The photocatalytic activity of the powders is evaluated through the degradation of methylene blue and isoproturon under UV illumination. The experiments are carried out in a set-up based on ISO 10678:2010(E)(Figure 2.3). A

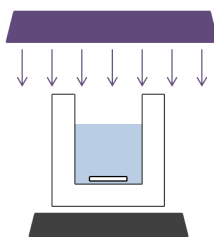


Figure 2.3: Schematic of aqueous photocatalytic test set-up.

Vilber Lourmat VL-315BLB blacklight blue fluorescent light tube, 15 cm from the dispersion surface, is used with a maximum emission at 365 nm and emitting 10 W/m^2 . The starting concentration of the aqueous methylene blue solution was 50 mg/L and 8 mg/L in the case of the isoproturon solution. Both experiments were conducted in the same way. Titania (0.3 g/L) was added to 50 mL pollutant solution in a photocatalytic cell which is kept at a constant temperature of $25 \text{ }^\circ\text{C}$. The suspension was stirred for 60 minutes in the dark to reach adsorption equilibrium. At frequent time intervals (time = 0, 15, 30 and 60 minutes in the case of methylene blue discoloration and time = 0, 30, 60 and 90 minutes in the case of isoproturon degradation) 2 mL dispersion was centrifuged for 5 minutes at 5000 rpm to separate the titania powder from the pollutant solution. The pollutant concentration was evaluated using a Shimadzu UV1800 UV spectrometer at 665 nm in the case of methylene blue and 245 nm in the case of isoproturon. These wavelengths are maintained during the whole test in order to avoid the interference of the degradation products. The degradation is normalized with respect to the starting concentration after reaching adsorption equilibrium. The degradation of methylene blue and isoproturon proceed with pseudo-first order kinetics. Rate

constants are derived from the $\ln(C/C_0)$ versus time graphs.

Air purification. All samples (20 mg) were first suspended in 1 g absolute ethanol and stirred ultrasonically. For each sample, two pre-cleaned glass slides ($2.5 \times 1.5 \text{ cm}^2$) were drop casted with $300 \mu\text{L}$ of its suspension. The slides were left to dry to the air and were then transferred to an oven at $100 \text{ }^\circ\text{C}$ for further drying overnight. Acetaldehyde was used as model pollutant. A polluted gas flow was generated by premixing 1% acetaldehyde in N_2 (Praxair) with synthetic air (Praxair), resulting in an acetaldehyde concentration of $30 \pm 3 \text{ ppmv}$. The samples were placed in the centre of a single pass, $150 \text{ mm} \times 20 \text{ mm} \times 2.75 \text{ mm}$ slit-shaped flatbed photoreactor (Figure 2.4). A Philips Cleo UVA tube (λ_{max} of

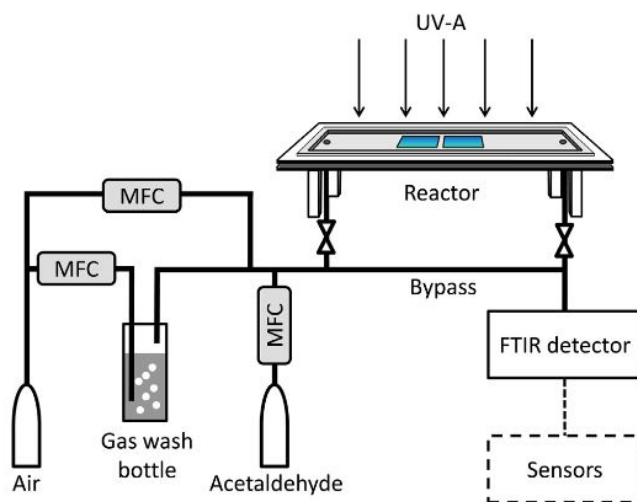


Figure 2.4: Schematic of gaseous photocatalytic test set-up. MFC: Mass Flow Controller.¹⁶

365 nm , incident intensity of 3 mW cm^{-2} at sample distance (2 cm) was used as light source. This test procedure is similar as described in earlier work.¹⁶⁻¹⁸ The measurements were carried out in several phases: 1) the dark reactor is flushed with clean air. 2) The reactor is illuminated and flushed with clean air. During this step, adsorbed rest fractions of solvents form the synthesis of coating protocols are photocatalytically removed from the substrate. 3) The pollutant reference level is measured by flowing polluted air directly to the detector, not passing the reactor. 4) Polluted air is passed through the dark reactor to determine the adsorption of the pollutant. 5) The reactor is illuminated and the photocatalytic activity is monitored. The concentrations of acetaldehyde and CO_2 are monitored on-line by FTIR spectroscopy. The FTIR absorbance is converted into an actual concentration using pre-established calibration curves constructed using an organic vapour sensor

and CO₂ sensor. For each sample an automated test protocol is run, that goes through the test phases, described above, three consecutive times, with 15 minutes polluted flow through the reactor in dark and 20 minutes under UV illumination.

2.3 Material properties

2.3.1 Specific surface area and crystallinity

Table 2.1: Crystal fractions and specific surface areas of the titania samples.

	EISA	MW 1 ^a	MW 2 ^a	MW 3 ^a
Anatase (%) ^b	35	57	82	50
Brookite (%) ^b	0	24	0	0
Other (%) ^c	65	19	18	50
S _{BET} (m ² /g)	318 ± 5	267 ± 2	202 ± 2	361 ± 4
Pore size ^d (nm)	3.5 - 4.5	2.5 - 4	5 - 6	3.5 - 4.5
Band gap ^e (eV)	3.1	3.2	3.1	3.0
Visual appearance				

^a The microwave treatment of MW 1 is performed before its transfer to a Petri Dish. In case of MW 2 and MW 3 the microwave treatment is performed respectively before and after the NaOH treatment.

^b When a crystal phase fraction of less than 1% is found, this is neglected.

^c Other includes amorphous fractions, undetermined crystalline phases and adsorbed molecules.

^d The average pore sizes are determined from the differential pore volume distributions (Figure A.4).

^e The band gap energy is calculated from the $[F(R) \cdot E]^2$ versus the energy (E) plot (Figure 2.6).

The effect of a microwave treatment, applied at different stages of the syntheses, on the degree of crystallinity and the specific surface area of titania was investigated. Table 1 shows quantitative information on the fractions of the crystal phases present in the different samples. In the supplementary information XRD spectra of all samples (Figure A.1 and the Rietveld convolutions of MW 1 and MW 2 (Figure A.2) are presented. The EISA sample is the least crystalline, with 35 wt% anatase. For all three microwave treated samples, the anatase phase increased with at least 15%. MW 1 exhibits a large fraction of brookite (24%), next to an increased anatase fraction of 57%. The microwave procedure for the MW 1 sample is performed on the ethanolic precursor solution, which results in higher pressures in the reaction vessels than with aqueous solutions. As brookite is gener-

ally formed at higher pressures, it explains why the brookite phase is only observed in this sample. MW 2 has the highest anatase fraction of 82%, but also the anatase content of MW 3 increased to 50%.

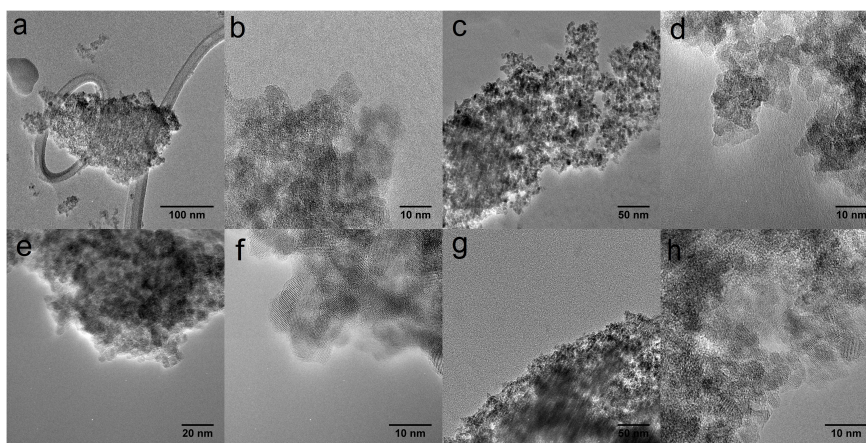


Figure 2.5: TEM images of the titania samples EISA (a, b), MW 1 (c, d), MW 2 (e, f) and MW 3 (g, h).

The nitrogen sorption isotherms of the samples exhibit type IV characteristics (A.3). EISA and MW 2 show more pore blocking, whereas MW 1 and MW 3 display capillary condensation at higher relative pressures. The average pore sizes are extracted from the differential pore size distributions (A.4). All samples exhibit pore sized in the lower mesoporous range and do not differ much. The specific surface areas of the mesoporous titania samples obtained from BET analysis are also listed in Table 2.1. The untreated EISA sample exhibits a specific surface area of $318 \text{ m}^2/\text{g}$. In most of the samples, the microwave treatment did not result in a large loss in specific surface area, except for MW 2, where a decrease to $202 \text{ m}^2/\text{g}$ is observed. The preservation of the specific surface area of MW 1 during the microwave treatment can be explained by the hydrolysis behavior of the titania precursor, preferentially leading to nanoparticles.¹⁹ This means that during microwave synthesis, particle formation is further enhanced, leading to increased crystallinity but leaving the specific surface area mainly unchanged. In the case of MW 2 and MW 3, the microwave treatment is performed after assembling the titania particles around the template by evaporating the solvent. For MW 2 the microwave treatment is done before the refluxing step with NaOH, leading to a collapse of the pore structure while in MW 3, including microwave treatment after refluxing with NaOH, the pore structure is maintained or even enhanced. Beyers *et al.*,¹² have shown that a NaOH treatment, after EISA and prior to calcination at elevated temperatures, stabilizes the porous structure by crystallization of the walls

of the mesoporous titania. This explains why the structure does not collapse when the microwave treatment is performed after the NaOH treatment (MW 3), but does collapse when it is performed prior to this treatment (MW 2). TEM analysis of the samples (Figure 2.5) shows that all samples have the same morphology namely an agglomeration of small (~ 6 nm) titania crystallites, forming large particles of 100 - 200 nm. MW 2 is more dense, but the crystallites are of the same size as the other samples.

Total reflectance UV-Vis measurements are performed to calculate the band gap energies (Table 2.1). The titania powders have a band gap of approximately 3.1 eV. The band gap energies are somewhat smaller than the 3.2 eV reported for anatase, but this can be attributed to measurement errors.

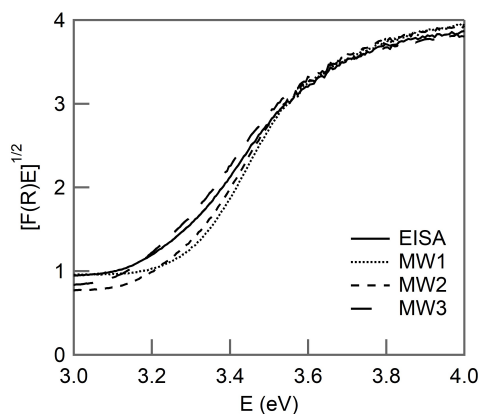


Figure 2.6: Plots of $[F(R)E]^{1/2}$ in function of E (eV).

2.3.2 Electronic properties

Surface photovoltage (SPV) measurements give a qualitative image of the formation capacity and stability of photogenerated charge carriers for the samples (Figure 2.7). MW 1 and MW 3 have an increased SPV signal compared to the non-treated (EISA) sample, which is in line with an increased degree of crystallinity, obtained from the microwave treatment. However, in the case of MW 2, no increase in SPV signal is observed. Its degree of crystallinity is increased, but its specific surface area has however decreased significantly, making it more difficult for the photogenerated charge carriers to reach the surface, resulting in approximately the same SPV signal. The SPV signal of MW 3 on the other hand is larger than expected when solely looking at the crystallinity degree as the crystallinity increase is smaller for MW 3 compared to MW 1. However, taking into account

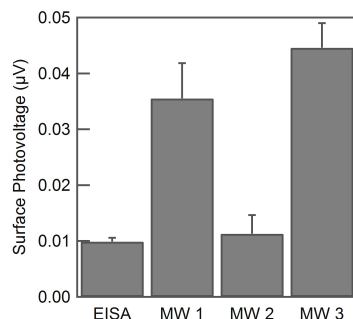


Figure 2.7: Surface photovoltage signals under UVA illumination. The error bars represent the standard deviation calculated from four independent measurements.

the differences in specific surface area for MW 3 (361 m²/g) versus MW 1 (267 m²/g), the resulting SPV signals can be explained, as the charge carriers can more easily reach the surface, when more surface is present.

2.4 Photocatalysis

The photocatalytic activity of the samples was tested in aqueous media by following the discolouration of methylene blue, a common dye in the textile industry and isoproturon, a herbicide used in the cultivation of grain. Furthermore, acetaldehyde was used as model pollutant for air purification.

2.4.1 Aqueous phase

A first evaluation of the photocatalytic activity of the samples in aqueous media was performed by following the discolouration of methylene blue as a test molecule for organic pollutants. We switched on the UV-lamps after the adsorption step described in the experimental section. The amount of methylene blue adsorbed at the beginning of the photocatalytic test is presented in Table 2.2. When compared to the starting concentration of 12 mM, this means that approximately 80% of the methylene blue molecules are adsorbed onto the surface. The moment the UV lamp is switched on, different concentration of methylene blue are measured for the different samples. However, as the major part of the methylene blue molecules are adsorbed onto the surface, these differences are only minimal. At regular time intervals an aliquot is taken from the reactor and analysed by UV-Vis spectroscopy. The resulting graph is depicted in Figure 2.8A. The rate constants are tabled in Table 2.2. When the rate constants are normalized with respect to

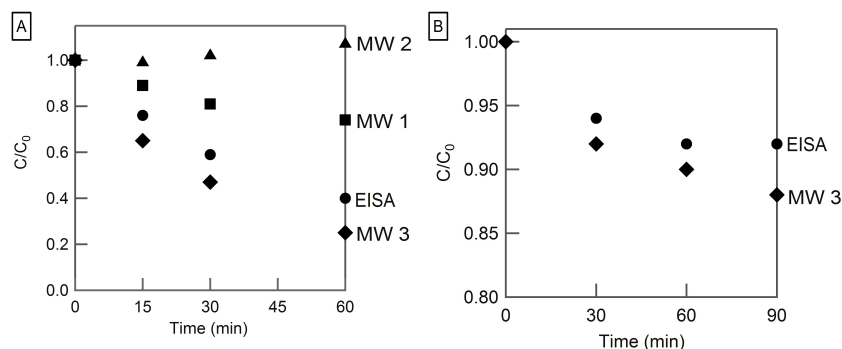


Figure 2.8: Photocatalytic degradation of aqueous A) methylene blue and B) isotroturon solutions as a function of time.

their respective specific surface areas, the same trends are still observed. This means that there is at least no linear correlation between the activity and the specific surface area. Even when corrected for the difference in specific surface area, the material with the highest specific surface area performs best. When the rate constants are normalized with respect to their respective anatase fractions, the rate constants of EISA and MW 3 and MW 1 and MW 2 are very similar, but there is a large difference between the two couples. Therefore there is again no linear relation between the photocatalytic activity and the anatase fraction.

Table 2.2: Amount of methylene blue adsorbed before catalysis and rate constants of the discolouration of methylene blue and isotroturon degradation.

	EISA	MW 1	MW 2	MW 3
Amount MB adsorbed (10^{-5} M)	10.2	9.8	8.4	10.6
Rate constant MB discolouration (min^{-1})	0.0153 ± 0.0009	0.0050 ± 0.0008	-0.0012 ± 0.0003	0.0227 ± 0.0012
Normalized rate constant MB discolouration ($\text{min}^{-1}/\text{m}^2 * 10^{-3}$)	3.21 ± 0.19	1.25 ± 0.20	-0.40 ± 0.10	4.19 ± 0.22
Normalized rate constant MB discolouration ($\text{min}^{-1}/\text{anatase fraction} * 10^{-3}$)	0.437 ± 0.257	0.088 ± 0.014	-0.015 ± 0.004	0.454 ± 0.024
Rate constant isotroturon degradation (min^{-1})	0.0009 ± 0.0003	-	-	0.0013 ± 0.0003

MW 1 is less active compared to the untreated titania material even though it shows an increased crystalline fraction and a higher SPV signal. However, its spe-

cific surface area is lower than the untreated sample. MW 2 is even less active as its specific surface area is even lower and its SPV signal is much lower than MW 1 and comparable to the untreated sample. MW 3 on the other hand has both a higher anatase fraction, leading to a high surface photovoltage and a higher specific surface area, resulting in an increased photocatalytic activity. The two most active samples were also tested for the photocatalytic degradation of a persistent herbicide, isotroturon (Figure 2.8B). Also in this application, the microwave treated sample, MW 3, was the most active.

2.4.2 Gaseous phase

The photocatalytic activity in air was investigated by the degradation of acetaldehyde. The activity is represented in terms of the steady state CO_2 levels (with CO_2 the final degradation product) generated during UV illumination at a total flow rate of $400 \text{ cm}^3 \text{ min}^{-1}$ and an acetaldehyde inlet concentration of $30 \pm 3 \text{ ppmv}$ (Figure 2.9). All microwave treated samples are more active than the untreated sample, but MW 1 and MW 2 clearly show the highest improvement.

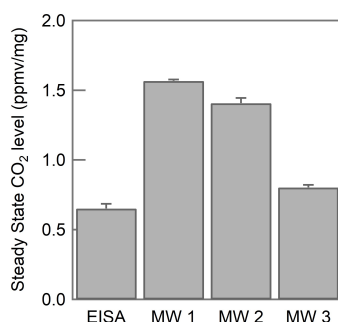


Figure 2.9: Photocatalytic steady state CO_2 formation during acetaldehyde degradation under UVA illumination.

In general, there is not really an agreement between the amount of CO_2 produced during the photocatalytic degradation of acetaldehyde and the SPV signal of the corresponding samples. To compare the samples with regard to their intrinsic electronic properties, the photocatalytic activities are represented per unit of area and compared to the anatase fraction in the samples (Figure 2.10). In the case of gaseous photocatalytic degradation of acetaldehyde, the higher the anatase fraction in the sample, the more active the sample is in terms of activity per unit of area, here the most active sample is MW 2. In the case of the absolute activity of the samples, the specific surface area has to be taken into account, which is lowest

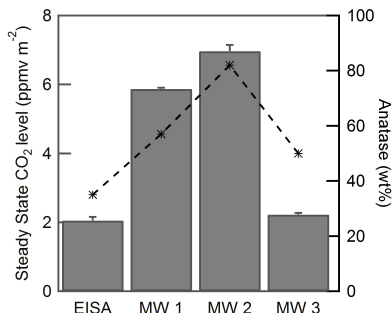


Figure 2.10: Area based photocatalytic activity during acetaldehyde degradation (left axis) and anatase fractions (right axis) of the samples.

for MW 2 compared to EISA, resulting in MW 1 being the most active sample overall.

2.4.3 Comparison of aqueous and gaseous photocatalysis

It should be noted that the relative activity of the samples is different for the aqueous phase and gas phase degradation reactions. Photocatalysis is a complex process that relies on an interplay of many parameters. Thus, not only the catalyst, but also the reaction conditions (irradiation intensity, reactor geometry, concentration, flow rate, *etc.*) have an important influence. The degradation rate is not only determined by the activity of the catalyst, but also by the ability of the pollutant molecules to reach the surface, the adsorption of the degradation products onto the surface and the removal of the degradation products from the interface region. It is therefore not possible to make conclusion about which parameter/characteristics of the catalysts are more important in the case of aqueous phase reactions or in the case of gaseous phase reactions as our test set-ups of aqueous and gaseous phase are too different. It is however reasonable to assume that incorporating the microwave treatment at different times of the synthesis will induce different additional variations in the catalyst properties that render them more (or less) suited for applications under a given set of reaction conditions. It is clear though, that these microwave treatments improve the crystallinity of the samples without greatly compromising the active surface area. As a result, the added value of the microwave treatment is also apparent from all conducted photocatalytic experiments under very divergent conditions, even though the order of reactivity is different. One can say that in our gaseous phase set-up, the samples with a high specific surface area and a high degree of crystallinity perform best, whereas in the case of the aqueous phase set-up, only the specific surface area seems to play an

important role.

2.5 Conclusions

Mesoporous titania was synthesized according to an evaporation induced self assembly synthesis. To enhance the crystallinity of the samples, a microwave treatment was added to the synthesis procedure at selected processing steps. XRD analysis confirms that it is indeed possible to increase the crystalline anatase fraction present. Furthermore, this increased crystallinity enhances the surface photovoltage, and does not substantially affect the specific surface area of the samples.

The photocatalytic activity of the samples was tested in both aqueous and gaseous media. Generally, it can be stated that the microwave treatment led to an increase in activity. In aqueous media, this was only the case for the sample with an increased specific surface area, but for the gaseous photocatalytic degradation all microwave treated samples have an increased performance. For gaseous degradation reactions, the best material combines a high surface photovoltage with high photocatalytic activity both in absolute terms as well as per unit of area. Overall, a high specific surface area and good electrical properties are necessary to perform well in both gaseous and aqueous applications. If one has a specific application in mind, the catalyst can be tuned so it has the best performance for that specific application.

References

- [1] Primo, A., Corma, A. & Garcia, H. Titania supported gold nanoparticles as photocatalyst. *Phys. Chem. Chem. Phys.* **13**, 886–910 (2011).
- [2] Dufour, F., Cassaignon, S., Durupthy, O., Colbeau-Justin, C. & Chaneac, C. Do TiO₂ nanoparticles really taste better when cooked in a microwave oven? *Eur. J. Inorg. Chem.* 2707–2715 (2012).
- [3] Arin, M. *et al.* Deposition of photocatalytically active TiO₂ films by inkjet printing of TiO₂ nanoparticle suspensions obtained from microwave-assisted hydrothermal synthesis. *Nanotechnology* **23**, 165603 (2012).
- [4] Arin, M. *et al.* Low temperature deposition of TiO₂ layers from nanoparticle containing suspensions synthesized by microwave hydrothermal treatment. *J. Sol-Gel Sci. Technol.* **66**, 100–111 (2013).
- [5] Baghbanzadeh, M., Carbone, L., Cozzoli, P. D. & Kappe, C. O. Microwave-assisted synthesis of colloidal inorganic nanocrystals. *Angew. Chem., Int. Ed.* **50**, 11312–11359 (2011).
- [6] Prado-Gonjal, J., Schmidt, R. & Moran, E. Microwave Assisted Synthesis and Characterization of Perovskite Oxides. *ArXiv e-prints* (2014).
- [7] Luque, R., Menendez, J. A., Arenillas, A. & Cot, J. Microwave-assisted pyrolysis of biomass feedstocks: the way forward? *Energy Environ. Sci.* **5**, 5481–5488 (2012).
- [8] Periyat, P. *et al.* Rapid microwave synthesis of mesoporous TiO₂ for electrochromic displays. *J. Mater. Chem.* **20**, 3650–3655 (2010).
- [9] Jena, A., Vinu, R., Shivashankar, S. A. & Madras, G. Microwave assisted synthesis of nanostructured titanium dioxide with high photocatalytic activity. *Ind. Eng. Chem. Res.* **49**, 9636–9643 (2010).
- [10] Suprabha, T., Roy, H. G., Thomas, J., Kumar, K. P. & Mathew, S. Microwave-assisted synthesis of titania nanocubes, nanospheres and nanorods for photocatalytic dye degradation. *Nanoscale Res. Lett.* **4**, 144–152 (2009).

- [11] Meynen, V., Cool, P. & Vansant, E. F. Verified syntheses of mesoporous materials. *Microporous Mesoporous Mater.* **125**, 170–223 (2009).
- [12] Beyers, E., Cool, P. & Vansant, E. F. Stabilisation of mesoporous TiO₂ by different bases influencing the photocatalytic activity. *Micropor. Mesopor. Mater.* **99**, 112–117 (2007).
- [13] Bish, D. L. & Howard, S. A. Quantitative phase analysis using the rietveld method. *J. Appl. Crystallogr.* **21**, 86–91 (1988).
- [14] Coelho, A. A. Topas academic version 4.1 (2007).
- [15] Verbruggen, S. W., Dirckx, J. J. J., Martens, J. A. & Lenaerts, S. Surface photovoltage measurements: A quick assessment of the photocatalytic activity? *Catal. Today* **209**, 215–220 (2013).
- [16] Verbruggen, S. W. *et al.* Photocatalytic acetaldehyde oxidation in air using spacious TiO₂ films prepared by atomic layer deposition on supported carbonaceous sacrificial templates. *Appl. Catal. B* **160**, 204–210 (2014).
- [17] Deng, S. *et al.* Atomic layer deposition-based synthesis of photoactive TiO₂ nanoparticle chains by using carbon nanotubes as sacrificial templates. *Rsc Advances* **4**, 11648–11653 (2014).
- [18] Verbruggen, S. W., Lenaerts, S. & Denys, S. Analytic versus cfd approach for kinetic modeling of gas phase photocatalysis. *Chem. Eng. J.* **262**, 1–8 (2015).
- [19] Brinker, C. J. & Scherer, G. W. *Sol-Gel Science: The Physics and Chemistry of Sol-Gel Processing.* (Academic Press, San Diego, 1990).

3

Synthesis of gold nanoparticles

In this chapter the addition of gold nanoparticles to the titania matrix is described. Gold nanoparticles are synthesized both in polar and apolar media. The obtained gold nanoparticles are added to the mesoporous titania precursor to form gold/titania composite materials.

3.1 Introduction

Increasing the photocatalytic activity of titania materials is important for a lot of its applications. One way to achieve this is increasing the degree of crystallinity of titania, but another method is the addition of noble metal nanoparticles to a titania matrix.

The Fermi level of the titania semiconductor (μ) is different from the Fermi level of noble metals (E_F) (Figure 3.1 left). Upon contact, a Schottky barrier is formed at the junction of a noble metal with a semiconductor (Figure 3.1 right). The electrons in the conduction band of the semiconductor can lower their energy by flowing to the metal, causing a charge to build-up at the metal-semiconductor interface, resulting in the deformation of the band structure of the semiconductor. This deformation of the bands is a potential energy barrier, also called Schottky barrier, that the electrons have to overcome to flow from the conduction band to the metal.¹ Upon irradiation of the noble metal functionalized titanium dioxide material, electrons and holes are created in the titania matrix. The electrons, however, can lower their potential energy by migrating to the noble metal, resulting in a separation of the electrons and holes, which leads to a lower recombination rate and therefore a higher photocatalytic activity.²⁻⁵

The addition of noble metal nanoparticles to the titania matrix can also have another enhancing effect as noble metal nanoparticles can absorb (visible) light. When metal nanoparticles are irradiated, the electrons in the conduction band begin to oscillate due to the electromagnetic field of the incident photon. This results in a oscillating charge separation between the surface electrons in the conduction band and the positive lattice. Light is adsorbed when the frequencies of the electron oscillation is in resonance with the frequency of the incident photons. This effect is called surface plasmon resonance (SPR).⁶⁻⁹ The absorption of light of noble metals broadens the absorption spectrum of the composite material compared

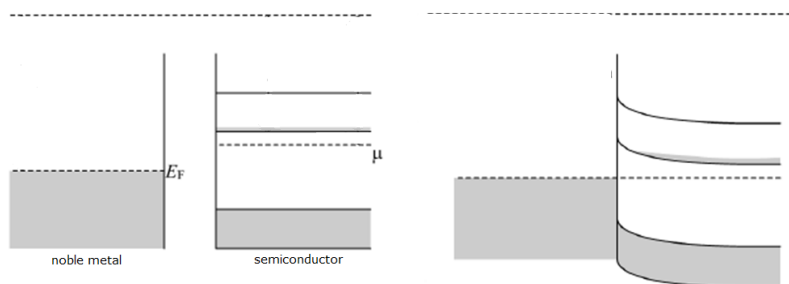


Figure 3.1: The energy levels of a noble metal and a semiconductor not in contact (left) or in contact (right).

to pure titania. This effect has however not been investigated as only UV light was used during the photocatalytic tests.¹⁰

Different noble metal nanoparticles, like Pt, Au, Pd and Ag, can be added to enhance the photocatalytic activity of titania up to 60% in the case of Pd.¹¹ As a model system we used gold as improvements up to 30% are reported in literature, which is less than Pd, but better than Pt and Ag.

Different synthetic approaches to obtain Au/TiO₂ composite materials have been described:¹² a) mixing of pre-synthesized Au nanoparticles with the TiO₂ material,¹³⁻¹⁵ b) adsorbing a gold salt onto a pre-formed titania powder followed by the reduction of the salt,^{10, 16, 17} c) blending pre-synthesized gold nanoparticles with the titanium precursor during the synthesis of the titania material^{18, 19} and d) combining a gold salt with a titanium precursor, simultaneously forming metal nanoparticles and titanium dioxide.^{20, 21}

In this chapter gold nanoparticles are synthesized in order to mix them with the titania precursor, to obtain homogeneous dispersed gold nanoparticles incorporated in the titania matrix. Because the gold nanoparticles are synthesized first and not simultaneously with the composite material, this method is referred to as the ex-situ synthesis of gold/titania composite materials.

The approach of first synthesizing the gold nanoparticles has the advantage that the properties (e.g. particle size, shape and distribution) of the particles can be controlled. However, the particles also have to fulfil some requirements to be able to produce the desirable composite materials:

- The particles have to be dispersible in the titania precursor to obtain a homogeneous distribution of gold particles in the mesoporous titania matrix. The titania precursor consists of ethanol, hydrochloric acid, titanium isopropoxide and water. This is a polar mixture, therefore the gold particles should also be stable in polar (water or ethanol) media.
- Small gold particles are preferred, as a larger number of particles are obtained for the same gold loading, leading to more electron sink centres for the same cost. Therefore, particles of maximum 5 nm in diameter are aimed for.

The most straightforward way to fulfil the first requirement is to synthesize the particles in aqueous media, because this will produce particles that are dispersible in water. This is desirable as water is a part of the titania precursor described in the previous chapter. However, most literature syntheses are performed in apolar solvent furthermore, the properties of the gold nanoparticles are much better controlled in apolar media, therefore this will be discussed in the second part of this chapter. Both types of particles will be incorporated in the titania precursor to determine if we are able to form the desirable composite material. A large number

of synthesis routes for gold nanoparticles have already been described, therefore we started from these methods.

3.2 Experimental section

Materials. Titanium(IV) isopropoxide ($\text{Ti}(\text{O}^i\text{Pr})_4$, $\geq 97\%$), sodium hydroxide (NaOH, reagent grade, $\geq 98\%$), gold(III) chloride trihydrate ($\text{HAuCl}_4 \cdot 3\text{H}_2\text{O}$, ACS reagent, $\geq 49\%$ Au basis), sodium borohydride ($\text{NaBH}_4 \geq 98\%$), tetraoctylammonium bromide ($\geq 98\%$), sodium citrate dihydrate ($\text{Na}_3\text{C}_6\text{H}_5\text{O}_7 \cdot 2\text{H}_2\text{O}$), mercaptopropionic acid ($\text{C}_3\text{H}_6\text{O}_2\text{S}$, $\geq 99\%$) and dodecanthiol (98%) are purchased from Sigma-Aldrich. Hydrochloric acid (HCl, 36%) is acquired from Fiers, N-cetyl-N,N-trimethylammonium bromide (CTAB, pro analysis) from Merck and ethanol (EtOH, absolute PA) from Panreac. All chemicals are used as received.

3.2.1 Synthesis of gold nanoparticles

Turkevich-Frens gold nanoparticle method. The synthesis is conducted as described by Frens.²² Gold chloride (0.05 g) and sodium citrate (0.01 g) are separately dissolved in respectively 50 mL and 1 mL distilled water. The gold chloride solution is heated to its boiling point, where after the sodium citrate solution is added under vigorously stirring. The reaction is complete after 5 minutes. In the case of the modified citrate route, the pH of the gold chloride solution is increased to 6 with a 20 mM aqueous NaOH solution. The solution is heated to 85 °C instead of its boiling point. The reaction is quenched 200 s after the sodium citrate solution is added, by pouring it in 200 mL ice water.

Carboxylate capped gold particles. The synthesis is based on a recipe described by Chen *et al.*²³ Gold chloride (0.197 g) was dissolved in 390 mL water and added to a 100 mL methanol solution containing 0.130 g mercaptopropionic acid. The gold salt is reduced by adding 25 mL 0.2 M sodium borohydride in water under vigorously stirring. After one hour, the gold particles were separated by centrifugation and washed two times with a 20% (v/v) water/methanol and two times with pure methanol.

Gold nanorods. The synthesis of gold nanorods starts from a seed solution. The preparation of the seed solution is as followed: an aqueous gold chloride solution (0.25 mL, 0.01 M) is added to an aqueous CTAB solution (9.75 mL, 0.1 M). Under vigorous stirring, a sodium borohydride solution (0.6 mL, 0.01 M) is added and stirred for 2 minutes. To synthesize the nanorods, an aqueous silver nitrate solution (0.075 mL, 0.01 M) and gold chloride solution (0.5 mL, 0.01 M) are added to a CTAB solution (9.5 mL, 0.1 M), forming a yellow-orange coloured solution. Ascorbic acid (0.055 mL, 0.1 M) is added, turning it into a colorless solution. The seed solution (12 μL) is added to start the formation of the nanorods and the reac-

tion is finished after 24 hours.

Brust synthesis. The recipe was described first by Brust.²⁴ An aqueous solution of gold chloride (30 mL, 0.03 M) was added to a solution of tetraoctylammonium bromide in toluene (80 mL, 0.05 M). The two-phase system was stirred vigorously until all gold was transferred to the toluene phase, where after dodecanethiol (0.17 g) was added. To form the nanoparticles, an aqueous solution of sodium borohydride (25 mL, 0.4 M) was added slowly, while vigorously stirring. After 3 hours, the organic phase was separated and the gold nanoparticles were precipitated and washed with ethanol.

Phosphine stabilized gold nanoparticles. This synthesis is based on the method of Brust, but instead of thiol ligands, phosphine ligands are used. The recipe we followed was described by Weare *et al.*²⁵ Gold chloride (0.1 g) and tetraoctylammonium bromide (0.16 g) were added to distilled water (5 mL) and toluene (6.5 mL). After all gold atoms are transferred to the organic phase, triphenylphosphine (0.232 g) was added, forming a white, cloudy emulsion. An aqueous sodium borohydride solution (1 mL, 3.7 M) was added and the resulting mixture was vigorously stirred overnight. The toluene phase was separated from the aqueous phase and the toluene was removed at the rotavapor. The resulting powder was washed with hexane. The particles could be dispersed in dichloromethane.

3.2.2 Synthesis of Au/TiO₂ materials

The standard synthesis of mesoporous titania using the EISA method is described in chapter 2. In short: an ethanolic solution containing CTAB is mixed with a solution of EtOH, Ti(O^{*i*}Pr)₄ and HCl. Distilled water is added to form the final titania precursor. The precursor transferred to a Petri Dish and placed in an oven at 75 °C for 3 days. The obtained solid is subjected to a base treatment consisting of 48 hours refluxing in NaOH solution. The final step is the calcination which proceeds for 2 hours at 450 °C (Figure 3.2 A).

In the case of the gold/titania composite materials, the distilled water or part of the ethanol was replaced by a dispersion containing gold nanoparticles. The pure, distilled water was replaced by an aqueous dispersion of gold nanoparticles when the nanoparticles were synthesized according to the Turkevich-Frens method or the carboxylate method (Figure 3.2 B). In the case of the phosphine stabilized gold nanoparticles, the ethanol used to dissolve the CTAB was replaced by the same amount of ethanolic dispersion of nanoparticles (Figure 3.2 C) as the phosphine capped particles were only dispersible in ethanol.

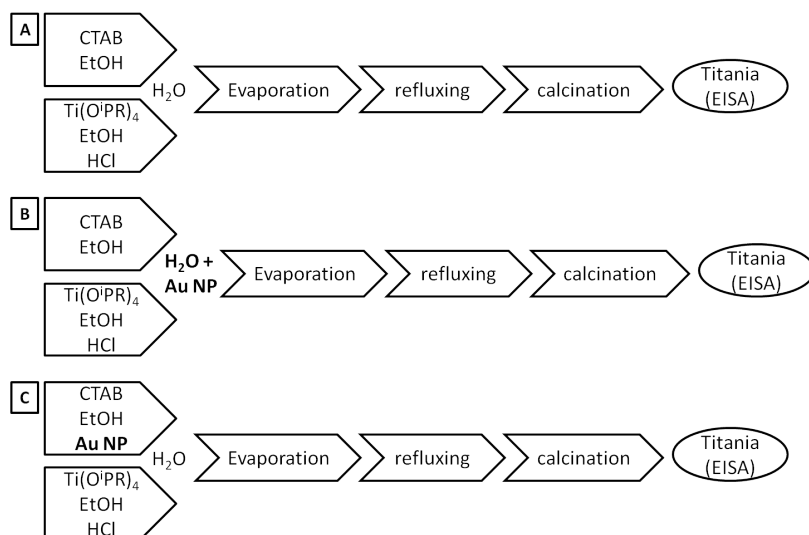


Figure 3.2: The different schemes to prepare A) pure mesoporous titania and B) and C) gold functionalized mesoporous titania.

3.2.3 Characterization

Nitrogen sorption experiments were carried out on a TriStar 3000 (Micromeritics) at $-196\text{ }^{\circ}\text{C}$. The specific surface areas were calculated using the Brunauer-Emmett-Teller (BET) method.²⁶ Samples for high angular annular dark field scanning transmission electron microscopy (HAADF STEM) were prepared by dispersing the powder in deionized water and dipping the copper support TEM grid (200 mesh) in the dispersion. The HAADF STEM samples were air-dried and measured using a JEOL JEM-2200FS transmission electron microscope with post-sample Cs corrector and an accelerating voltage of 200 kV.

3.3 Aqueous synthesis of gold nanoparticles

First, aqueous synthesis methods that produce particles dispersible in water were explored, starting with the most known aqueous synthesis, namely citrate route of Turkevich-Frens. This is one of the oldest synthesis methods for gold nanoparticles and is very simple and straightforward.^{22, 27} In addition, we also explored the synthesis of Chen,²³ Li²⁸ and Gou.²⁹

3.3.1 Turkevich-Frens Method

The most commonly used aqueous synthesis of gold nanoparticles was invented in 1951 by John Turkevich and uses sodium citrate both as stabilizing and reducing agent.²⁷ An aqueous solution of HAuCl_4 is heated to its boiling point, whereupon an aqueous solution of sodium citrate is added to reduce the gold salt. The reaction is complete after 5 minutes. In 1973 Frens improved the synthesis method by changing the gold/citrate ratio to be able to obtain a wide range of gold particle sizes (16 - 150 nm).²²

The smallest nanoparticles (16 nm diameter) are obtained when using the smallest gold/citrate ratio. Because more ligands are present per gold atom, they are able to stabilize more particles, resulting in smaller particle sizes. As we need the gold particle to be as small as possible, we used a 5/10 $\text{HAuCl}_4/\text{Na}_3\text{C}_6\text{H}_5\text{O}_7$ ratio. Stable, red dispersions were obtained, but the particles were polydisperse with a particles size of 15 - 35 nm and agglomerated (Figure 3.3). The particles are somewhat larger than described in the article and more agglomerated, therefore they were not suitable to be incorporated in a titania matrix.

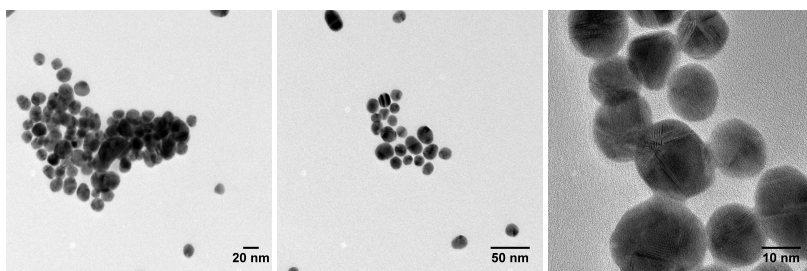


Figure 3.3: TEM images of gold nanoparticles synthesized according to the Turkevich-Frens method.

To obtain somewhat smaller (10 - 20 nm) and more monodisperse nanoparticles, Li *et al* proposed a pH and temperature controlled synthesis based on the Turkevich-Frens method.²⁸ By lowering the temperature to 70 °C or 85 °C and increasing the pH with NaOH to 6 - 7.5, uniform gold particles can be obtained. Especially, the pH increase is crucial to obtain monodisperse nanoparticles, but lowering the temperature helps to reduce the cost of the synthesis.

We reproduced the modified citrate route described by Li at a pH of 6 and a lowered the reaction temperature of 85 °C, but coalesced particles were obtained (Figure 3.4).

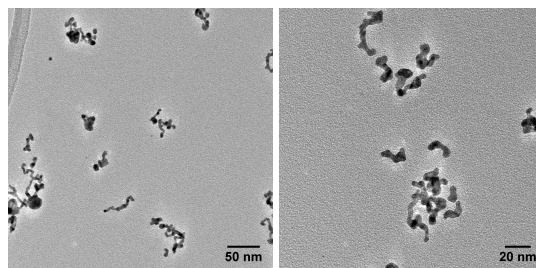


Figure 3.4: TEM images of gold nanoparticles produced using the modified citrate route.

3.3.2 Carboxylate capped gold particles

A synthesis that results in smaller particles (1 - 4 nm) is described by Chen.²³ The synthesis itself is conducted in methanol, but the carboxylate capped particles are dispersible in water. An aqueous solution of HAuCl_4 was added to a solution of the ligand in methanol. In the article, mercaptosuccinic acid is used as ligand, but we used mercaptopropionic acid ($\text{C}_3\text{H}_6\text{O}_2\text{S}$) instead. An aqueous solution of NaBH_4 was added slowly while vigorously stirring to reduce the gold salt.

TEM image of the produced gold particles showed both large gold structures ($0.5 \mu\text{m}$) and small nanoparticles (1.5 - 4 nm) (Figure 3.5). The small gold nanoparticles synthesized using this method are indeed smaller than the ones produced using the Turkevich-Frens method, but because of the presence of the larger structures, these particles are also not very suitable to be incorporated in the titania matrix.

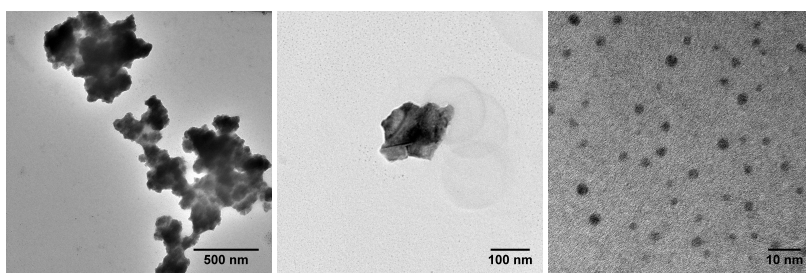


Figure 3.5: TEM images of carboxylate capped gold nanoparticles.

3.3.3 Gold nanorods

Cetyltrimethylammonium bromide (CTAB) is used as pore forming agent in the synthesis of mesoporous titania. Therefore gold nanoparticles that are capped with CTAB should be stable in the titania precursor. The synthesis of gold nanorods de-

scribed by Gou et al, uses CTAB as ligand and silver ions to control the aspect ratio of the gold rods.^{29, 30} The minimal amount of silver (< 10%) present in the gold rods, should have no influence on the ability of the gold particles to act as electron sink. The addition of AgNO₃ is necessary to form uniform nanorods. The exact mechanism is not yet know, but there are different theories.³¹ The first theory suggests that the silver ions modify the CTAB micelle formation, making them more rodlike. The second theory is the preferential underpotential deposition of silver onto the {110} facet,^{32, 33} resulting in the growth of rods along the other crystal facets. The last theory is the preferential adsorption of a CTAB-AgBr complex on the {520} facets, assisting in the reduction of Au ion at these facets, resulting in rodshaped particles.³⁴

To synthesize the nanorods, first a seed solution has to be made. For this seed solution an aqueous solution of HAuCl₄ containing CTAB is reduced using NaBH₄, which results in gold 'seeds' of 1.5 nm. We tried to purify the gold seeds to use them as nanoparticles for the incorporation into the titania matrix, but it was not possible to precipitate and purify the gold seeds themselves.

To obtain the gold nanorods, the seed solution is added to a mixture of CTAB, AgNO₃, HAuCl₄ and ascorbic acid as reducing agent. After 24 hours the nanorods were fully formed.

We were able to form the gold nanorods, as two adsorption peaks could be observed using UV-Vis spectroscopy (Figure 3.6). But we were not able to purify the sample as only part of the gold rods and a lot of the ligand precipitated.

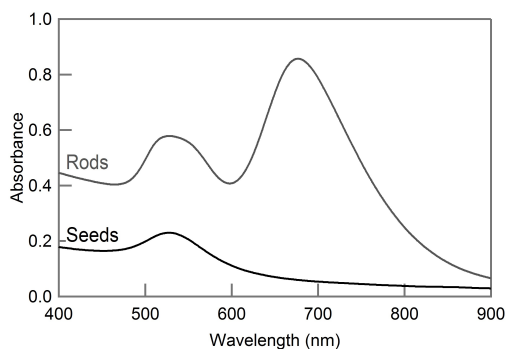


Figure 3.6: UV-Vis spectra of the gold seeds and gold rods.

3.3.4 Incorporation in mesoporous titania matrix

The gold nanoparticles that were obtained using aqueous synthesis methods did not meet the requirements that were proposed as the particles were a bit too large

or agglomerated. However, to investigate if it could be possible to incorporate gold nanoparticles by mixing them with the titania precursor, we did some tests with the carboxylate capped gold nanoparticles and the nanoparticles produced using the Turkevich-Frens method, as these methods resulted in the most stable gold dispersions.

During a standard mesoporous titania synthesis, water is added as part of the precursor solution. In the case of the gold/titania composite materials, the pure water was replaced by an aqueous solution of gold nanoparticles. When the carboxylate capped gold nanoparticles were added to the precursor solution, the powder obtained after the oven treatment at 75 °C, was inhomogeneous, as little "islands" of gold particles were found in a yellow titania matrix. Therefore these particles are not applicable to form good gold/titania composite materials.

If the Turkevich-Frens particles are added to the precursor solution, it was possible to obtain a homogeneous powder during the complete synthesis. However, the obtained powder exhibits a specific surface area of only 78 m²/g. This is much lower compared to the more than 300 m²/g of the unfunctionalized mesoporous titania powder. Due to the low surface area, the catalytic activity is not investigated.

3.4 Non-Aqueous synthesis of gold nanoparticles

More literature on small (< 5 nm) nanoparticles is available in the case of non-aqueous syntheses. The obtained particles are however not dispersible in polar media. Nevertheless, a ligand exchange step, during which the apolar ligands are replaced by polar ligands, can be conducted to make the nanoparticles dispersible in polar media. Therefore non-aqueous syntheses, look promising for obtaining the desired gold nanoparticles. The most well known synthesis of small gold nanoparticles (1 - 3 nm) in toluene was invented in 1994 by Brust *et al.*²⁴ and will be researched first.

3.4.1 Brust synthesis

The Brust synthesis makes use of a two-phases system. The aqueous phase contains the gold salt, while tetraoctylammonium bromide is dissolved in the toluene phase and acts as a phase transfer reagent. When these phases are stirred vigorously, the gold salt will be transferred to the organic phase. A ligand (dodecanethiol) is added and the gold ions are reduced using sodium borohydride. The organic phase is separated from the aqueous phase and purified to obtain the 1 - 3 nm gold nanoparticles.

TEM images of the resulting gold nanoparticles show that they are indeed smaller than the ones obtained from the aqueous syntheses, but more important, they are also not agglomerated (Figure 3.7). Therefore, they are very suitable for

the incorporation in the titania matrix, although they are not yet dispersible in polar media. So, a ligand exchange procedure has to be performed.

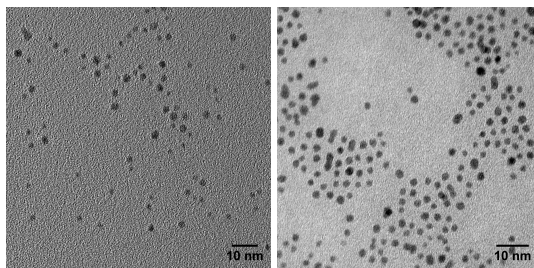


Figure 3.7: TEM images of the gold nanoparticles in toluene synthesized according to the two-phases method of Brust.

Different ligands like mercaptopropionic acid, ammonium sulfide and sodium sulfide in polar solvents like water, ethanol and formamide have been tested in ligand exchange experiments,³⁵ but none of them was successful to obtain stable suspensions in polar media. Stirring for 8 hours did not give rise to any visible change. When the dispersions were stirred longer (overnight or over the weekend) all color disappeared, a result of the dissolution of the gold nanoparticles. The gold nanoparticles synthesized according to the Brust method could therefore not be added to the titania precursor to form gold/titania composite materials.

3.4.2 Phosphine stabilized gold nanoparticles

The dodecanethiol ligands used in the Brust method are too tightly bound to the gold nanoparticles to be exchanged for other ligands. The conditions to be able to do this are too harsh, causing the particles to dissolve before the ligands can be exchanged. A possibility to overcome this problem is to start from gold particles capped with ligands that have smaller interactions with the gold atoms and exchange these with ligands that have stronger interactions with the gold atoms. According to the Pearson acid-base theory sulfur binds very strongly with gold, where phosphorus has a somewhat smaller binding affinity to gold. Weare *et al.* proposed a synthesis very similar to the method of Brust, but using triphenylphosphine as ligand instead of dodecanethiol.²⁵ The particle size of these phosphine capped gold nanoparticles is the same as the particle size of the dodecanethiol capped particles, namely 1 - 3 nm (Figure 3.8 left).

Woehrle *et al.* described different procedures for ligand exchange reaction with a wide range of sulfur containing ligands.³⁶ We performed a ligand exchange of the phosphine ligands with mercaptopropionic acid, as the latter is solvable in both water and ethanol and therefore the titania precursor. The triphenylphosphine capped gold nanoparticles are dispersed in dichloromethane. A phosphate buffer

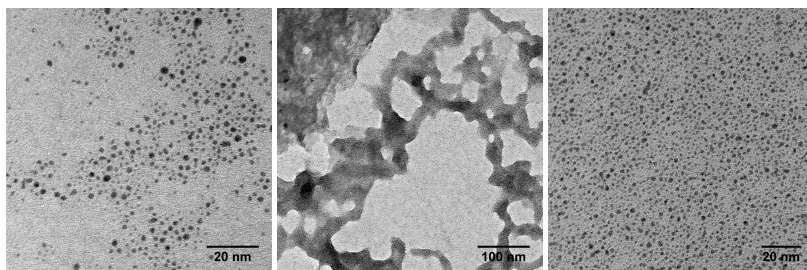


Figure 3.8: TEM images of gold nanoparticles synthesized according to the Weare method before (left figure) and after ligand exchange (middle and right figure).

(pH 8) is added to this dispersion together with mercaptopropionic acid and stirred vigorously for 2.5 hours. The dichloromethane phase became colourless, but the particles are situated between the organic and aqueous phases. However, after removing both the organic and the aqueous phases, they could be dispersed in ethanol. Purification was difficult as the gold nanoparticles could not be selectively precipitated. TEM images show that the sample is indeed not pure (3.8 middle image), but the particles have not grown and are not agglomerated (Figure 3.8 right image).

3.4.3 Incorporation in mesoporous titania matrix

The gold nanoparticles synthesized according to Weare *et al.* are small and dispersible in ethanol. So, even though the nanoparticle dispersion was not completely pure, they are still suitable to be incorporated into the titania matrix. The organic impurities present will be removed during the calcination step of the composite material.

An ethanolic dispersion of the gold nanoparticles was used to dissolve CTAB, instead of the pure ethanol in the standard mesoporous titania synthesis. The other steps were the same as in the standard procedure. A homogeneous dispersion was obtained, the resulting composite material however was yellow - white. This color is the same as the unfunctionalized material indicating no gold particles are present as the powder is blue-purple when gold nanoparticles are present. This implies the gold particles have dissolved during the synthesis, probably due to the harsh HCl conditions.

3.5 Adsorption of gold nanoparticle on the titania matrix

Another route to obtain Au/TiO₂ composite materials starting from previously formed gold nanoparticles is the adsorption of gold nanoparticles onto a preformed titania matrix. Zheng *et al.* described a general method to adsorb gold nanoparticles onto different metaloxide supports (Fe₂O₃, TiO₂, Al₂O₃, ZnO, SiO₂).¹⁶ The titania support was synthesized according to the standard procedure described in chapter 2, while the gold nanoparticles were produced following the Brust method. After purification, the gold nanoparticles were dispersed in dichloromethane with a concentration of approximately 1 μg/mL. Mesoporous titania powder (0.5 g) was added to 5 mL of the gold nanoparticle dispersion and stirred for 3 hours. After 3 hours, the dichloromethane was still brown, indicating that not all gold nanoparticles are adsorbed onto the titania support. The dispersion was stirred further overnight, but the dichloromethane phase did not become completely colorless. Nonetheless, the dispersion was filtrated and the powder was dried at 100 °C and calcined at 300 °C for 1 hour to remove the ligands. The powder was analysed using TEM. This showed that the gold nanoparticles have grown much, resulting in gold particles of 50-100 nm (Figure 3.9).

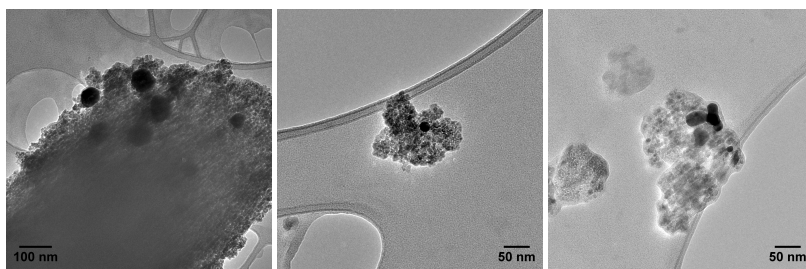


Figure 3.9: TEM images of the gold composite materials formed by adsorbing Brust gold nanoparticles onto a mesoporous titania matrix.

The powder was tested for leaching, but 48 hours of stirring in water, did not lead to leaching of the gold particles. However, this procedure is also not very ideal because of the growth of the gold particles and incomplete adsorption of the gold nanoparticles onto the titania support, making it very hard to produce a Au/TiO₂ composite material with a defined gold loading.

3.6 Conclusions

In this chapter, we wanted to synthesize gold nanoparticles that were dispersible in the titania precursor to form homogeneous gold/titania composite materials. A

first approach was the synthesis of gold nanoparticles dispersible in aqueous media. Different synthesis methods were tested, but none of them resulted in small, non agglomerated particles that were homogeneously dispersible in the titania precursor. A second approach was the synthesis of gold nanoparticles in apolar media and exchange the ligands for ligands that can stabilize the particles in a polar phase. One of the most used synthesis method is the one of Brust, which results in thiol capped gold particles. These thiol ligands however have a too strong interaction with the gold particles to be able to be exchanged for other ligands. Therefore the Brust synthesis was adapted for the use of phosphines as ligands, which are exchangeable with thiol ligands to obtain particles that are dispersible in ethanol. Unfortunately it was not possible to obtain a gold/titania composite using these particles as they dissolve during the synthesis of mesoporous titania, probably due to the harsh acid conditions.

As it was not possible to synthesize appropriate Au/TiO₂ materials, other methods have to be found to obtain these materials. The next chapter describes the synthesis of gold/titania composites using an in-situ approach.

References

- [1] Ismail, A. A. & Bahnemann, D. W. Mesoporous titania photocatalysts: preparation, characterization and reaction mechanisms. *Journal of Materials Chemistry* **21**, 11686–11707 (2011).
- [2] Carneiro, J. T., Savenije, T. J. & Mul, G. Experimental evidence for electron localization on Au upon photo-activation of Au/anatase catalysts. *Phys. Chem. Chem. Phys.* **11**, 2708–2714 (2009).
- [3] Mizukoshi, Y. *et al.* Immobilization of noble metal nanoparticles on the surface of TiO₂ by the sonochemical method: Photocatalytic production of hydrogen from an aqueous solution of ethanol. *Ultrason. Sonochem.* **14**, 387–392 (2007).
- [4] Iliev, V., Tomova, D., Bilyarska, L. & Tyuliev, G. Influence of the size of gold nanoparticles deposited on TiO₂ upon the photocatalytic destruction of oxalic acid. *Journal of Molecular Catalysis a-Chemical* **263**, 32–38 (2007).
- [5] Mehta, A., Sharma, M., Kumar, A. & Basu, S. Effect of au content on the enhanced photocatalytic efficiency of mesoporous au/tio₂ nanocomposites in uv and sunlight. *Gold Bulletin* **50**, 33–41 (2017).
- [6] Ghosh, S. K. & Pal, T. Interparticle coupling effect on the surface plasmon resonance of gold nanoparticles: From theory to applications. *Chem. Rev.* **107**, 4797–4862 (2007).
- [7] Huang, X. & El-Sayed, M. A. Gold nanoparticles: Optical properties and implementations in cancer diagnosis and photothermal therapy. *J. Adv. Res.* **1**, 13 – 28 (2010).
- [8] Liu, L., Ouyang, S. & Ye, J. Gold-nanorod-photosensitized titanium dioxide with wide-range visible-light harvesting based on localized surface plasmon resonance. *Angewandte Chemie* **125**, 6821–6825 (2013).
- [9] Juve, V. *et al.* Size-Dependent Surface Plasmon Resonance Broadening in Nonspherical Nanoparticles: Single Gold Nanorods. *nano Letters* **13**, 2234–2240 (2013).

- [10] Kowalska, E., Abe, R. & Ohtani, B. Visible light-induced photocatalytic reaction of gold-modified titanium(iv) oxide particles: action spectrum analysis. *Chem. Commun.* 241–243 (2009).
- [11] Wang, X. D., Waterhouse, G. I. N., Mitchell, D. R. G., Prince, K. & Caruso, R. A. Noble metal-modified porous titania networks and their application as photocatalysts. *ChemCatChem* **3**, 1763–1771 (2011).
- [12] Wang, X. D. & Caruso, R. A. Enhancing photocatalytic activity of titania materials by using porous structures and the addition of gold nanoparticles. *J. Mater. Chem.* **21**, 20–28 (2011).
- [13] Li, J. & Zeng, H. C. Preparation of monodisperse Au/TiO₂ nanocatalysts via self-assembly. *Chem. Mater.* **18**, 4270–4277 (2006).
- [14] Subramanian, V., Wolf, E. E. & Kamat, P. V. Catalysis with TiO₂/gold nanocomposites. effect of metal particle size on the fermi level equilibration. *J. Am. Chem. Soc.* **126**, 4943–4950 (2004).
- [15] zlem Hamalolu, K., Sa, E. & Tuncel, A. Bare, gold and silver nanoparticle decorated, monodisperse-porous titania microbeads for photocatalytic dye degradation in a newly constructed microfluidic, photocatalytic packed-bed reactor. *Journal of Photochemistry and Photobiology A: Chemistry* **332**, 60 – 65 (2017).
- [16] Zheng, N. & Stucky, G. D. A general synthetic strategy for oxide-supported metal nanoparticle catalysts. *J. Am. Chem. Soc.* **128**, 14278–14280 (2006).
- [17] Claus, P., Bruckner, A., Mohr, C. & Hofmeister, H. Supported gold nanoparticles from quantum dot to mesoscopic size scale: Effect of electronic and structural properties on catalytic hydrogenation of conjugated functional groups. *J. Am. Chem. Soc.* **122**, 11430–11439 (2000).
- [18] Pradhan, S., Ghosh, D. & Chen, S. W. Janus nanostructures based on Au-TiO₂ heterodimers and their photocatalytic activity in the oxidation of methanol. *Acs Appl. Mater. Interfaces* **1**, 2060–2065 (2009).
- [19] Zhao, J. *et al.* Direct coating of mesoporous titania on CTAB-capped gold nanorods. *Nanoscale* **8**, 5417–5421 (2016).
- [20] Xie, Y. *et al.* In situ controllable loading of ultrafine noble metal particles on titania. *J. Am. Chem. Soc.* **131**, 6648–6649 (2009).
- [21] Wang, P. *et al.* Synthesis and plasmon-induced charge-transfer properties of monodisperse gold-doped titania microspheres. *Chem.-Eur. J.* **15**, 4366–4372 (2009).

- [22] Frens, G. Controlled nucleation for the regulation of the particle size in monodisperse gold suspensions. *Nature* **241**, 20–22 (1973).
- [23] Chen, S. H. & Kimura, K. Synthesis and characterization of carboxylate-modified gold nanoparticle powders dispersible in water. *Langmuir* **15**, 1075–1082 (1999).
- [24] Brust, M., Walker, M., Bethell, D., Schiffrin, D. J. & Whyman, R. Synthesis of thiol-derivatised gold nanoparticles in a two-phase liquid-liquid system. *Journal of the Chemical Society Chemical Communications* 801–802 (1994).
- [25] Weare, W. W., Reed, S. M., Warner, M. G. & Hutchison, J. E. Improved synthesis of small (d(core) approximate to 1.5 nm) phosphine-stabilized gold nanoparticles. *Journal of the American Chemical Society* **122**, 12890–12891 (2000).
- [26] Brunauer, S., Emmett, P. H. & Teller, E. Adsorption of gases in multimolecular layers. *J. Am. Chem. Soc.* **60**, 309–319 (1938).
- [27] Turkevich, J., Stevenson, P. C. & Hillier, J. A study of the nucleation and growth processes in the synthesis of colloidal gold. *Discuss. Faraday Soc.* **11**, 55–75 (1951).
- [28] Li, C., Li, D., Wan, G., Xu, J. & Hou, W. Facile synthesis of concentrated gold nanoparticles with low size-distribution in water: temperature and pH controls. *Nanoscale Research Letters* **6** (2011).
- [29] Gou, L. F. & Murphy, C. J. Fine-tuning the shape of gold nanorods. *Chemistry of Materials* **17**, 3668–3672 (2005).
- [30] Smith, D. K. & Korgel, B. A. The importance of the ctab surfactant on the colloidal seed-mediated synthesis of gold nanorods. *Langmuir* **24**, 644–649 (2008).
- [31] Jackson, S. R., McBride, J. R., Rosenthal, S. J. & Wright, D. W. Where's the Silver? Imaging Trace Silver Coverage on the Surface of Gold Nanorods. *J. Am. Chem. Soc.* **136**, 5261–5263 (2014).
- [32] Liu, M. & Guyot-Sionnest, P. Mechanism of silver(I)-assisted growth of gold nanorods and bipyramids. *Journal of physical chemistry B* **109**, 22192–22200 (2005).
- [33] Scarabelli, L., Sanchez-Iglesias, A., Perez-Juste, J. & Liz-Marzan, L. M. A “Tips and Tricks” Practical Guide to the Synthesis of Gold Nanorods. *J. Phys. Chem. Lett.* **6**, 4270–4279 (2015).

- [34] Almora-Barrios, N., Novell-Leruth, G., Whiting, P., Liz-Marzan, L. M. & Lopez, N. Theoretical Description of the Role of Halides, Silver, and Surfactants on the Structure of Gold Nanorods. *nano Lett.* **14**, 871–875 (2014).
- [35] Nag, A. *et al.* Metal-free inorganic ligands for colloidal nanocrystals: S^{2-} , HS^- , Se^{2-} , HSe^- , Te^{2-} , HTe^- , TeS_3^{2-} , OH^- , and NH_2^- as surface ligands. *Journal of the American Chemical Society* **133**, 10612–10620 (2011).
- [36] Woehrle, G. H., Brown, L. O. & Hutchison, J. E. Thiol-functionalized, 1.5-nm gold nanoparticles through ligand exchange reactions: Scope and mechanism of ligand exchange. *Journal of the American Chemical Society* **127**, 2172–2183 (2005).

4

Gold/titania composites: Synthesis and Characterisation

This chapter describes the synthesis of gold/titania materials synthesized by the impregnation and reduction of a gold salt on a titania matrix. The oxidation state of the gold atoms after reduction are studied using XANES. Neutral or positively charged gold particles are obtained depending on the used reduction method. Their photocatalytic activity is evaluated by following the degradation of phenol under UV illumination

Adapted from:

Meire, M.; Tack, P.; De Keukeleere, K.; Balcaen, L.; Pollefeyt, G.; Vanhaecke, F.; Vincze, L.; Van Der Voort, P.; Van Driessche, I.; Lommens, P., Gold/titania composites: An X-ray absorption spectroscopy study on the influence of the reduction method. Spectrochim. Acta B 2015, 110 (0), 45-50.

4.1 Introduction

In Chapter 3, the gold nanoparticles were synthesized separately before they were mixed with the titania precursor to produce gold/titania composite materials. Unfortunately it was not possible to obtain good composites through this route, as most gold nanoparticles were not dispersible in the titania precursor, or they formed heterogeneous composites.

In this chapter, the development of Au/TiO₂ materials using another method is discussed. A mesoporous titania powder is impregnated with an aqueous solution of HAuCl₄. In a subsequent step, the salt is reduced using different reduction methods: chemical (citrate, NaBH₄,...),^{1,2} thermal (H₂ atmosphere)^{3,4} or by UV irradiation.^{5,6}

Several papers discuss the influence of the used synthesis method on the obtained materials and noticed large differences in terms of gold particle size, specific surface area of the titania matrix and (photo)catalytic activity depending on the production procedure.^{3,4,7-10} Yet, only few papers address the determination of the oxidation state of the gold atoms present in the composite material.^{11,12} Positively charged gold ions have other properties than metallic gold particles and this can increase or decrease the activity of these materials depending on the application. A positive charge on gold particles increases the activity in the case of CO conversion due to a better adsorption of CO,¹¹ but in the case of photocatalytic hydrogen production on a Pt/TiO₂ material, the ionized atoms have a smaller effect than the metallic atoms.¹³ Therefore, it is important to investigate the oxidation states present in a synthesized material. In most cases, X-ray photoelectron spectroscopy (XPS) is used to determine the oxidation state of the gold atoms. However, shifting of the binding energies due to support interactions, particle size/shape and geometric effects make correct analysis of the spectra complex, as it is very difficult to determine the exact cause of the observed shift.^{14,15}

To overcome these problems, we used X-ray absorption spectroscopy (XAS) as an alternative and improved method. XAS is an element-specific technique that allows for the determination of oxidation state as well as local chemical environment of the probed atoms by monitoring the amount of X-ray absorption as a function of excitation beam energy. Using XAS, the oxidation state can be determined based on the so-called absorption edge position, the energy above which the incident X-ray photons have sufficient energy to eject an electron from a given shell of the absorbing atom into an unbound state, characterized by a sharp increase in X-ray absorbance. As such, a shift in absorption edge position relates to a shift in oxidation state of the absorbing atom. Additionally, XAS also provides information on the absorbing atoms local structure and is able to resolve mixtures of differently coordinated species of the absorbing atom by means of linear combination analysis.¹⁶ X-ray absorption near edge structure (XANES) spectroscopy

is the part of XAS situated from approximately 20 eV below to 100 eV above the absorption edge. Information on the local structural environment of the gold atoms can help to better identify the gold species that are present and, in turn, to better understand the nature of their interaction with the titania matrix. This has already been demonstrated for the case of gold on ceria.¹⁷

Different composite materials were prepared following a synthesis approach that involves adsorption and reduction of HAuCl_4 on mesoporous titania, using different reduction methods. In this way we can investigate the effect of the reduction method (NaBH_4 , H_2 , UV irradiation and microwave irradiation) on material parameters such as particle size, oxidation state and interactions with the titania support. Their photocatalytic activity was evaluated for the degradation of phenol in aqueous solutions.

4.2 Experimental section

Materials. Titanium(IV) isopropoxide ($\text{Ti}(\text{O}^i\text{Pr})_4$, $\geq 97\%$), gold(III) chloride trihydrate ($\text{HAuCl}_4 \cdot 3\text{H}_2\text{O}$, ACS reagent, $\geq 49\%$ Au basis), sodium hydroxide (NaOH , reagent grade, $\geq 98\%$), sodium borohydride (NaBH_4 $\geq 98\%$) and phenol are purchased from Sigma-Aldrich. N-cetyl-N,N,N-trimethylammonium bromide (CTAB, pro analysis) is acquired from Merck, hydrochloric acid (HCl , 36%) from Fiers and ethanol (EtOH , absolute PA) from Panreac. All chemicals are used as received.

4.2.1 Synthesis

Mesoporous titania. Mesoporous titania was prepared using the synthesis method described in chapter 2, without the additional microwave treatments.

Au/TiO₂ powders. The as-synthesized titania (1.5 g) was dispersed in a yellow, aqueous solution of HAuCl_4 (0.015 g) and the pH was adjusted to 10 with NaOH . Additionally, water was added to obtain a total volume of 20 mL. The dispersion was stirred for 18 hours in the dark, to avoid reduction of the salt. The dispersion was filtered, resulting in a white powder and a colorless filtrate. The powder was dried in the dark under ambient conditions, and split into 5 equal portions. One part was kept as a reference while the other four portions were subjected to different reduction procedures: (1) illumination for 6 hours with a UV black light (Vilber, $136 \mu\text{W}/\text{cm}^2$, maximum intensity at 365 nm), every half hour, the powder is turned in order to illuminate other parts of the powder, (2) thermal reduction for 2 hours at 200 °C under 5% H_2/Ar atmosphere, (3) microwave (MW) irradiation for 1 hour at 120 °C, dispersed in 4 mL aqueous solution of NaOH (pH =10). The powder was washed with water and dried at room temperature in the dark and finally (4) 0.2 mL of 0.1 M NaBH_4 was added to a dispersion of Au/TiO_2 in 15 mL deionized

water and stirred for 3 hours. Afterwards, the powder was washed with deionized water and dried at room temperature in the dark. All samples were stored in the dark at 25°C and the characterizations performed within a week after synthesis.

4.2.2 Characterization

Nitrogen sorption experiments were carried out on a TriStar 3000 (Micromeritics) at -196 °C. The specific surface areas were calculated using the Brunauer-Emmett-Teller (BET) method.¹⁸ Samples for high angular annular dark field scanning transmission electron microscopy (HAADF STEM) were prepared by dispersing the powder in deionized water and dipping the copper support TEM grid (200 mesh) in the dispersion. The HAADF STEM samples were air-dried and measured using a JEOL JEM-2200FS transmission electron microscope with post-sample CS corrector and an accelerating voltage of 200 kV. The gold load of the samples was quantitatively determined using inductively coupled plasma mass spectrometry (ICP-MS, Perkin Elmer Elan DRC).

XANES spectroscopy experiments were performed at BM26A, the XAS station of the Dutch-Belgian beamline (DUBBLE) at the European Synchrotron Radiation Facility (ESRF) located in Grenoble, France.¹⁹ The beamline uses a 0.40 T bending magnet as a primary radiation source. The energy of the X-ray beam was tuned by a double-crystal Si(111) monochromator (energy resolution $\Delta E/E$ of $\sim 1.7 \times 10^{-4}$ at 9.659 keV) operating in a fixed-exit mode. The beam size at the sample position was approximately $3 \times 1 \text{ mm}^2$, limited by slit systems. Samples were fixed as powder between two 25 μm polyimide tapes (Goodfellow SARL). The X-ray absorption signal was monitored in emission mode using a Vortex-EM silicon drift detector. A XANES scan consisted of 139 energy steps, with an acquisition time of 1 s/step. High resolution XANES data were acquired at ID26 (ESRF, Grenoble, France) using a Si(311) monochromator (energy resolution $\Delta E/E$ of $\sim 0.3 \times 10^{-4}$). A wavelength dispersive spectrometer with an energy resolution better than the core-hole lifetime broadening (5.41 eV for the Au-L₃ edge)²⁰ was used to monitor the emitted radiation, resulting in significantly sharpened spectral features.²¹⁻²³ The spectrometer was tuned to 9.713 keV (Au-L _{α} fluorescence line) using the spherically bent Ge(600) wafer Bragg reflection. A beam size of $0.3 \times 1 \text{ mm}^2$ at the sample position was used. Samples were pressed to pellets (5 mg powder dispersed in cellulose). The X-ray beam could induce changes to the sample, e.g. reduce unreduced gold atoms, resulting in changing XAS spectra in function of X-ray irradiation time. A spectrum averaged over time, would therefore not represent the original sample. To avoid these beam induced changes, the sample was moved through the beam after each scan. By doing so, different scans of the 'pristine' sample could be taken, resulting in an improved signal to noise ratio, while measuring only a limited amount of beam induced changes. A XANES scan

consisted of 1003 energy steps, with an acquisition time of 30 s/scan. 60 scans were averaged to obtain better counting statistics. At both beamlines experiments were performed at room temperature (298 K). Raw XANES data were normalized for incident beam flux using the primary ionization chamber signal, pre-edge subtracted using a linear function and post-edge normalized at an energy of $E_0 + 50$ eV. Additionally, the slow variations caused by the atomic absorption profile before and after the edge were subtracted to facilitate linear combination analysis spectra comparisons.¹⁶ The obtained XANES profiles were compared to the transmission mode XANES profiles of a series of reference compounds (Au foil, AuCN, KAu(CN)₂ and HAuCl₄) by means of linear combination fitting, resulting in the semi-quantitative chemical speciation of the gold in the sample.^{24, 25}

4.2.2.1 Photocatalytic degradation

The photocatalytic activity of the powders is evaluated through the degradation of phenol under UV illumination. The experiments are carried out in a setup based on ISO 10678:2010(E) (Figure 4.1). A Vilber Lourmat VL-315BLB blacklight blue fluorescent light tube, 15 cm from the dispersion surface, is used with a maximum emission at 365 nm and emitting $136 \mu\text{W}/\text{cm}^2$. The starting concentration of the aqueous phenol solution was 30 mg/L. Titania (0.5 g/L) was added to 50 mL pollutant solution in a photocatalytic cell which is kept at a constant temperature of 25 °C. The suspension was stirred for 60 minutes in the dark to reach adsorption equilibrium. Every 30 minutes 2 mL dispersion was centrifuged for 5 minutes at 5000 rpm to separate the titania powder from the pollutant solution. The pollutant concentration was evaluated using HPLC with an UV detector. The degradation is normalized with respect to the starting concentration after reaching adsorption equilibrium. The degradation of phenol proceeds with a pseudo-first order kinetic. Rate constants are derived from the $\ln(C/C_0)$ versus time graph. Illumination of the phenol solution without the presence of a catalyst, also results in a small amount of degradation. This measurement is not added, as it is the same for all samples.

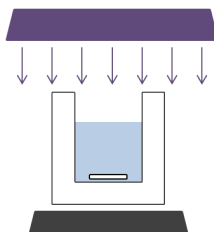


Figure 4.1: Schematic of aqueous photocatalytic test set-up.

4.3 Material properties

In-house synthesized mesoporous titania was impregnated with Au^{3+} ions by stirring the titania matrix in an aqueous HAuCl_4 solution overnight prior to the reduction of the salt. The pH of the $\text{TiO}_2/\text{HAuCl}_4$ dispersion was adjusted to 9-10 resulting in a negatively charged titania surface, facilitating the adsorption of the positively charged gold atoms.¹⁴ Neither the impregnation step nor any of the four different reduction methods (UV, MW, H_2 and NaBH_4) changed the specific surface area of the materials, which was approximately $100 \text{ m}^2/\text{g}$ for all samples (Table 4.1). It did also not alter the pore size distributions (A.6) or the nitrogen sorption isotherms (A.5), which are exactly the same for all samples. The samples exhibit an average pore size of 6.2 nm, which is well within the desired mesoporous range. Due to problems with the drying furnace and new flasks, the specific surface area of these samples are smaller than in the other chapters of this manuscript. The amount of gold deposited on the matrix was determined using ICP-MS to be approximately 0.3 wt% (nominal concentration 0.5 wt%) and did not differ much among the samples aside from the NaBH_4 reduced sample which has a smaller load of 0.23 wt% (Table 4.1). Reduction using NaBH_4 involves the re-dispersion of the powder in excess water after HAuCl_4 adsorption, leading to leaching of the gold salt and thus a lower Au load.

Table 4.1: Properties of the mesoporous titania host and the different Au/TiO_2 composite materials.

	TiO_2	$\text{TiO}_2 + \text{HAuCl}_4$	Au/TiO_2 (UV)	Au/TiO_2 (MW)	Au/TiO_2 (H_2)	Au/TiO_2 (NaBH_4)
S_{BET} (m^2/g)	96 ± 1	106 ± 1	105 ± 1	104 ± 1	102 ± 1	100 ± 1
Au wt% ^a	-	0.296 ± 0.010	0.303 ± 0.005	$0.30^b \pm 0.005$	0.301 ± 0.012	0.234 ± 0.002
Au particle diameter (nm) ^c	-	-	11.5 ± 6.2	10.5 ± 8.4	2.4 ± 0.8	4.7 ± 1.3
Visual appearance						

^a The standard deviation is calculated based on three separate ICP-MS analyses of the samples

^b There was only enough sample for one analysis, therefore it was not possible to calculate a standard deviation.

^c Determined from HAADF STEM images (Figure 4.2)

The diameter of the gold nanoparticles obtained on the titania host after full synthesis was determined using high angular annular dark field scanning transmission electron microscopy (HAADF STEM). HAADF STEM imaging is based on atomic number (Z) contrast, therefore the heavier gold atoms can be clearly distinguished from the titania matrix. The gold nanoparticles appear as white spots in the image shown in Figure 4.2. EDX analysis of these spots confirmed that

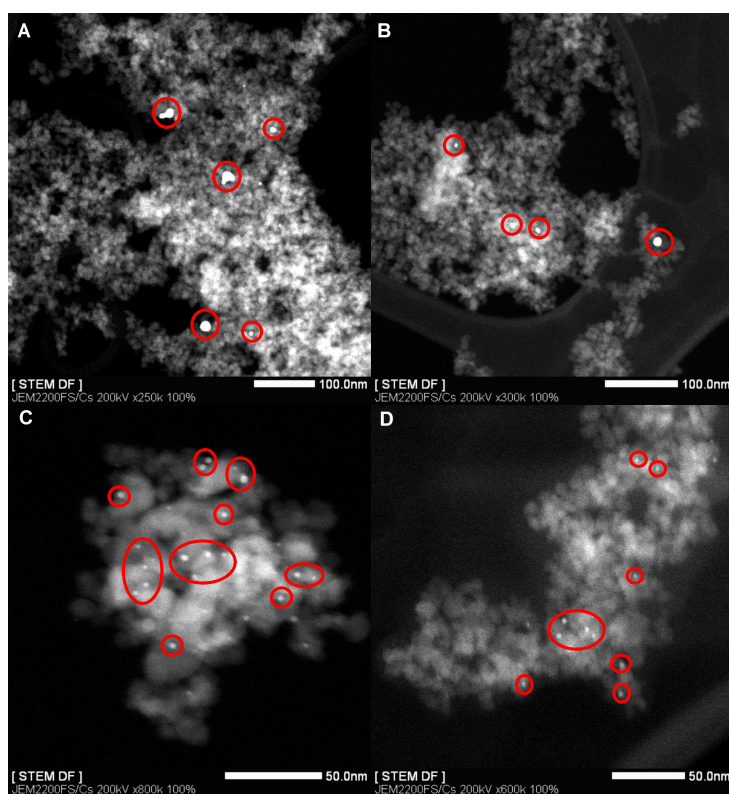


Figure 4.2: HAADF STEM images of the Au/TiO₂ composite materials using the A) UV, B) MW, C) H₂ and D) NaBH₄ reduction. Some of the gold nanoparticles are encircled.

these were indeed gold nanoparticles. At least 50 gold particles were measured for each sample in order to determine the mean particle size and the corresponding standard deviation (Figure 4.3). The mean diameters of the gold particles obtained after reduction using microwave and UV irradiation are more or less the same, respectively 10.5 nm and 11.5 nm. Both samples exhibit a broad size distribution, resulting in large standard deviations of 8.4 nm and 6.2 nm respectively. Reduction under H₂ atmosphere leads to much smaller Au particles and a more narrow size distribution with a mean diameter of 2.4 nm and standard deviation of 0.8

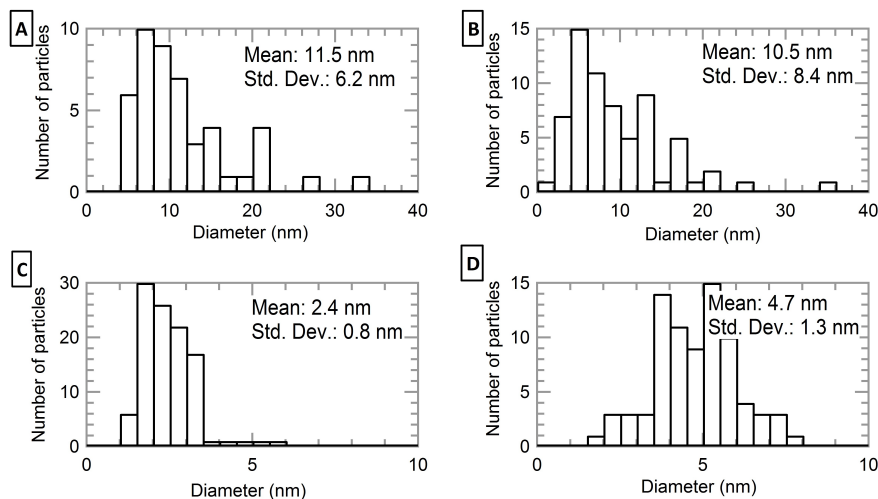


Figure 4.3: Particle size distribution of the gold nanoparticles obtained by A) UV, B) MW, C) H₂ and D) NaBH₄ reduction.

nm. The chemical reduction with NaBH₄ results in gold particles with a mean diameter of 4.7 nm and a standard deviation of 1.3 nm. Due to the smaller size of the gold nanoparticles obtained in the case of H₂ or NaBH₄ reduction compared to the UV and microwave reduction, the number of gold particles present on the titania matrix is much larger. As in the case of the NaBH₄ reduced sample a lower gold loading is achieved, the number of gold nanoparticles present on the sample is smaller compared to the H₂ reduced sample. The smaller particle sizes observed in case of H₂ or NaBH₄ reductions might be caused by the much faster kinetics of these processes, leading to more nucleation events and a higher number of smaller nanoparticles. The difference in particle size is also reflected in the different colors of the composite materials as gold particles with different sizes absorb different wavelengths due to plasmon resonance shifts. (Table 4.1)

4.4 Oxidation state

It has been shown in literature, using XPS, that not all synthesis methods for Au/TiO₂ materials lead to the complete reduction of the gold salt, subsequently influencing the catalytic activity of the material.¹¹ The reduction yield of each of the methods studied in this work was investigated using Au-L₃ XANES on the composite materials. The measured XANES spectra are displayed in Figure 4.4. The first peak (~11.918 keV) after the absorption edge, known as the white line, represents the 2p-5d electron transition, providing information on the density of

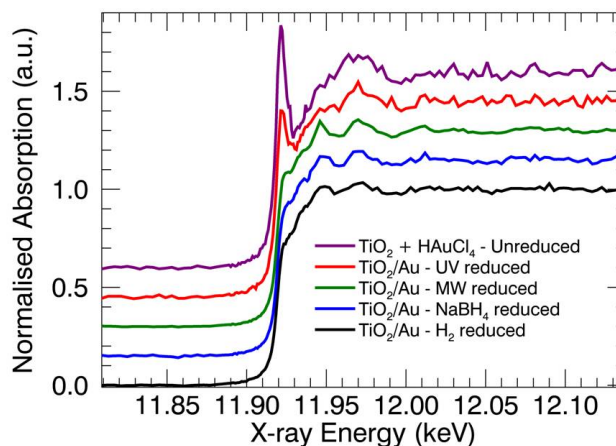


Figure 4.4: Au- L_3 XANES spectra of the different Au/TiO₂ materials.

the unoccupied 5d states near the Fermi level and is therefore closely related to the oxidation state of the gold atoms.^{17, 26} The decrease of the white line represents a smaller density of unoccupied 5d states and thus a reduction in oxidation state. For each sample, multiple fast scans as a function of energy were acquired to obtain better statistics and to allow detection of beam induced changes. In case of the unreduced and UV reduced samples, the white line was clearly present (Figure 4.4), yet decreased in intensity as a function of time (amount of scans) (Figures 4.5). For this reason only the first measured XANES scan of these samples was used as representative of the sample's initial state. The white line of the UV reduced sample was significantly smaller than the one of the unreduced sample, indicating that some reduction took place during the UV irradiation. In case of the other samples, no white line was present and the spectra did not change as a function of time.

Linear combination fitting was performed using an Au foil and the unreduced sample XANES spectra. The unreduced sample XANES was used as a reference for the sample initial state instead of the pure HAuCl₄ XANES, as the surrounding titania matrix has an influence on the XANES shape. The fitting results showed that in case of the thermal and chemical reduction, transformation from Au³⁺ to Au⁰ was complete, while MW reduction left 4% unreduced and UV irradiation only reduced half (52%) of the gold atoms.

Using high resolution XANES, the energy dependent post-edge features can be observed in more details showing more fluctuations and more pronounced amplitudes, allowing a better determination of the edge position and surroundings of the adsorbing atom. Consequently, a more detailed determination of the oxidation state can be performed.

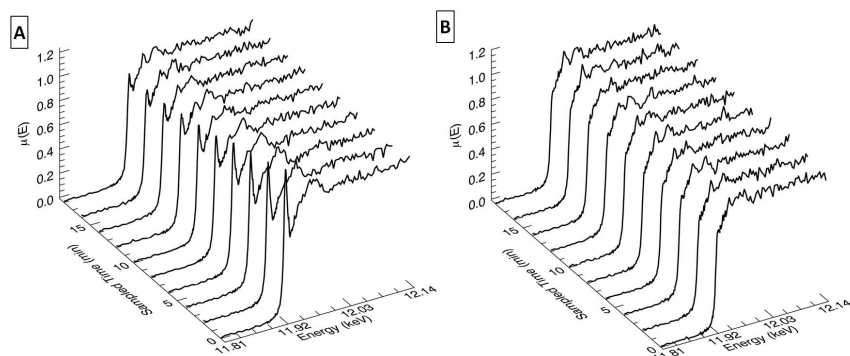


Figure 4.5: Au-L₃ XANES spectra of A) the unreduced sample and B) the microwave reduced sample as a function of irradiation time.

In contrast to the low resolution XANES experiments, no spectral changes were observed as a function of time during the high resolution XANES experiments as this was evaded by scanning over the sample. It was previously shown for gold on different oxide supports that a correlation exists between the size and shape of the Au-L₃ XANES post-edge features and the probed particle size.^{27, 28} Therefore, it was decided to perform high resolution XANES for the microwave and UV reduced Au/TiO₂ samples which have gold particles of 11.5 nm and 10.5 nm, respectively (Figure 4.6).

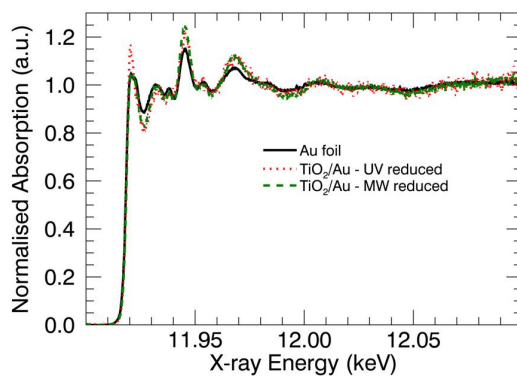


Figure 4.6: High resolution Au-L₃ XANES of the microwave and UV reduced sample. The Au foil spectrum is used as reference.

For the two Au/TiO₂ samples, the post-edge features are nearly identical, except for the white line, which is more intense in the case of the UV reduced sample (Figure 4.6). The latter arises from a larger density of unoccupied 5d states. This

suggests that in case of UV reduction, the Au atoms in the metal particles are oxidized. At the same time, the absorption edge position for the two Au/TiO₂ samples and the gold foil reference all coincide, showing that the gold in the composite materials has the same oxidation state as the metal foil. As also the post-edge features of the XANES spectra of the samples are similar to those of the XANES features of the metal foil, it can be concluded the gold in the Au/TiO₂ samples has a similar surrounding as found in metallic gold. Therefore, the oxidized Au species in the UV reduced sample cannot be identified as unreduced salt (HAuCl₄), as in that case, the absorption edge should be shifted to lower energies and the post-edge features observed for the Au/TiO₂ samples should clearly differ from those of the Au foil. As such, the increase of the white line intensity of the UV reduced sample can only be explained as originating from a positive charge on the gold particles. As it is likely the charge is spread over the gold particle, resulting in a small charge on each gold atom in the cluster. Yet, it is not impossible that the local Au structure does not change significantly compared to the case with no charge, as seen in Figure 4 when comparing the XANES post-edge regions. This also shows that the low resolution XANES does not tell the complete story, because there, an increase in white line intensity was explained by the presence of unreduced starting material (HAuCl₄), as the resolution of the post-edge features was too low to make a clear comparison with the gold foil.

The increase in white line intensity of the UV reduced sample can be explained by a different interaction with the titania support compared to the microwave reduced sample. As the MW reduced sample does not show an increase in white line intensity, the gold nanoparticles have only limited interaction with the titania support. An explanation for the positive charge might be found in the used reduction method. The UV reduction is the only reduction that uses the photoelectrical properties of the titania matrix to reduce the gold salt. The other reduction methods are based on external influences. The use of the titania matrix during the reduction step might cause a stronger interaction between the gold nanoparticles and the titania matrix. One explanation for the positive charge on the gold nanoparticles could be the following. During UV illumination electron and hole pairs are formed in the titania matrix. The electrons will reduce the gold ions to form gold nanoparticles, and the holes will be scavenged by surface bound hydroxyl groups. As the experiment is performed on dry Au³⁺/TiO₂ powder, the amount of surface bound hydroxyl groups present might not be sufficient to scavenge all photogenerated holes produced during 6 hours of illumination and part of these photogenerated holes will oxidise the gold nanoparticles, generating a partial positive charge. A positive charge on the gold nanoparticles can lead to a reduction in photocatalytic activity of the composite materials as photogenerated electrons will neutralize this positive charge and therefore will not participate in the generation of a photocurrent.

4.5 Photocatalysis

To investigate the effect of the (charged) gold nanoparticles on the photocatalytic activity of mesoporous titania, the degradation of phenol under UV illumination is followed (Figure 4.7). The resulting rate constants for the first order kinetics are tabled in Table 4.2. The UV and thermally reduced samples are somewhat better than the pure titania reference catalyst during the first two hours of the reaction. However, at the end of the test unfunctionalized titania has degraded the highest amount of phenol, although there is not much difference between all samples.

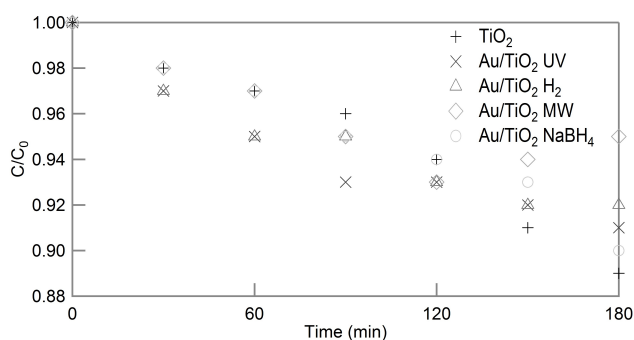


Figure 4.7: Photocatalytic degradation of phenol under UV illumination using Au/TiO₂ catalysts and unfunctionalized TiO₂ as reference.

Table 4.2: Rate constants of the degradation of phenol for pure TiO₂ and the different Au/TiO₂ composite materials.

	TiO ₂	Au/TiO ₂ (UV)	Au/TiO ₂ (MW)	Au/TiO ₂ (H ₂)	Au/TiO ₂ (NaBH ₄)
Rate constant (min ⁻¹)	0.00061 ± 0.00005	0.00050 ± 0.00006	0.00032 ± 0.00009	0.00046 ± 0.00005	0.00053 ± 0.00004

The (charged) gold nanoparticles do not have a large influence on the photocatalytic activity of mesoporous titania, which was not expected. To investigate if the in-house produced titania matrix is causing this effect, gold nanoparticles were also deposited onto commercially available powders. Gold nanoparticles were deposited onto Evonik P25 and Hombikat UV 100 using the thermal process (H₂ atmosphere) and the UV reduction. The photocatalytic activity of both the Evonik P25 (Figure 4.8 left) and Hombikat UV 100 (Figure 4.8 right) samples showed no

difference between the functionalized and unfunctionalized samples. Varying the gold load (0.5 wt% - 5 wt% nominal concentration, 0.1 wt% - 2.5 wt% effective concentration) also did not change the photocatalytic activity. One can also note that the photocatalytic activity of the Evonik P25 and Hombikat UV100 is larger than the in-house synthesized titania powders.

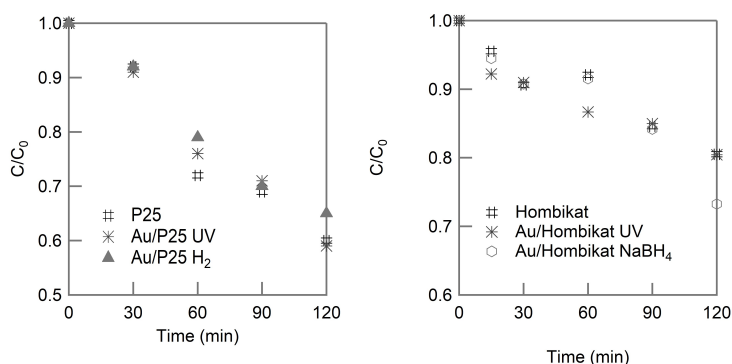


Figure 4.8: Photocatalytic degradation of phenol under UV illumination using Au/P25 catalysts and unfunctionalized Evonik P25 (left) and Au/Hombikat and unfunctionalized Hombikat UV100 (right).

The deposition of gold nanoparticles on a titania matrix does, in our case, not result in improvement (or diminishment) of the photocatalytic activity of the titania matrix. Up till now, we did not find a clear explanation. As the titania matrix is not causing this effect, the deposition method will probably be the cause, but none of the gold functionalized materials showed any improvement. Furthermore, the syntheses are literature based where improvement is noticed. The only difference with some articles is the drying step of the powders after adsorption, whereas most articles reduce the gold immediately after impregnation. However even the samples synthesized according to a 'wet' reduction method do not have improved activities. Another possible explanation could be the UV lamp used during the photocatalytic test. If the UV lamp used by other groups emits a larger fraction of visible light, this could lead to improved activities as the gold nanoparticles can absorb this visible light. While this is not possible if there is no visible light present in the irradiation spectrum.

4.6 Conclusions

When synthesizing Au/TiO₂ composites by impregnation of a mesoporous titania host with HAuCl₄ and subsequent reduction to Au⁰, the reduction method determines many properties of the final material e.g. particle size, oxidation state, etc..

In this research four different reduction methods were investigated *i.e.* UV irradiation, microwave irradiation, thermal reduction under 5% H₂/Ar atmosphere and chemical reduction with NaBH₄. The reduction method did not have any influence on the specific surface area of the final Au/TiO₂ composite. The gold loading was more or less the same for all samples. The Au mean particle size on the other hand is greatly influenced by the reduction method. The largest particles (~11 nm) are obtained using UV and MW irradiation while the smallest mean particle size (2.4 nm) was observed for the H₂ reduced sample. Using XANES spectroscopy, we showed that the gold in almost all samples was completely reduced to the metallic state except for the UV reduced composite material where partially charged Au particles are present, caused by a strong interaction with the titania support, influencing the density of state of the gold nanoparticles. However, the (charged) gold nanoparticles did not improve the photocatalytic activity of mesoporous titania. Using the same deposition methods, gold nanoparticles did also not improve the photocatalytic activity of commercially available titania powders. The influence of the positive charge will therefore be investigated for the carbonylation of glycerol, a reaction catalysed by gold particles.

References

- [1] Hidalgo, M. C., Maicu, M., Navio, J. A. & Colon, G. Effect of sulfate pretreatment on gold-modified TiO₂ for photocatalytic applications. *J. Phys. Chem. C* **113**, 12840–12847 (2009).
- [2] Zheng, N. & Stucky, G. D. A general synthetic strategy for oxide-supported metal nanoparticle catalysts. *J. Am. Chem. Soc.* **128**, 14278–14280 (2006).
- [3] Claus, P., Bruckner, A., Mohr, C. & Hofmeister, H. Supported gold nanoparticles from quantum dot to mesoscopic size scale: Effect of electronic and structural properties on catalytic hydrogenation of conjugated functional groups. *J. Am. Chem. Soc.* **122**, 11430–11439 (2000).
- [4] Bamwenda, G. R., Tsubota, S., Nakamura, T. & Haruta, M. The influence of the preparation methods on the catalytic activity of platinum and gold supported on TiO₂ for CO oxidation. *Catal. Lett.* **44**, 83–87 (1997).
- [5] Kowalska, E., Abe, R. & Ohtani, B. Visible light-induced photocatalytic reaction of gold-modified titanium(iv) oxide particles: action spectrum analysis. *Chem. Commun.* 241–243 (2009).
- [6] Zhang, D. Q. *et al.* Au nanoparticles enhanced rutile TiO₂ nanorod bundles with high visible-light photocatalytic performance for CO oxidation. *Appl. Catal. B-Environ.* **147**, 610–616 (2014).
- [7] Dozzi, M. V., Prati, L., Canton, P. & Selli, E. Effects of gold nanoparticles deposition on the photocatalytic activity of titanium dioxide under visible light. *Phys. Chem. Chem. Phys.* **11**, 7171–7180 (2009).
- [8] Haruta, M. Size- and support-dependency in the catalysis of gold. *Catal. Today* **36**, 153–166 (1997).
- [9] Haruta, M. *et al.* Low-temperature oxidation of CO over gold supported on TiO₂, -Fe₂O₃, and Co₃O₄. *J. Catal.* **144**, 175–192 (1993).
- [10] Grunwaldt, J. D. & Baiker, A. Gold/titania interfaces and their role in carbon monoxide oxidation. *J. Phys. Chem. B* **103**, 1002–1012 (1999).

- [11] Casaletto, M. P., Longo, A., Martorana, A., Prestianni, A. & Venezia, A. M. XPS study of supported gold catalysts: the role of Au⁰ and Au^{+δ} species as active sites. *Surf. Interface Anal.* **38**, 215–218 (2006).
- [12] Li, H. *et al.* Mesoporous Au/TiO₂ nanocomposites with enhanced photocatalytic activity. *J. Am. Chem. Soc.* **129**, 4538–4539 (2007).
- [13] Parayil, S. K. *et al.* Synthesis-dependent oxidation state of platinum on TiO₂ and their influences on the solar simulated photocatalytic hydrogen production from water. *J. Phys. Chem. C* **117**, 16850–16862 (2013).
- [14] Kydd, R., Scott, J., Teoh, W. Y., Chiang, K. & Amal, R. Understanding photocatalytic metallization of preadsorbed ionic gold on titania, ceria, and zirconia. *Langmuir* **26**, 2099–2106 (2010).
- [15] Radnik, J., Mohr, C. & Claus, P. On the origin of binding energy shifts of core levels of supported gold nanoparticles and dependence of pretreatment and material synthesis. *Phys. Chem. Chem. Phys.* **5**, 172–177 (2003).
- [16] Calvin, S. *XAFS for Everyone* (Taylor and Francis Inc, Bosa Roca, 2013), 1st edn.
- [17] Longo, A. *et al.* Structure of the metal-support interface and oxidation state of gold nanoparticles supported on ceria. *J. Phys. Chem. C* **116**, 2960–2966 (2012).
- [18] Brunauer, S., Emmett, P. H. & Teller, E. Adsorption of gases in multimolecular layers. *J. Am. Chem. Soc.* **60**, 309–319 (1938).
- [19] Nikitenko, S. *et al.* Implementation of a combined SAXS/WAXS/QEXAFS set-up for time-resolved in situ experiments. *J. Synchrotron Radiat.* **15**, 632–640 (2008).
- [20] Krause, M. O. & Oliver, J. H. Natural widths of atomic K and L levels, Ka X-ray lines and several K_{LL} auger lines. *J. Phys. Chem. Ref. Data* **8**, 329–338 (1979).
- [21] de Groot, F. M. F., Krisch, M. H. & Vogel, J. Spectral sharpening of the Pt L edges by high-resolution X-ray emission. *Phys. Rev. B* **66** (2002).
- [22] Glatzel, P. *et al.* Reflections on hard X-ray photon-in/photon-out spectroscopy for electronic structure studies. *J. Electron Spectrosc. Relat. Phenom.* **188**, 17–25 (2013).
- [23] Hamalainen, K., Siddons, D. P., Hastings, J. B. & Berman, L. E. Elimination of the inner-shell lifetime broadening in X-ray-absorption spectroscopy. *Phys. Rev. Lett.* **67**, 2850–2853 (1991).

-
- [24] Samain, L. *et al.* Fading of modern prussian blue pigments in linseed oil medium. *J. Anal. Atom. Spectrom.* **26**, 930–941 (2011).
- [25] Silversmit, G. *et al.* Three-dimensional Fe speciation of an inclusion cloud within an ultradeep diamond by confocal mu-x-ray absorption near edge structure: Evidence for late stage overprint. *Anal. Chem.* **83**, 6294–6299 (2011).
- [26] Reifsnnyder, S. N. & Lamb, H. H. Characterization of silica-supported Pd-Au clusters by X-ray absorption spectroscopy. *J. Phys. Chem. B* **103**, 321–329 (1999).
- [27] Schwartz, V. *et al.* XAS study of Au supported on TiO₂: Influence of oxidation state and particle size on catalytic activity. *J. Phys. Chem. B* **108**, 15782–15790 (2004).
- [28] Miller, J. T. *et al.* The effect of gold particle size on Au-Au bond length and reactivity toward oxygen in supported catalysts. *J. Catal.* **240**, 222–234 (2006).

5

Gold/titania composites: carbonylation of glycerol with urea

In this chapter, the catalytic activity of gold nanoparticles deposited on titania (chapter 4) is evaluated by following the carbonylation of glycerol with urea. The positive charge on the gold nanoparticles of the UV reduced sample leads to a higher amount of Lewis acid places and results in a higher conversion, but lower selectivity.

5.1 Introduction

The Au/TiO₂ composites synthesized in the previous chapter showed some remarkable differences (e.g. positive charge on gold nanoparticles), unfortunately they displayed no high photocatalytic activity. To investigate the effect of this positive charge, the catalytic activity of the gold nanoparticles is evaluated.

Gold nanoparticles can be used for many catalytic applications, e.g. deoxygenation of epoxides into alkenes,^{1,2} hydroamination of alkynes,³ hydrosilylation of alkynes,⁴ hydrogenation of unsaturated C-C bonds⁵ and Suzuki coupling reactions.^{6,7} The catalytic applications become very interesting when the gold particles are deposited onto a substrate because this results in regenerable heterogeneous catalyst. Moreover, the support itself can have a beneficial effect,⁸ which makes our gold/titania composites also desirable for gold catalysed applications.

The carbonylation of glycerol with urea is a very interesting reaction from environmental point of view as it net consists of the incorporation of CO₂ (Figure 5.1). Both glycerol and urea are cheap reaction products. Glycerol is a byproduct resulting from the production of biodiesel and therefore plentiful abundant and cheap.⁹ The conversion of glycerol into value added chemicals is a very desired process. Glycerol carbonate is one of those valuable products as it is a building block in the synthesis of fine chemicals like pharmaceuticals, textiles, cosmetics and polymers. It has a low toxicity and high boiling point which makes it useful as electrolyte and solvent in lithium ion batteries.^{10,11} It is also biodegradable.

Although the reaction of glycerol with urea can proceed by increasing the temperature of the system, several heterogeneous catalysts have been found to improve its rate and selectivity to glycerol carbonate.¹³ Some of these heterogeneous catalyst are W-Sn mixed oxides,¹⁴ zinc containing catalysts¹⁵ and gold particles deposited on a wide range of supports going from MgO¹⁶ and CaO¹¹ to mixed oxides (Al/Mg, Al/Li)¹¹ and TiO₂, SiO₂ and ZnO.¹⁶ Hutchings et al. presented

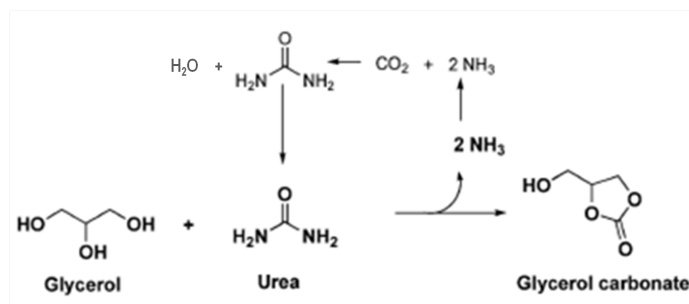


Figure 5.1: Reaction scheme for the synthesis of glycerol carbonate from glycerol and urea as CO₂ donor.¹²

a gold supported on magnesia catalyst as a high active and selective system for the glycerolysis of urea.¹⁶ These authors suggest that the combination of the basic properties of the support with the Lewis acidity of the gold-supported nanoparticles results in the improvement of the yield and selectivity. Moreover, the support can also play an additional role concerning to the stabilization of the gold nanoparticles and/or the occurrence of different metal-support interaction effects (e.g. charge withdrawing effects).

In chapter 4 we studied the influence of different reduction methods on the material properties of gold/titania composite materials. We found that the use of UV irradiation as reduction method for the gold salt deposited on a titania matrix results in positively charged gold nanoparticles.¹⁷ In this research, the catalytic behaviour of the different Au/TiO₂ materials is investigated by following the synthesis of glycerol carbonate from glycerol and urea. The synthesized materials are also tested for their stability and reusability.

5.2 Experimental section

Materials. Titanium(IV) isopropoxide (Ti(OⁱPr)₄, 97%), gold(III) chloride trihydrate (HAuCl₄·3H₂O, ACS reagent, ≥ 49% Au basis), sodium hydroxide (NaOH, reagent grade, ≥ 98%), sodium borohydride (NaBH₄ ≥ 98%), glycerol (ACS reagent ≥ 99,5%) and urea ((NH₂)₂CO) are purchased from Sigma-Aldrich, diethylene glycol monoethyl ether (≥ 99%) is acquired from SAFC and methanol (MeOH, > 99,8%) from ROMIL - Pure Chemistry. Hydrochloric acid (HCl, 36%) is obtained from Fiers, N-cetyl-N,N,N-trimethylammonium bromide (CTAB, pro analysis) from Merck and ethanol (EtOH, absolute PA) from Panreac. All chemicals are used as received.

5.2.1 Characterisation

Nitrogen sorption experiments were carried out on a TriStar 3000 (Micromeritics) at -196 °C. Samples were pretreated at 120 °C for 18 hours under vacuum. The specific surface areas were calculated using the Brunauer-Emmett-Teller (BET) method.¹⁸ Samples for high angular annular dark field scanning transmission electron microscopy (HAADF STEM) were prepared by dispersing the powder in deionized water and dipping the copper support TEM grid (200 mesh) in the dispersion. The HAADF STEM samples were air-dried and measured using a JEOL JEM-2200FS transmission electron microscope with post-sample Cs corrector and an accelerating voltage of 200 kV. The particle size of the gold nanoparticles was determined by measuring the diameter of at least 50 gold particles of each sample. The gold load of the samples was quantitatively determined using inductively coupled plasma mass spectrometry (ICP-MS, Perkin Elmer Elan DRC). Leaching of

gold after catalysis was investigated using XRF analysis (Nex CG, Rigaku) on the reaction products, after removal of the catalyst.

Surface concentrations of the acidic sites were determined by temperature-programmed desorption of ammonia (NH₃-TPD), using an Autosorb iQ TPX device, from Quantachrome. In a typical experiment, about 100 mg of catalyst was placed in a quartz reactor (quartz-wool bed) and pretreated at 120 °C for 1 h, under He flow (30 mL/min). In the case of the UV reduced sample, the He flow was switched to pure H₂ (30 mL/min) for 1h, in order to guarantee the reduction of all the gold-cationic species. Subsequently, the sample was cooled down to 40 °C and saturated under a flow of gas mixture containing 5 vol% of NH₃ in He, during 30 minutes. The weakly adsorbed NH₃ was removed by flushing the sample with He (30 mL/min) at the adsorption temperature (40 °C), during 30 min. Desorption was carried out with a linear heating rate (10 °C/min) in a flow of He (30 mL/min) up to 600 °C. The composition of the effluent gases was measured using a TCD detector.

Au *L_{III}*-edge ($E_0 = 11,919$ eV) X-ray absorption spectroscopy (XAS) measurements were carried out at the Swiss-Norwegian Beam Line (SNBL) BM01B, at the European Synchrotron Radiation Facility (ESFR), Grenoble-France. A Si(111) channel-cut monochromator was used and higher harmonics were rejected by a Cr-coated mirror. The samples were mixed with starch and pressed into pellets before being analysed. All spectra were recorded in transmission mode using ionization chambers for detection. To avoid beam induced changes, the sample was moved through the beam after each scan. By doing so, different scans of the 'pristine' sample could be taken, resulting in an improved the signal to noise ratio, while measuring only a limited amount of beam induced changes.

5.2.2 Carbonylation of glycerol with urea

Approximately 4 g glycerol in a three neck flask was heated to 140 °C to remove the water present in the starting product. After 30 minutes an equimolar amount of urea (2.69 g) and the 1 wt% Au/TiO₂ catalyst (0.2 g), representing a $0.115 \cdot 10^{-3}$ catalyst/substrate ratio, were added while maintaining 140 °C. A vacuum pump was used to reduce the pressure to 500 mbar to remove the ammonia that is formed during the reaction. After 4 hours, the reaction was stopped by cooling the reaction mixture to room temperature. The internal standard (25 mL, 200 mg/mL of diethylene glycol monoethyl ether in methanol) was added to reduce the viscosity of the reaction mixture. The resulting dispersion was centrifuged for 5 minutes at 4000 rpm to remove the catalyst. The reaction products (630 μ L) were diluted with methanol (25 mL) prior to GC analysis (HP 5890 series II). The reaction products are separated on a Superox II column, using the following sequence: 3 minutes at 50 °C, heating to 240 °C with a heating rate of 20 °C/min and 17.5 minutes at 240

°C. The components are detected with a TCD detector. The catalyst was washed two times with acetone and dried at 100 °C before the reuse experiments.

5.3 Material properties

An overview of the properties of the Au/TiO₂ materials can be found in Table 5.1. The samples all display very similar type IV nitrogen sorption isotherms (A.7A). The specific surface areas and average pore sizes of all powders are respectively approximately 300 m²/g and 4 nm (A.8). The particle size of the gold nanoparticles is different for all samples, but the H₂ and NaBH₄ reduced samples possess the smallest particles (8 - 9 nm) and the UV reduced sample the largest (17 nm). The standard deviation on the particle size is rather high for all samples. HAADF STEM images of all samples and gold particle size distributions are shown in Figures 5.2 and 5.3, respectively. One can note that the properties of these materials are different from the materials in the previous chapter. As already discussed in the previous chapter, there were some problem with the reproducibility of the high specific surface areas due to problems with the drying furnace and new flasks. These problems are solved and it is again possible to obtain high specific surface areas. However, the gold nanoparticles are bigger than in the previous chapter. This can possibly be caused by the higher specific surface area, making it more difficult for the reducing agents to reach the gold ions, resulting in a smaller amount of nuclei and therefore larger particles. The gold loading is similar in the case of the thermally and UV reduced samples (respectively 0.85 wt% and 0.79 wt%) and for the microwave and NaBH₄ reduced samples (respectively 0.10 wt% and 0.15 wt%). However between these two couples of samples, there is a large difference in loading. This is probably caused by the fact that the latter reduction methods are performed in water, leading to a much higher amount of leaching compared to the dry reduction methods.

5.4 Catalysis

The catalytic conversion of glycerol to glycerol carbonate with urea was investigated using four different gold/titania catalysts (Table 5.2). These results are compared with the blank reaction, using only the TiO₂ matrix and a commercially available ZnO powder catalyst as benchmark. In literature, selectivities over 90% are reached.^{11, 19} The ZnO benchmark has a conversion of 67% and the highest selectivity (62%). The UV reduced sample has the highest conversion, but a very low selectivity, even lower than the blank reaction. The other Au/TiO₂ samples have a lower conversion, but a good selectivity. The gold particle size does not have a large influence on the selectivity: the H₂ and NaBH₄ reduced samples have

Table 5.1: Material properties of all gold/titania catalysts before and after one catalytic run. A standard deviation was calculated for the gold particles sizes.

	Au/TiO ₂ UV	Au/TiO ₂ H ₂	Au/TiO ₂ MW	Au/TiO ₂ NaBH ₄
S_{BET} (m ² /g) before catalysis	305 ± 4	299 ± 4	298 ± 4	263 ± 4
Mean Au NP size (nm) before catalysis	17.0 ± 10.3	8.4 ± 4.9	14.7 ± 5.8	8.8 ± 3.4
Au wt% before catalysis	0.85	0.79	0.10	0.15
S_{BET} (m ² /g) after catalysis	248 ± 4	255 ± 4	244 ± 4	263 ± 4
Mean Au NP size (nm) after catalysis	16.5 ± 11.9	17.3 ± 9.6	14.3 ± 7.4	25.0 ± 8.7
Au wt% after catalysis	0.77	0.76	0.09	0.13

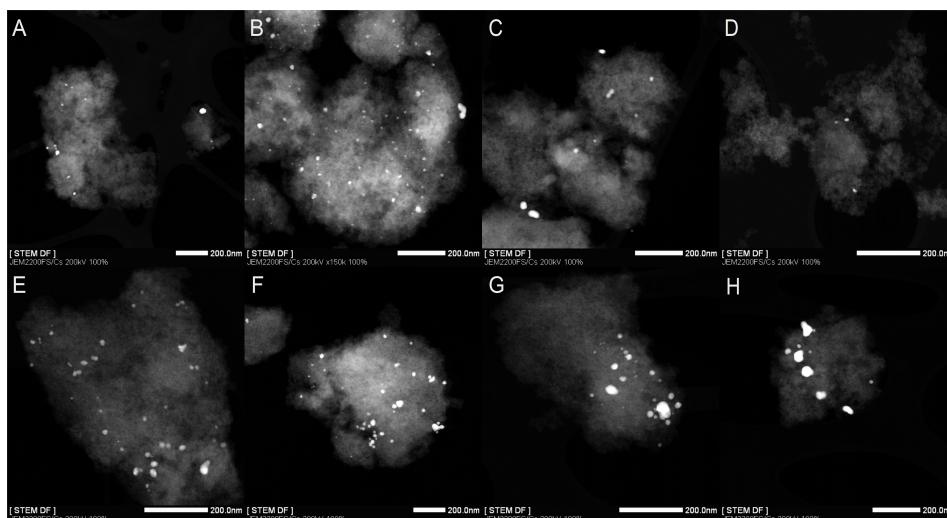


Figure 5.2: HAADF STEM images of the UV (A, E), thermally (B, F), microwave (C, G) and NaBH₄ (D, H) reduced samples before (A-D) and after (E-H) catalysis.

the highest selectivity ($\sim 55\%$) and the smallest particles (~ 8 nm), however the selectivity of the microwave reduced sample is only slightly smaller ($\sim 52\%$) and the gold particles are much larger (~ 15 nm). The selectivity of the UV reduced sample is much smaller (24%), while the increase in particle size is rather small (17 nm). The cause of the low selectivity of the UV reduced samples can therefore not be found in the larger gold particle size. This is not unexpected as the gold particle size distribution is broad for all samples.

In the previous chapter, we noted a positive charge on the UV reduced gold

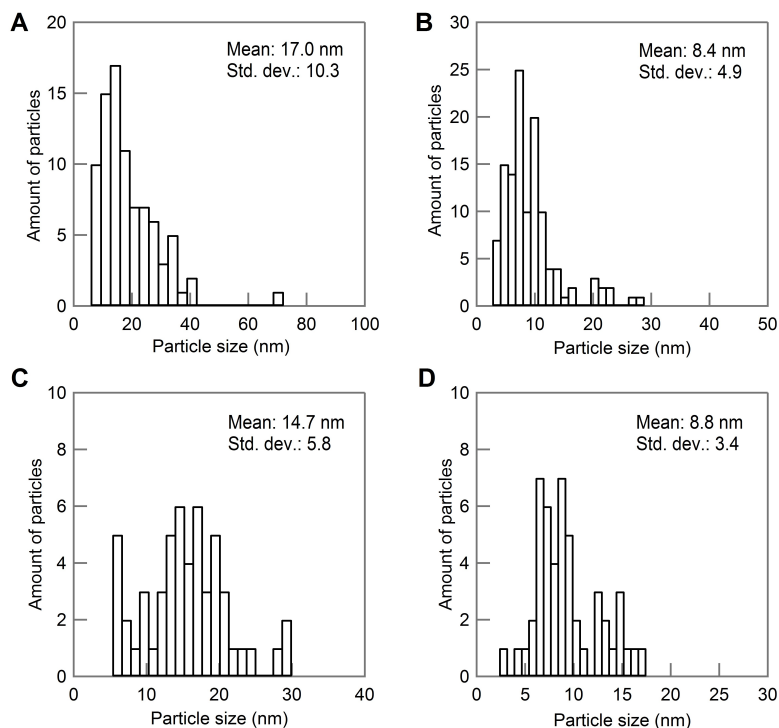


Figure 5.3: Gold particle size distributions of the UV (A), thermally (B) microwave (C) and NaBH₄ (D) reduced samples before catalysis.

particles, which was not present on the other samples. These positively charged gold particles can behave as Lewis-acid sites on the surface of the catalyst, favoring the activation of the carbonyl group of urea. This leads to a high conversion as an alcoholic group of glycerol has to attack urea to form dihydroxypropyl carbamate in the first reaction step.¹⁶ The second reaction step consists of a ring closing reaction, to form glycerol carbonate (Figure 5.4). Next to the desired glycerol carbonate, other products (e.g. 4-(hydroxymethyl)oxazolidin-2-one and (2-oxo-1,3,-dioxolan-4-yl)methyl carbamate) can be formed.

In literature it can be found that a basic support favors the ring closing reaction to form the glycerol carbonate.¹¹ The low yield to the production of glycerol carbonate observed for this catalyst suggests a poor role of the support (TiO₂) to drive the reaction to the target molecule. Thus, on the UV reduced sample, the predominant presence of acid sites (Au δ^+) is not compensated by the basicity of the TiO₂ used as support, leading to a low yield of glycerol carbonate. To confirm this hypothesis NH₃-TPD has been performed on the bare titania support,

Table 5.2: Results of the first catalytic conversion of glycerol to glycerol carbonate using gold/titania catalysts and pure titania and commercial ZnO as references.

	Au/TiO ₂ UV	Au/TiO ₂ (H ₂)	Au/TiO ₂ (MW)	Au/TiO ₂ (NaBH ₄)	TiO ₂	ZnO
% conversion (glycerol)	74	53	66	62	56	67
% yield (glycerol carbonate)	18	29	34	35	18	42
% selectivity (glycerol carbonate)	24	55	52	56	31	62
reaction rate ($\frac{\mu\text{mol}(\text{glycerolcarbonate})}{g_{\text{cat}}s}$)	2.64	4.40	5.19	5.23	-	-

The conversion is described as $\frac{C_{0,\text{glycerol}} - C_{\text{end},\text{glycerol}}}{C_{0,\text{glycerol}}}$

The yield is defined as $\frac{C_{\text{glycerolcarbonate}}}{C_{0,\text{glycerol}}}$

The selectivity is calculated as $\frac{\text{yield}}{\text{conversion}}$.

the UV reduced sample with the high conversion, but low yield and the H₂ reduced sample, representing the other catalysts but with a gold loading very similar to the UV reduced sample (Figure 5.5).

The ammonia uptake was calculated from the respective TPD profiles and normalized as a function of the mass of sample or their surface area (Table 5.3). These values represent the total amount of acid sites (both Brønsted and Lewis type sites), while the temperature of the maxima of the desorption profile are indicative of the strength of the acid sites.

Table 5.3: Ammonia uptake calculated from the NH₃-TPD profiles, from 50 to 550 °C.

Sample	Ammonia uptake	
	$\mu\text{mol NH}_3/\text{g cat.}$	$\mu\text{mol NH}_3/\text{m}^2$
TiO ₂	1143	3.63
Au/TiO ₂ UV	1305	4.28
Au/TiO ₂ H ₂	1142	3.82

The three analyzed materials showed similar NH₃-TPD profiles characterized by an evolution of ammonia occurring with a broad shape in a wide temperature range (50-550 °C). This indicates the presence of several NH₃ adsorbed species with different thermal stability, suggesting that acid sites of weak strength (below 200 °C) and moderate strength (from 200 °C to 450 °C) are present on these materials.²⁰⁻²² Bigger differences can be observed from the quantitative data presented

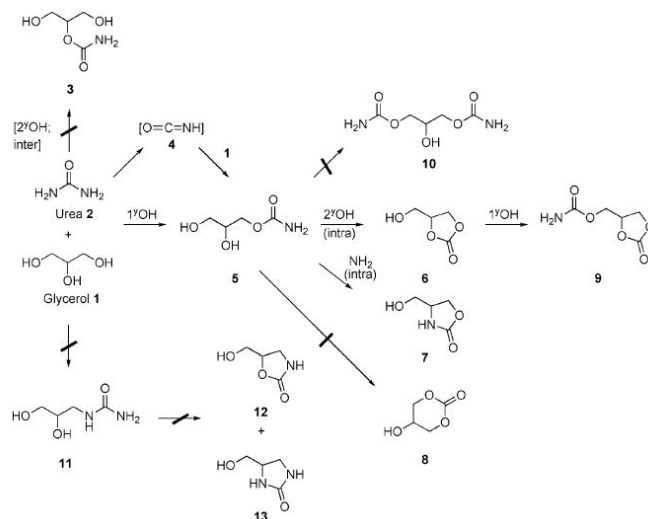


Figure 5.4: Possible reaction pathways for the reaction between glycerol and urea.¹⁶

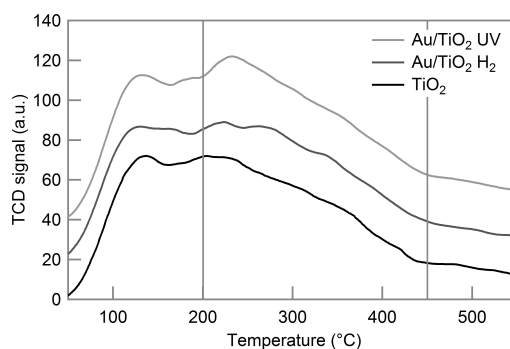


Figure 5.5: NH_3 -TPD profiles of the studied materials.

in Table 5.3. Whereas the bare TiO_2 support and the H_2 reduced catalysts showed a similar ammonia uptake (indicating a similar concentration of acidic sites), the UV reduced catalyst showed an enhanced concentration of acidic sites per gram and per surface area of sample. In such a way, the $\text{Au}(\delta^+)$ species stabilized on the TiO_2 surface can behave as additional Lewis acidic places, which are accessible to the NH_3 used as a probe-basic molecule. This clearly supports our hypothesis.

After catalysis, the samples are reanalysed for structural changes (Table 5.1). The nitrogen sorption isotherms exhibit the same shape as before catalysis (A.7B). The specific surface areas are approximately $250 \text{ m}^2/\text{g}$ for all samples, which is a

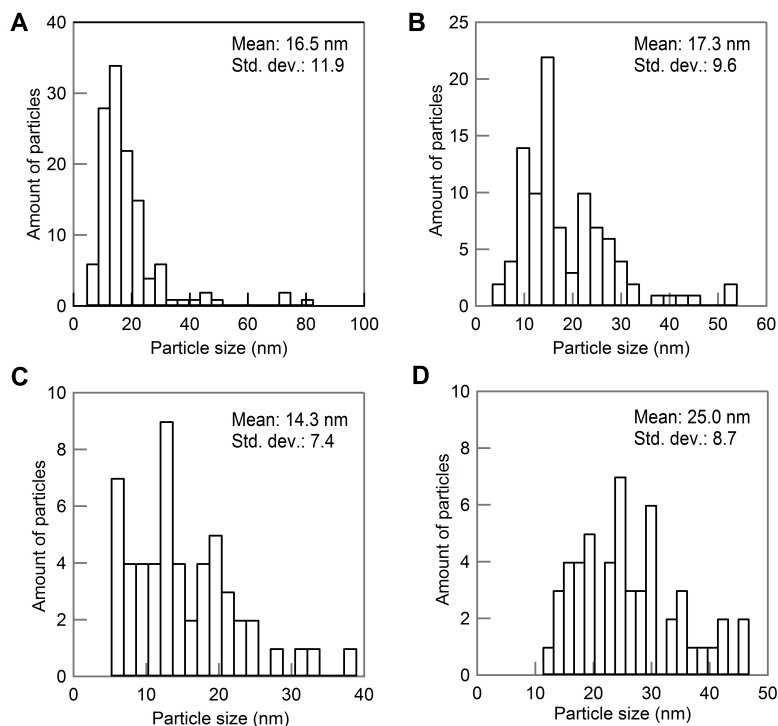


Figure 5.6: Gold particle size distributions of the UV (A), thermally (B) microwave (C) and NaBH₄ (D) reduced samples after catalysis.

decrease compared to the fresh catalysts. The average pore sizes likewise decrease only a limited amount to 3.9 nm (A.9). The decrease in both specific surface area and average pore size could result from organic material which is still present from the catalytic reaction. STEM images of the samples did not show visual differences in the titania matrix (Figure 5.2). Therefore it can be concluded that the matrix is relatively stable under the catalytic conditions. After catalysis, one can observe that the smallest gold particles have grown considerably, while the bigger gold particles on the UV and microwave reduced samples remain more or less the same size. The gold particle size distribution broadened for all samples (Figure 5.6). The growth of the small nanoparticles is almost inevitable at the higher temperatures at which the catalytic reaction is taking place due to the low melting points and high surface energies of gold nanoparticles. To reduce their surface energy, the particles sinter together.^{23, 24} There are different mechanisms to achieve this: crystallite migration or atom migration, both leading to the disappearance of small particles and the formation of larger particles. The small particles with high surface energies

are present on the thermally and chemically reduced samples. After catalysis, these particles have sintered together. In the case of the microwave and UV reduced samples, larger gold particles with smaller surface energies are already present from the start. During catalysis at higher temperatures, the force to sinter together is much smaller for these two samples as the reduction in surface energies is much smaller for larger particles. The used catalysts were analysed with NH_3 -TPD, but were contaminated with adsorbed organic molecules from the reaction, resulting in TPD profiles which are not comparable with the TPD profiles of the fresh catalysts.

Hot filtration tests are not possible because it is impossible to remove the catalyst due to the viscosity of the reaction mixture. After dilution with methanol, it was however possible to remove the catalyst. The filtrate was analysed using XRF and no gold atoms could be detected. ICP-MS analysis of the catalysts after the first catalytic run also showed only a minimal decrease in gold loading, confirming there is no leaching of the gold catalyst. Hence the catalytic reaction proceeds heterogeneous.

The catalysts are recovered and a second and third catalytic run is performed (Figure 5.7). The selectivity of the H_2 , MW and NaBH_4 reduced samples remained approximately the same (55% - 60%) for each run. The conversion and yield do also not differ in various runs. On the other hand, the selectivity of the UV reduced sample increased from 24% in the first run to 40% in the second and third run. This again indicates that the particle size has no large influence on the selectivity of the reaction as the gold particles sinter together during the catalytic reaction, as the selectivity remains constant. The selectivity of the UV reduced sample increases, but the mean gold particle size has not changed. The unchanged selectivity of the H_2 , MW and NaBH_4 reduced samples also shows that there is no poisoning of the catalyst.

X-ray absorption spectroscopy (XAS) experiments were performed on the UV reduced sample, before and after catalysis (Figure 5.8) to investigate its increase in selectivity. The spectrum of the catalyst before catalysis shows a large peak (white line) at 11.92 keV corresponding to the 2p - 5d electron transition, indicating a positive charge on gold. However, after catalysis this peak has almost completely disappeared, causing the spectrum to look almost identical to the metallic foil reference spectrum, meaning the positive charge has vanished during/after the first catalytic run. As the positive charge was the main difference with the other Au/ TiO_2 samples, the simultaneous disappearance of the charge and the increase in selectivity, suggests that the charge has indeed an influence on the reaction.

The removal of the charge results in a lower concentration of Lewis-acid sites, which provokes a more favourable ratio of these sites with respect to the basicity of the support. Although this situation decreases the conversion capacity of the gold-supported catalyst, it is in favour of an improved selectivity. A UV cure on the recovered catalyst did not increase the conversion (or decrease the selectiv-

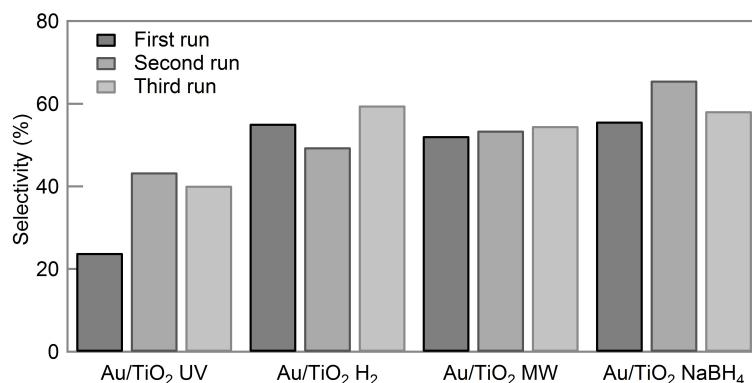


Figure 5.7: The selectivity towards glycerol carbonate for three runs of the different gold/titania catalysts.

ity). More research using XAS has to be performed to investigate the cause of the disappearance of the positive charge during the reaction.

5.5 Conclusions

The gold/titania catalysts synthesized in chapter 4, showed no improved photocatalytic activity. Therefore, we researched the activity of the materials in gold catalysed reactions. The conversion of glycerol to glycerol carbonate using urea was followed. The thermally, microwave and chemically reduced samples had a good selectivity of 55%. This is lower than state of the art catalysts which reach selectivities up to 98%. Titania is a too acidic support to produce very high selectivities. The UV reduced sample had a low selectivity of 24% but a higher conversion (74%). Analysis of the powders after catalysis showed that the catalysts are stable and no leaching of gold was observed. The selectivity of the catalysts remained the same in a second and third catalytic run, except for the UV reduced catalyst which even showed an increase in selectivity after the first run.

The gold particle size had no influence on the selectivity of the materials as the particles sinter together during the catalytic reaction, and this does not result in differences in selectivity. The amount of Lewis acid sites however, has an influence on the selectivity of the reaction. The positive charge present on the gold nanoparticles of the UV reduced sample, results in more acid sites. This positive charge and corresponding acid sites can activate urea, leading to a high conversion, but the positive charge is not favourable for the ring closure in the reaction, leading to a low yield of glycerol carbonate. After the first catalytic run, the positive charge

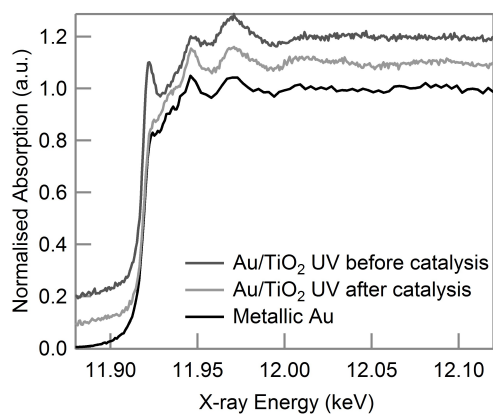


Figure 5.8: XAS spectra of the UV reduced sample before and after catalysis and the metallic foil reference.

is removed as shown by XAS, resulting in similar properties of the UV reduced sample compared to the other samples, expressed by a comparable selectivity for all catalysts in the second and third catalytic run. This information can be used to synthesize superior catalysts if the UV reduction method is used to deposit gold nanoparticles on a more basic support than TiO₂ like MgO, K₂O and Ca₂SiO₄. In this way a more balanced amount of Lewis acid/base sites can be created which improve both the activation of urea and the ring closure reaction. This should lead to both a high conversion and selectivity for the carbonylation of glycerol with urea.

References

- [1] Mitsudome, T. *et al.* Supported Gold and Silver Nanoparticles for Catalytic Deoxygenation of Epoxides into Alkenes. *Angew. Chem. Int. Ed.* **49**, 5545–5548 (2010).
- [2] Ni, J. *et al.* Mild and efficient CO-mediated eliminative deoxygenation of epoxides catalyzed by supported gold nanoparticles. *Chem. Comm.* **47**, 812–814 (2011).
- [3] Corma, A., Concepcion, P., Dominguez, I., Fornes, V. & Sabater, M. J. Gold supported on a biopolymer (chitosan) catalyzes the regioselective hydroamination of alkynes. *J. Catal.* **251**, 39–47 (2007).
- [4] Corma, A., Gonzalez-Arellano, C., Iglesias, M. & Sanchez, F. Gold nanoparticles and gold(III) complexes as general and selective hydrosilylation catalysts. *Angew. Chem. Int. Ed.* **46**, 7820–7822 (2007).
- [5] Hashmi, A. S. K. & Hutchings, G. J. Gold catalysis. *Angew. Chem. Int. Ed.* **45**, 7896–7936 (2006).
- [6] Willis, N. G. & Guzman, J. Influence of the support during homocoupling of phenylboronic acid catalyzed by supported gold. *Appl. Catal. A* **339**, 68–75 (2008).
- [7] Han, J., Liu, Y. & Guo, R. Facile Synthesis of Highly Stable Gold Nanoparticles and Their Unexpected Excellent Catalytic Activity for Suzuki-Miyaura Cross-Coupling Reaction in Water. *J. Am. Chem. Soc.* **131**, 2060–2061 (2009).
- [8] Stratakis, M. & Garcia, H. Catalysis by Supported Gold Nanoparticles: Beyond Aerobic Oxidative Processes. *Chem. Rev.* **112**, 4469–4506 (2012).
- [9] Teng, W. K., Ngoh, G. C., Yusoff, R. & Aroua, M. K. A review on the performance of glycerol carbonate production via catalytic transesterification: Effects of influencing parameters. *Energy Convers. Manage.* **88**, 484–497 (2014).

- [10] Sonnati, M. O. *et al.* Glycerol carbonate as a versatile building block for tomorrow: synthesis, reactivity, properties and applications. *Green Chem.* **15**, 283–306 (2013).
- [11] Climent, M. J. *et al.* Chemicals from biomass: Synthesis of glycerol carbonate by transesterification and carbonylation with urea with hydrotalcite catalysts. the role of acid-base pairs. *J. Catal.* **269**, 140–149 (2010).
- [12] Ab Rahim, M. H. *et al.* Gold, palladium and gold-palladium supported nanoparticles for the synthesis of glycerol carbonate from glycerol and urea. *Catal. Sci. Tech.* **2**, 1914–1924 (2012).
- [13] Aresta, M., Dibenedetto, A., Nocito, F. & Ferragina, C. Valorization of bio-glycerol: New catalytic materials for the synthesis of glycerol carbonate via glycerolysis of urea. *J. Catal.* **268**, 106–114 (2009).
- [14] Jagadeeswaraiiah, K., Kumar, C. R., Prasad, P. S. S., Loridant, S. & Lingaiah, N. Synthesis of glycerol carbonate from glycerol and urea over tin-tungsten mixed oxide catalysts. *Appl. Catal. A* **469**, 165–172 (2014).
- [15] Fujita, S.-i., Yamanishi, Y. & Arai, M. Synthesis of glycerol Carbonate from glycerol and urea using zinc-containing solid catalysts: A homogeneous reaction. *J. Catal.* **297**, 137–141 (2013).
- [16] Hammond, C. *et al.* Synthesis of glycerol carbonate from glycerol and urea with gold-based catalysts. *Dalton Transactions* **40**, 3927–3937 (2011).
- [17] Meire, M. *et al.* Gold/titania composites: An x-ray absorption spectroscopy study on the influence of the reduction method. *Spectrochim. Acta B* **110**, 45–50 (2015).
- [18] Brunauer, S., Emmett, P. H. & Teller, E. Adsorption of gases in multimolecular layers. *J. Am. Chem. Soc.* **60**, 309–319 (1938).
- [19] Kondawar, S. E. *et al.* Carbonylation of glycerol with urea to glycerol carbonate over supported zn catalysts. *Applied Petrochemical Research* **7**, 41–53 (2017).
- [20] Chang, F.-W. *et al.* Production of hydrogen by partial oxidation of methanol over bimetallic Au-Cu/TiO₂-Fe₂O₃ catalysts. *J. Mol. Catal. A* **313**, 55–64 (2009).
- [21] Venezia, A., La Parola, V., Pawelec, B. & Fierro, J. Hydrogenation of aromatics over Au-Pd/SiO₂-Al₂O₃ catalysts; support acidity effect. *Appl. Catal. A* **264**, 43–51 (2004).

-
- [22] Heracleous, E., Machli, M., Lemonidou, A. & Vasalos, L. Oxidative dehydrogenation of ethane and propane over vanadia and molybdena supported catalysts. *J. Mol. Catal. A* **232**, 29–39 (2005).
- [23] Ma, Z. & Dai, S. Chapter 1 stabilizing gold nanoparticles by solid supports. In *Heterogeneous Gold Catalysts and Catalysis*, 1–26 (The Royal Society of Chemistry, 2014).
- [24] Goudeli, E. & Pratsinis, S. E. Crystallinity dynamics of gold nanoparticles during sintering or coalescence. *AIChE Journal* **62**, 589–598 (2016).

6

Platinum/titania composites: synthesis and characterisation

This chapter describes the synthesis of platinum/titania materials produced by the impregnation of a platinum salt in a titania matrix and the subsequent reduction of the salt. Not all synthesis methods reduce the platinum ions, while the ones that do, produce large, irregular platinum particles. The photocatalytic activity of the composite materials is increased in comparison with pure mesoporous titania for the degradation of the herbicide isoproturon.

6.1 Introduction

Chapter 4 covers the synthesis of mesoporous titania functionalized with gold nanoparticles. Functionalized titania with noble metal nanoparticles should improve the photocatalytic activity of titania.¹⁻³ However, this is not the case for the Au/TiO₂ materials synthesized in the scope of this PhD research. This is not expected and to investigate if this effect is caused by the synthesis methods, Pt/TiO₂ materials are synthesized according to the same recipes. As platinum is a noble metal, a Schottky barrier is created at the junction of Pt and TiO₂. This results in the physical separation of the photogenerated electron and holes, which should result in an increased photocatalytic activity.

Pt/TiO₂ materials are also good catalyst for the water splitting reaction, which produces hydrogen gas.⁴⁻⁶ It has a better activity than Au/TiO₂ materials.⁷ Due to time limitations, it unfortunately was not possible to investigate this reaction during the scope of this PhD research.

6.2 Experimental section

Materials. Titanium(IV) isopropoxide (Ti(OⁱPr)₄, 97%), sodium borohydride (NaBH₄ ≥ 98%), sodium hydroxide (NaOH, reagent grade, ≥ 98%) and isoproturon (PESTANAL®), analytical standard) are purchased from Sigma-Aldrich. N-cetyl-N,N,N-trimethylammonium bromide (CTAB, pro analysis) is acquired from Merck, dihydrogen hexachloroplatinate (IV) hexahydrate (H₂PtCl₆·3H₂O, ACS, 99.95% (materials basis) Pt 37.5% min) from Alfa Aesar, hydrochloric acid (HCl, 36%) from Fiers and ethanol (EtOH, absolute PA) from Panreac. All chemicals are used as received.

6.2.1 Synthesis

Mesoporous titania. Mesoporous titania was prepared using the synthesis method described in chapter 2, without the additional microwave treatments.

Pt/TiO₂ powders. The as-synthesized titania (2 g) was dispersed in an orange, aqueous solution of H₂PtCl₆ (0.0273 g) and the pH was adjusted to 9.5 with NaOH. Additionally, water was added to obtain a total volume of 20 mL. The dispersion was stirred for 3 hours in the dark, to avoid reduction of the salt. The dispersion was filtered, resulting in a very light yellow powder and a light yellow filtrate. The powder was dried in the dark under ambient conditions, and split into 4 equal portions. Each is subjected to a different reduction procedure: (1) illumination for 6 hours with a mercury lamp (UVP Pen-Ray®, primary energy at 254 nm), every half hour, the powder is turned in order to illuminate other parts of the powder, (2) thermal reduction for 2 hours at 200 °C under 5% H₂/Ar atmosphere,

(3) microwave (MW) irradiation for 1 hour at 120 °C, dispersed in 4 mL water. The powder was washed with water and dried at room temperature in the dark and finally (4) 2 mL of 0.2 M NaBH₄ was added to a dispersion of Au/TiO₂ in 15 mL deionized water and stirred for 3 hours. Afterwards, the powder was washed with deionized water and dried at room temperature in the dark.

6.2.2 Characterization

Nitrogen sorption experiments were carried out on a TriStar 3000 (Micromeritics) at -196 °C. The specific surface areas were calculated using the Brunauer-Emmett-Teller (BET) method.⁸ Samples for high angular annular dark field scanning transmission electron microscopy (HAADF STEM) were prepared by dispersing the powder in deionized water and dipping the copper support TEM grid (200 mesh) in the dispersion. The HAADF STEM samples were air-dried and measured using a JEOL JEM-2200FS transmission electron microscope with post-sample CS corrector and an accelerating voltage of 200 kV. The platinum load of the samples was quantitatively determined using X-ray Fluorescence (XRF) spectrometry (PANalytical, Epsilon 3^{XLE}). A calibration curve between 0 wt% and 1 wt% was compost. The signals obtained from the samples were fitted to the calibration curve to determine the exact Pt concentration of the samples.

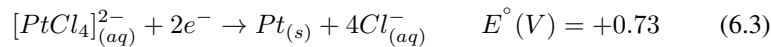
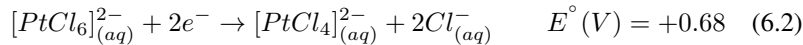
6.2.3 Photocatalytic degradation

The photocatalytic activity of the powders is evaluated through the degradation of isoproturon under UV illumination. The experiments are carried out in a setup based on ISO 10678:2010(E). A Vilber Lourmat VL-315BLB blacklight blue fluorescent light tube is used with a maximum emission at 365 nm and emitting 136 $\mu\text{W}/\text{cm}^2$ (Figure 2.3). The starting concentration of the aqueous isoproturon solution is 10 mg/L. Titania (0.4 g/L) was added to 50 mL pollutant solution in a photocatalytic cell which is kept at a constant temperature of 25 °C. The suspension is stirred for 60 minutes in the dark to reach adsorption equilibrium. At time = 0, 15, 30, 60, 90, 120, 150 and 180 minutes, 2 mL aliquots are taken. The dispersion is centrifuged for 5 minutes at 5000 rpm to separate the titania powder from the pollutant solution. The pollutant concentration is evaluated using a HPLC-MS system (Thermo-Scientific). The degradation is normalized with respect to the starting concentration after reaching adsorption equilibrium. The degradation of isoproturon proceeds with a pseudo-first order kinetic. Rate constants are derived from the $\ln(C/C_0)$ versus time graph.

6.3 Material properties

An overview of the properties of the Pt/TiO₂ materials can be found in Table 6.1. The specific surface areas of all powders are approximately 330 m²/g. The mesoporous titania structure remains intact after the impregnation of the titania host with the Pt⁴⁺ salt and the subsequent reduction to Pt⁰. However, only a limited amount, approximately 5%, of Pt salt is adsorbed on titania. This is very low compared to the 60% adsorption of the gold salt. The dry reduction methods (UV reduction or H₂ reduction) exhibit a higher loading (0.067% and 0.063%) compared to the wet reduction methods (MW and NaBH₄ reduction) which both have a Pt load of 0.045%. The decreased loading of the wet reduction methods can be explained by the possible desorption of the Pt ions from the titania surface during the reduction method in water, whereas this is not possible if the powder is reduced in dry conditions. The same trend was observed for the Au/TiO₂ samples.

The UV and microwave reduction could not reduce the platinum salt, as no particles are observed in the STEM image (Figure 6.1 A and B). Additionally the obtained powders have a white color, whereas the thermally and chemically reduced samples have a light grey color, due to the surface plasmon resonance of the nanoparticles (Table 6.1). This is probably due to the smaller reduction potential of [PtCl₆]²⁻ (+ 0.705 V) compared to [AuCl₄]⁻ (+ 1 V). This makes it more difficult to completely reduce the platinum salt than the gold salt to their respective metal states.



Respectively, dendrite particles and large particles are produced when the H₂ and NaBH₄ reduction is performed (Figure 6.1 C and D). The STEM images of the UV, MW and H₂ reduced samples, show the titania matrix as an agglomerate of small particles. The large particle on the image of the NaBH₄ reduced samples exhibits a smooth surface and edges, typical of metal particles. The light dendritic structures on Figure 6.1C are Pt particles.

The obtained Pt particles are very different in shape compared to the gold nanoparticles, which were small and spherical. This is probably also due to the smaller reduction potential of the platinum salt.

Table 6.1: Properties of the mesoporous titania host and the different Pt/TiO₂ composite materials.

	TiO ₂	Pt/TiO ₂ (UV)	Pt/TiO ₂ (MW)	Pt/TiO ₂ (H ₂)	Pt/TiO ₂ (NaBH ₄)
Specific surface area (m ² /g)	341 ± 5	336 ± 3	344 ± 4	327 ± 4	323 ± 4
Pt wt%	-	0.067	0.045	0.063	0.045
Pt particle shape ^a	-	-	-	dendrites	irregular
Visual appearance					

^a Determined from HAADF STEM images (Figure 6.1)

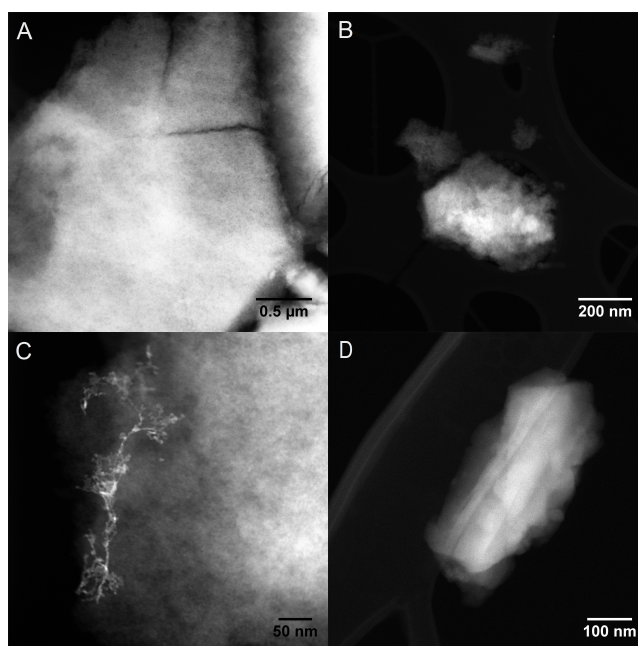


Figure 6.1: HAADF STEM images of the Pt/TiO₂ composite materials using the A) UV, B) MW, C) H₂ and D) NaBH₄ reduction.

6.4 Photocatalysis

The photocatalytic activity of the samples was tested in aqueous media by following the degradation of isoproturon, a herbicide harmful for aquatic life. As the UV

and MW reduced samples do not contain Pt nanoparticles, only the UV reduced sample was tested and compared to pure titania and the H₂ and NaBH₄ reduced Pt/TiO₂ samples. The resulting graph is depicted in Figure 6.2. The degradation of isoproturon with titania can be described by a pseudo-first order reaction.^{9, 10} The resulting rate constants are presented in 6.2.

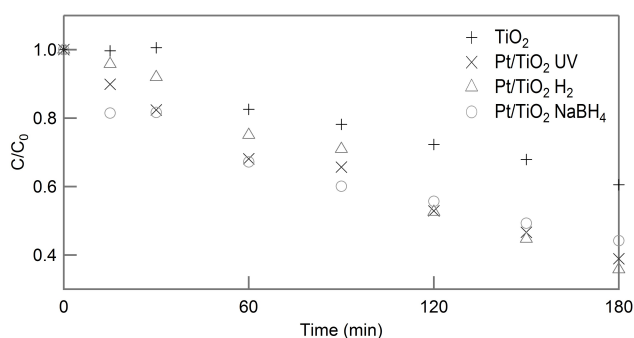


Figure 6.2: Photocatalytic degradation of an isoproturon solution as a function of time.

Table 6.2: Isoproturon degradation rate constants derived from the $\ln(C/C_0)=kt$ graph.

	TiO ₂	Pt/TiO ₂ (UV)	Pt/TiO ₂ (H ₂)	Pt/TiO ₂ (NaBH ₄)
Rate constant (min ⁻¹)	0.0029 ± 0.0002	0.0050 ± 0.0002	0.0058 ± 0.003	0.0042 ± 0.0003

All platinum functionalized mesoporous titania samples are more photocatalytically active than their pure mesoporous titania counterpart as their rate constants are significantly larger than the rate constant of pure TiO₂. This is even the case for the UV reduced sample, which does not contain Pt nanoparticles (but only Pt ions). There is not much difference between the Pt/TiO₂ materials, especially after 2-3 hours of photodegradation. This means that Pt ions versus Pt metal and dendritic particles versus large irregular particles have the same effect in enhancing the photocatalytic effect of mesoporous titania. Pt-doped titania is known to enhance the photocatalytic activity of titania by reducing the recombination rate.^{11, 12} In these cases the Pt ions are incorporated into the titanium dioxide crystal structure. This is not the case in our materials as Pt ions are only adsorbed onto the surface. Yet, it seems like the adsorbed ions already have the same effect.

6.5 Conclusions

Platinum/titania mesoporous materials are synthesized according to the same synthesis methods as the gold/titania mesoporous titania materials. The specific surface areas are also in this case not altered by the reduction methods. Nevertheless, the shape of the obtained particles are completely different as the thermal H₂ reduction produces dendritic particles, the chemical, NaBH₄ reduction large irregular particles and the UV and MW reduction do not even produce particles. This is probably due to the smaller reduction potential of H₂PtCl₆ compared to HAuCl₄.

The photocatalytic activity of the samples is tested for the degradation of isoproturon and compared with pure mesoporous titania. All tested composite materials have an almost equally enhanced photocatalytic activity compared to pure titania. The shape of Pt does not effect this enhancement.

More research has to be performed to produce Pt/TiO₂ materials functionalized with small, uniform Pt particles. With these materials the effect of the size on the photocatalytic activity could be tested.

The same synthesis procedure is used for the Pt/TiO₂ and the Au/TiO₂ composites. We still need to investigate why an enhancement of the photocatalytic activity was obtained in the case of Pt/TiO₂, which contains none ideal particles, and not in the case of Au/TiO₂, which does contain the desired particle shape. In literature, the Au functionalized samples always have a bigger increase in photocatalytic activity compared to Pt functionalized samples, when using the same synthesis method.^{1, 2, 13} Possibly the junction between the gold particles and titania is not as strong as in the case of the platinum/titania materials, creating an incomplete Schottky barrier. XANES spectroscopy can be used to analyse bond distances and could help to explain our findings.

References

- [1] Wang, X. D., Waterhouse, G. I. N., Mitchell, D. R. G., Prince, K. & Caruso, R. A. Noble metal-modified porous titania networks and their application as photocatalysts. *ChemCatChem* **3**, 1763–1771 (2011).
- [2] Bamwenda, G. R., Tsubota, S., Nakamura, T. & Haruta, M. The influence of the preparation methods on the catalytic activity of platinum and gold supported on TiO₂ for CO oxidation. *Catal. Lett.* **44**, 83–87 (1997).
- [3] Li, F. B. & Li, X. Z. The enhancement of photodegradation efficiency using Pt-TiO₂ catalyst. *Chemosphere* **48**, 1103–1111 (2002).
- [4] Parayil, S. K. *et al.* Synthesis-dependent oxidation state of platinum on TiO₂ and their influences on the solar simulated photocatalytic hydrogen production from water. *J. Phys. Chem. C* **117**, 16850–16862 (2013).
- [5] Yi, H. *et al.* Photocatalytic H₂ production from methanol aqueous solution over titania nanoparticles with mesostructures. *Int. J. Hydrogen Energy* **33**, 672–678 (2008).
- [6] Yu, J., Qi, L. & Jaroniec, M. Hydrogen production by photocatalytic water splitting over Pt/TiO₂ nanosheets with exposed (001) facets. *J. Phys. Chem. C* **114**, 13118–13125 (2010).
- [7] Bamwenda, G. R., Tsubota, S., Nakamura, T. & Haruta, M. Photoassisted hydrogen-production from a water-ethanol solution - a comparison of activities of Au-TiO₂ and Pt-TiO₂. *J. Photochem. Photobiol. A* **89**, 177–189 (1995).
- [8] Brunauer, S., Emmett, P. H. & Teller, E. Adsorption of gases in multimolecular layers. *J. Am. Chem. Soc.* **60**, 309–319 (1938).
- [9] Geltmeyer, J. *et al.* TiO₂ functionalized nanofibrous membranes for removal of organic (micro)pollutants from water. *Sep. Purif. Technol.* **179**, 533–541 (2017).

- [10] Verma, A., Prakash, N. T. & Toor, A. P. Photocatalytic degradation of herbicide isoproturon in TiO₂ aqueous suspensions: Study of reaction intermediates and degradation pathways. *Environmental Progress and Sustainable Energy* 1–7 (2013).
- [11] Vijayan, B. K., Dimitrijevic, N. M., Wu, J. & Gray, K. A. The effects of pt doping on the structure and visible light photoactivity of titania nanotubes. *The Journal of Physical Chemistry C* **114**, 21262–21269 (2010).
- [12] Chen, X. & Mao, S. S. Titanium dioxide nanomaterials: Synthesis, properties, modifications, and applications. *Chem. Rev.* **107**, 2891–2959 (2007).
- [13] Zhao, Q., Li, M., Chu, J., Jiang, T. & Yin, H. Preparation, characterization of au (or pt)-loaded titania nanotubes and their photocatalytic activities for degradation of methyl orange. *Appl. Surf. Sci.* **255**, 3773–3778 (2009).

7

General conclusion and future perspectives

7.1 General summary

The goal of this research project was the synthesis of mesoporous titania with enhanced photocatalytic activity. Two routes are investigated to achieve this goal. In a first part, the degree of crystallinity of mesoporous titanium dioxide is increased by introducing a microwave treatment during the synthesis. The second method is the functionalization of mesoporous titania with noble metal nanoparticles. The largest part of this thesis covers the synthesis of Au/TiO₂ composite materials, but at the end, the deposition of platinum nanoparticles is also discussed.

7.2 Microwave assisted synthesis

The biggest problem in the synthesis of mesoporous titania is the trade-of between a high specific surface area and a high degree of crystallinity, because of the high temperatures necessary to crystallize titanium dioxide. The polymeric template molecules are not stable at these temperatures, resulting in collapsing of the pores and a small specific surface area. We incorporated a microwave treatment during the synthesis to increase the degree of crystallinity, without the loss of specific surface area when this treatment is performed after the stabilization step in sodium hydroxide. The specific surface areas achieved in this research are amongst the

highest reported in literature. The synthesis of mesoporous titania without the microwave treatment is also very reproducible, resulting in mesoporous titania with a specific surface area of $340 \text{ m}^2/\text{g} \pm 27 \text{ m}^2/\text{g}$. In literature, the amorphous fraction of mesoporous titania is never quantified, even though this is an important factor in the evaluation of the photocatalytic activity of the materials. They only report the relative crystal fraction. In this research, special attention is paid to the quantification of the amorphous fractions present. In the case of the untreated material, amorphous fractions higher than 60 wt% are observed, but this could be reduced to less than 20 wt% when a microwave treatment was added to the synthesis procedure.

The materials were tested for their photocatalytic activity in aqueous and gaseous media. In both cases, microwave treated materials performed better than their untreated counterpart. In the aqueous tests, the specific surface area was the most important factor for good activities. The higher the specific surface area, the higher the photocatalytic activity, independent of the degree of crystallinity. In the case of the gaseous tests, materials with both a high degree of crystallinity and a high specific surface area perform best. Due to the completely different set-ups of the gaseous and the aqueous tests, it is not possible to make general conclusions about the characteristics necessary for aqueous or gaseous applications. It is however clear that in both cases a microwave treatment could improve the performance of titanium dioxide.

7.3 Functionalization with noble metal nanoparticles

A second way to improve the photocatalytic activity of titania is the incorporation of noble metal nanoparticles. At the junction of the noble metal and titania, a Schottky barrier is created, resulting in the physical separation of the photogenerated electrons and holes, diminishing the recombination rate.

7.3.1 Gold nanoparticles

There are different possibilities to synthesize the composite materials, but this research focussed on two. The first is the incorporation of pre-synthesized gold nanoparticles in the titania precursor and subsequent synthesis of the hybrid Au/TiO₂ material by following the mesoporous titania recipe. The second synthesis route starts from a pre-synthesized mesoporous titania powder, which is impregnated with a metal salt. In a following step the salt is reduced to form nanoparticles.

Gold nanoparticles have been synthesized in polar and apolar media. The particles obtained from the polar syntheses were too large and agglomerated and therefore not suited for the synthesis of composite materials. In literature, smaller non agglomerated particles are obtained, but we could not reproduce this. In the case of

the apolar syntheses, it was possible to obtain small, uniform nanoparticles. However, these particles could not be dispersed in the titania precursor. Unfortunately it was not possible to exchange the apolar ligand for more polar ones, without solving the gold nanoparticles. This was unexpected as these ligand exchange methods have already been performed by other groups.

The second synthesis route of gold functionalized mesoporous titanium dioxide materials compares four reduction methods (thermal, microwave, chemical and UV) of the gold salt. In literature, little attention is paid to the oxidation state of the obtained gold species as they assume complete reduction of the gold salt. In some cases XPS is used to evaluate the oxidation state, but shifting of the binding energies due to support interactions, particle shape/size and geometric effects makes analysis of the spectra complex. Therefore we used XANES spectroscopy to determine the oxidation state of the gold species. All reduction methods resulted in completely reduced gold species except for the UV reduction. This reduction method results in partially positively charged gold nanoparticles. This could have an important effect on the photocatalytic activity of the materials. Unfortunately, the addition of gold nanoparticles did not lead to an improvement of the photocatalytic activity, making it impossible to investigate the effect of the positive charge on the photocatalytic activity of mesoporous titania. This was unexpected as other groups observe increased photocatalytic activities by the addition of gold nanoparticles. We did not find an explanation why this is not the case for our materials.

In order to research the effect of the positive charge present on the gold atoms, the catalytic conversion of glycerol to glycerol carbonate using urea is followed. This reaction is catalysed by gold particles. In a first run, the UV reduced samples has a low selectivity, but a high conversion, compared to samples containing completely reduced, neutral gold nanoparticles. The positive charge and corresponding acid sites can activate urea, leading to a high conversion rate. On the other hand, the positive charge is not favourable for the ring closure step in the formation of glycerol carbonate, leading to a low yield of the desired product. The selectivity of the neutral catalysts remains constant in a second and third run. In the case of the UV reduced catalyst the selectivity increases as the positive charge disappears during/after the first run. The Au/TiO₂ materials do not perform as good as the benchmark catalyst with a more basic nature, but this reaction could prove that the positive charge present after UV reduction has an important influence on the catalytic (and possibly photocatalytic) activity of the materials.

7.3.2 Platinum nanoparticles

In order to investigate if it is possible to increase the photocatalytic activity of mesoporous titania with noble metal nanoparticles using our synthesis methods, a platinum salt is adsorbed onto the titania matrix and subsequently reduced. The

reduction of H_2PtCl_6 is more difficult compared to HAuCl_4 due to the smaller reduction potential of the platinum salt. Hence, not all reduction methods lead to the formation of nanoparticles. Furthermore, the other reduction methods (thermal and chemical) did not produce small, uniform nanoparticles. However, an improvement of the photocatalytic activity is observed. This is the case for all Pt/TiO₂ materials, whether or not the platinum ions are reduced to form particles or not. This outcome is completely different from the case of gold functionalized materials even though the same synthesis methods are used. Therefore we can conclude that it is possible to increase the photocatalytic activity of mesoporous titania through the functionalization with noble metal nanoparticles as is observed in literature. In our case it is however not possible through the decoration of mesoporous titania with gold nanoparticles.

7.4 Future perspectives

As a lot of syntheses routes did not work out as planned, more research can be performed to investigate the cause of these problems and new synthesis routes can be explored to achieve an increased photocatalytic activity of mesoporous titania.

The first, and most important, observation that has to be clarified is the inability of the gold nanoparticles to increase the photocatalytic activity of mesoporous titania. A possible method to give inside in the problem is looking at the bond distances of Au-Ti, Au-O and Au-Au of materials with and without an increased activity, with EXAFS. By evaluating this information, one can see if the gold nanoparticles on materials with an increased activity have the same interaction with the titania matrix as the gold nanoparticles on the materials without an increased activity. Yet, it is a very complex topic and it will be very difficult to achieve a convincing explanation for these observations.

Next to the clarification of lack of improved photocatalytic activity of Au/TiO₂ materials, there are also alternative routes to obtain gold functionalized titanium dioxide materials. These can possibly have an improved photocatalytic activity. Microwave treated mesoporous titania can be used as the matrix material for the decoration with noble metals. The ex-situ route can be reinvestigated. Especially the Turkevich-Frens method has the ability to result in homogeneous composite materials. It should also be possible to achieve a ligand exchange reaction with the phosphine capped particles. Next to these methods to create Au/TiO₂ materials, other noble metals (Pd, Ag), oxide (SiO₂, Fe₂O₃,) or other (CdS) nanoparticles could be added to titania to increase its photocatalytic activity.

Although the Au/TiO₂ materials produced during this project did not have improved photocatalytic activities, they were able to convert glycerol into glycerol carbonate. Albeit the a good indication that the positive charge on the gold particles of the UV reduced composite material has a remarkable influence on the

conversion of glycerol to glycerol carbonate, more research has to be performed in order to obtain more conclusive proof. The determination of the formed products in function of the reaction time can help to evaluate the differences between the catalysts. Also in-situ evaluation of the oxidation state and charge on the gold atoms, using XANES, will give more information on the reaction mechanism. Together this could give definite proof that the gold charge has indeed a large influence on the reaction mechanism. This knowledge can on its turn, help to develop new catalysts with a superior activity in the conversion of glycerol to glycerol carbonate.

As the UV reduced materials show the most interesting characteristics, more research can be performed on the influence of the UV reduction. Irradiation time, power of the UV lamp, type of lamp are all factors which can play a role in the resulting charge on the gold nanoparticles. It should also be investigated if it is possible to re-establish the positive charge after catalysis.

A last possible research topic is the use of the composite materials and especially the microwave treated mesoporous titania materials for other applications such as batteries, dye sensitized solar cells and electrochromic devices.

A

Supporting information

A.1 Chapter 2

A.1.1 X-ray diffraction

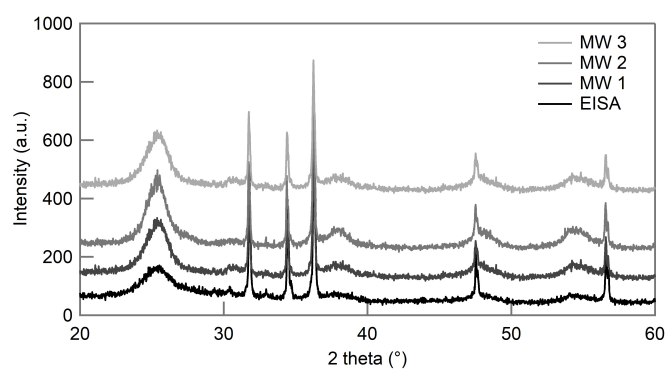


Figure A.1: XRD spectra of the EISA, MW 1, MW 2 and MW 3. The sharp peaks are generated from ZnO with is present to determine the degree of crystallinity.

A.1.2 Rietveld analysis

Rietveld refinement is a method for crystal structure refinement. Known crystal structures are fitted to the experimental spectrum using a least square method, in order to obtain as much agreement as possible. The refinement is used to determine the weight percentage of the crystal phases present. A known weight percentage of a completely crystalline material, in this case approximately 10 wt% ZnO, is added to be able to calculate the amount of amorphous phase present in the sample. Two examples of XRD spectra with their refined spectra are presented below.

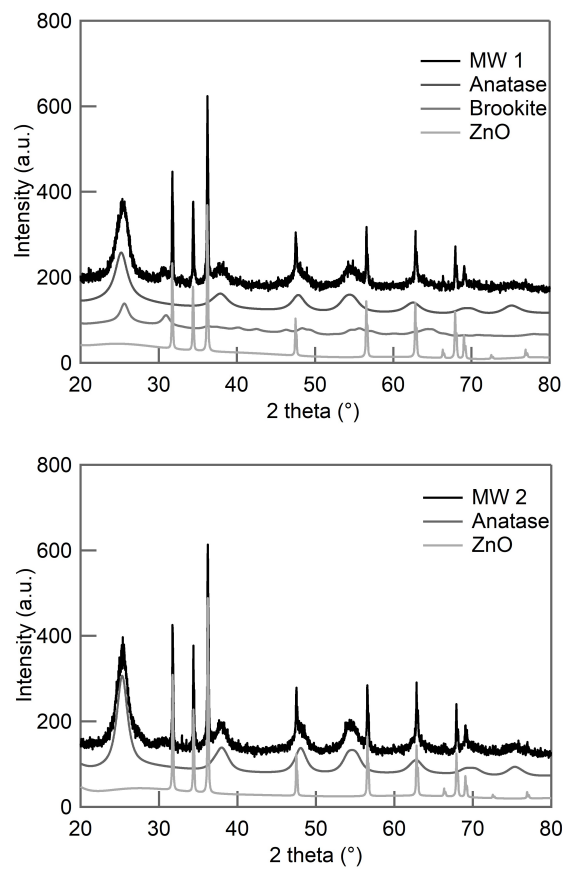


Figure A.2: XRD spectra and Rietveld convolutions of MW 1 (above) en MW 2 (below).

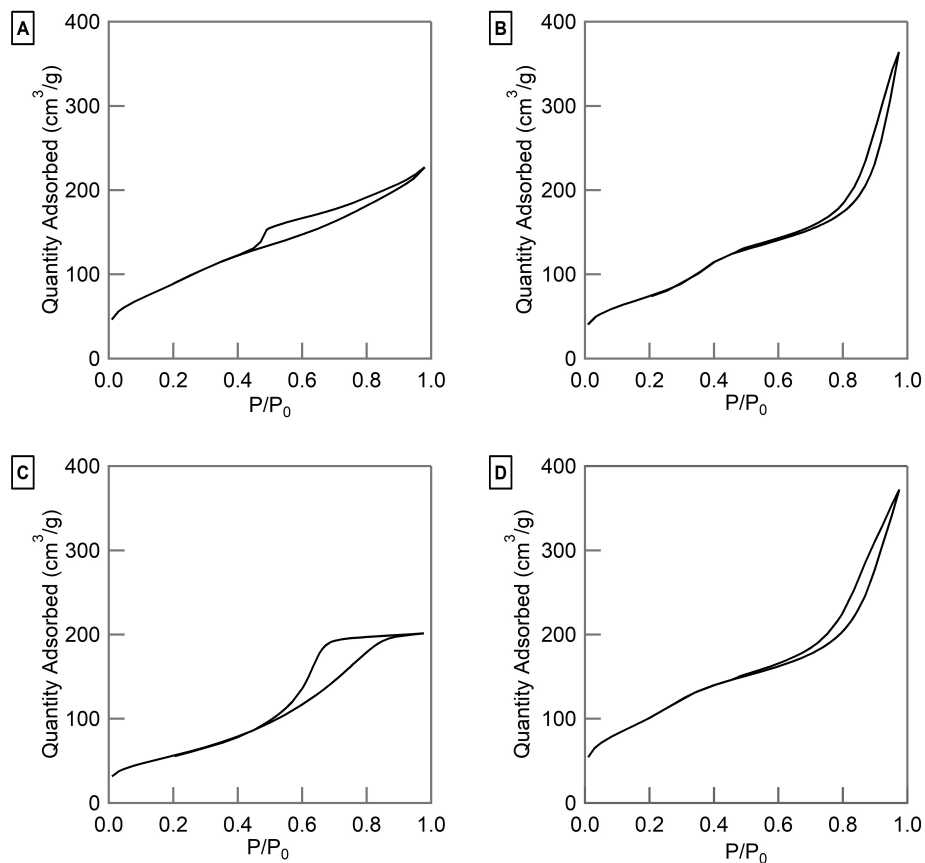
A.1.3 Nitrogen sorption isotherms of mesoporous titania

Figure A.3: Nitrogen sorption isotherms of A) EISA, B) MW 1, C) MW 2 and D) MW 3.

A.1.4 Differential pore size distributions mesoporous titania

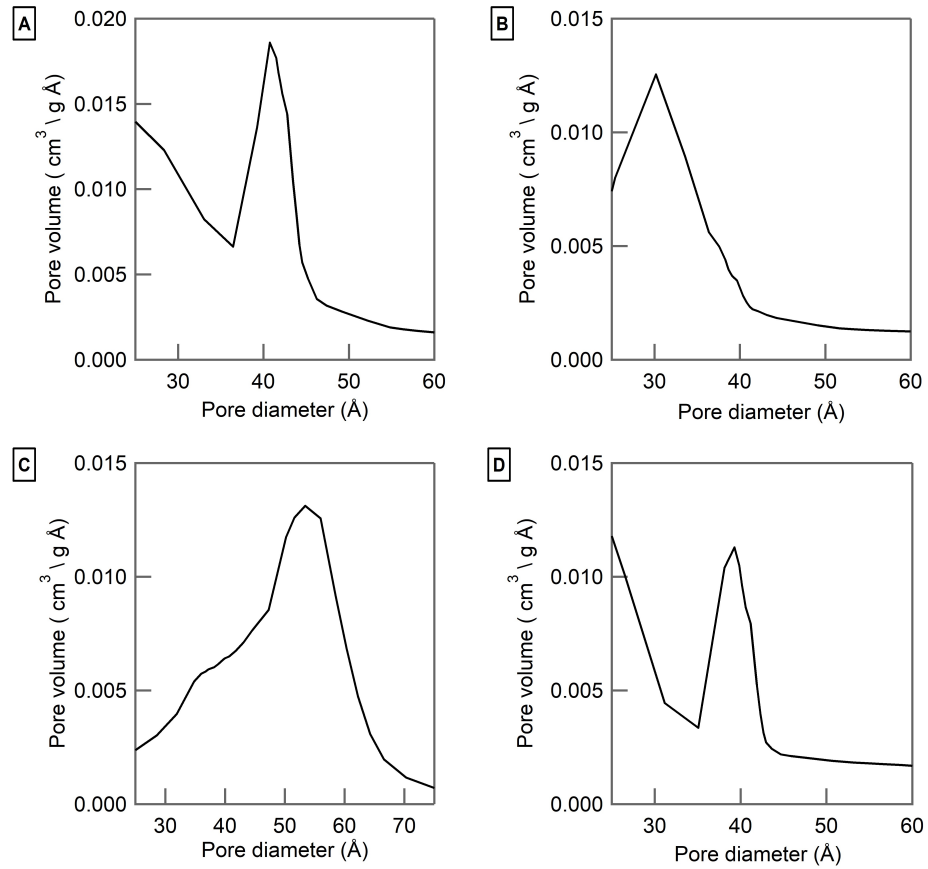


Figure A.4: Differential pore size distributions of A) EISA, B) MW 1, C) MW 2 and D) MW 3.

A.2 Chapter 4

A.2.1 Nitrogen sorption isotherms of gold functionalized mesoporous titania

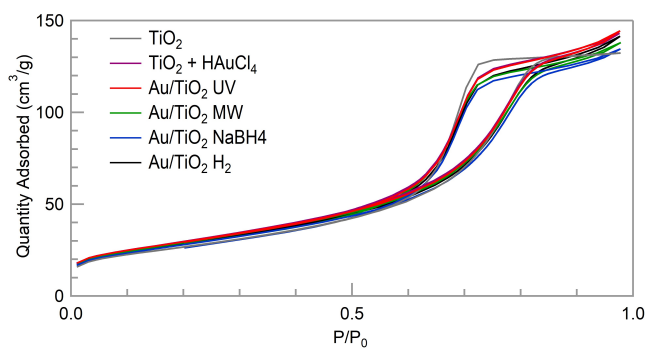


Figure A.5: Nitrogen sorption isotherms of the pure and gold functionalized mesoporous titania samples.

A.2.2 Differential pore size distributions of gold functionalized mesoporous titania

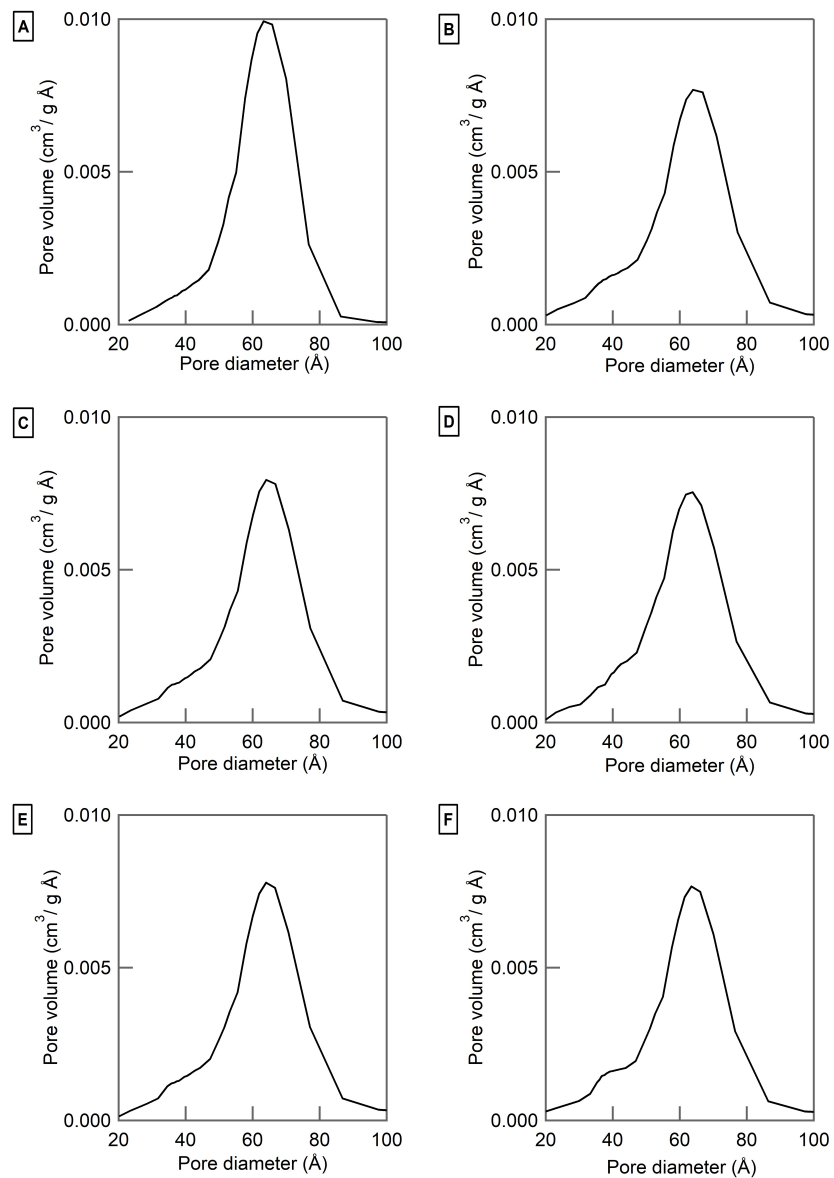


Figure A.6: Differential pore size distributions of A) TiO_2 , B) $\text{TiO}_2 + \text{HauCl}_4$, C) Au/TiO_2 UV, D) Au/TiO_2 MW, E) Au/TiO_2 H_2 and F) Au/TiO_2 NaBH_4 .

A.3 Chapter 5

A.3.1 Nitrogen sorption isotherms of gold functionalized mesoporous titania

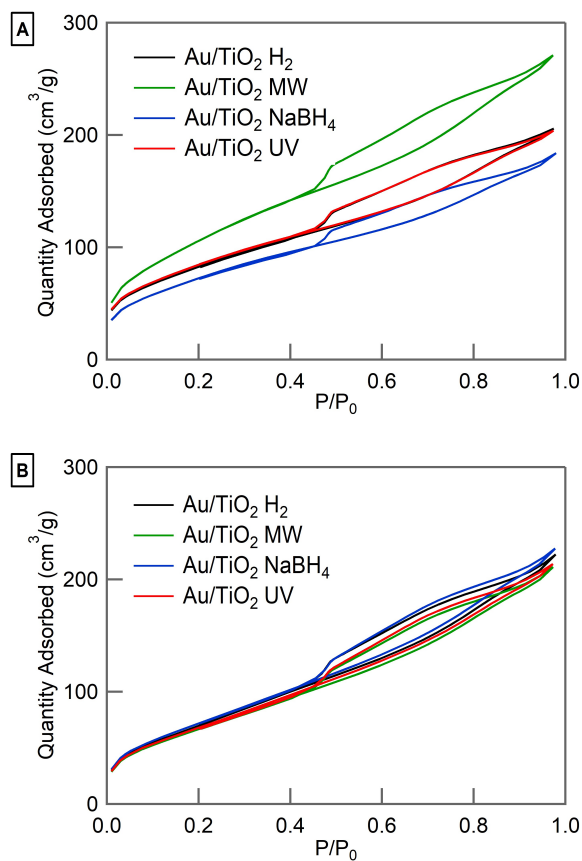


Figure A.7: Nitrogen sorption isotherms of the pure and gold functionalized mesoporous titania samples A) before and B) after catalysis.

A.3.2 Differential pore size distributions of gold functionalized mesoporous titania before catalysis

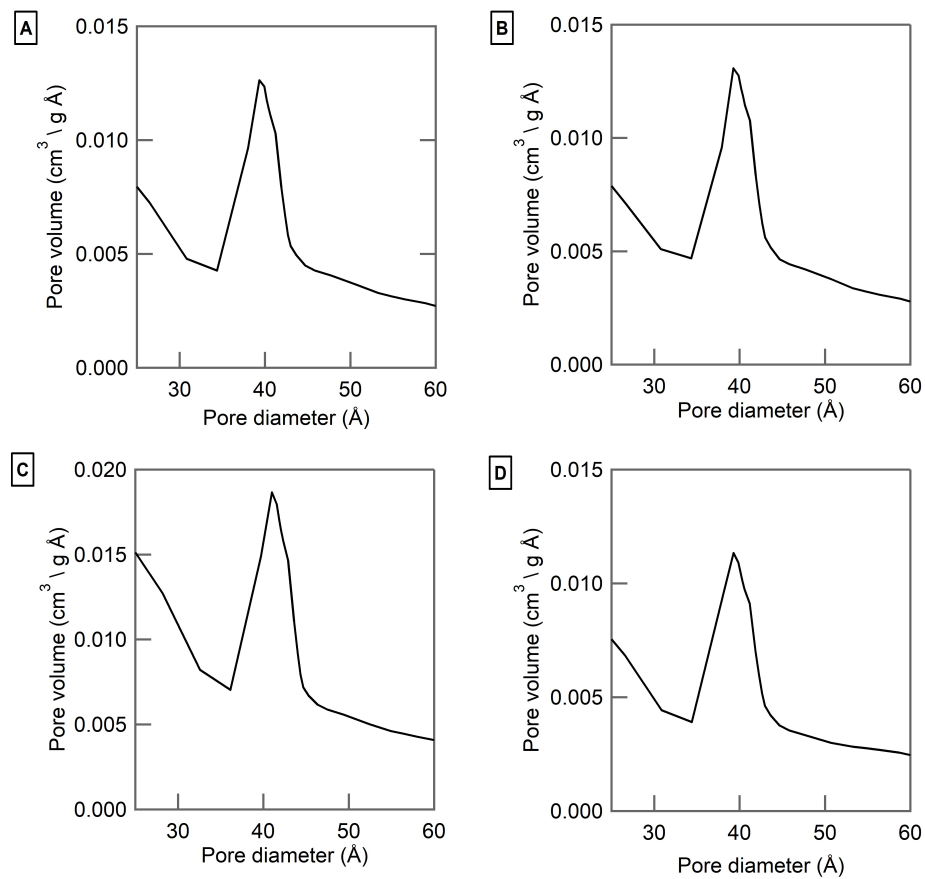


Figure A.8: Differential pore size distributions of the A) UV, B) thermally, C) microwave and D) NaBH₄ reduced gold/titania materials before catalysis.

A.3.3 Differential pore size distributions of gold functionalized mesoporous titania after catalysis

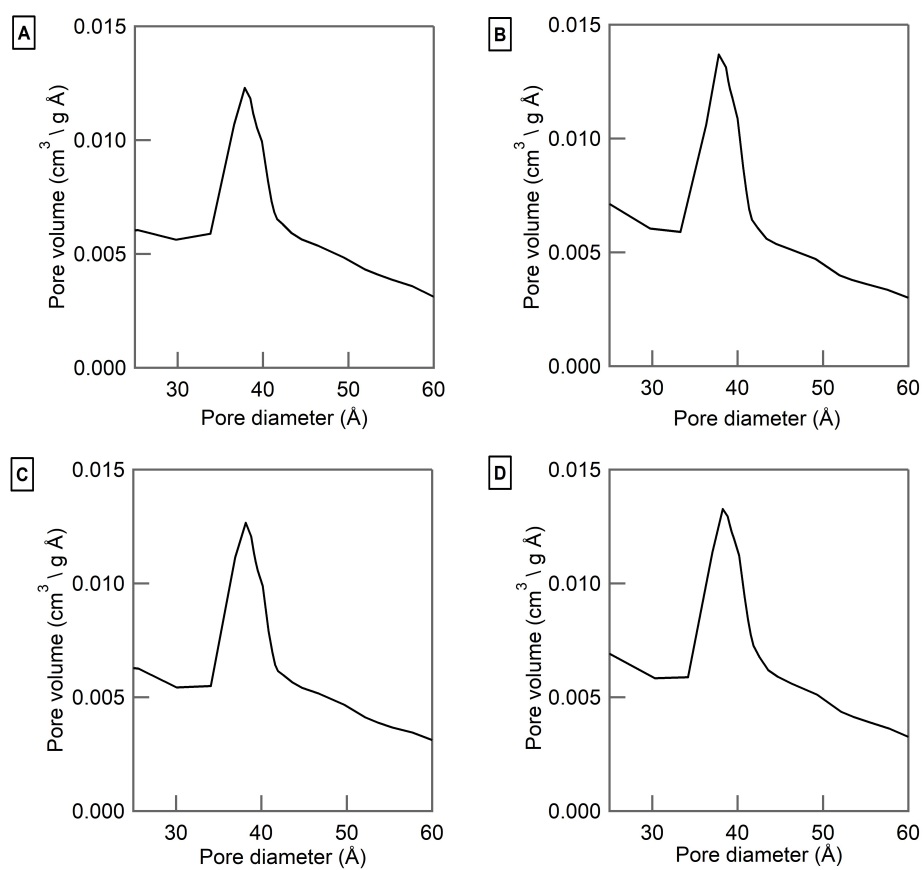


Figure A.9: Differential pore size distributions of the A) UV, B) thermally, C) microwave and D) NaBH₄ reduced gold/titania materials after catalysis.

B

Scientific disseminations

B.1 A1 publicatons

- **Solution-based synthesis of BaZrO₃ nanoparticles: conventional versus microwave synthesis**
De Keukeleere, K.; Feys, J.; Meire, M.; De Roo, J.; De Buysser, K.; Lommens, P.; Van Driessche, I. *Journal of Nanoparticle Research* 2013 15(11).
- **Gold/titania composites: An X-ray absorption spectroscopy study on the influence of the reduction method**
Meire, M.; Tack, P.; De Keukeleere, K.; Balcaen, L.; Pollefeyt, G.; Vanhaecke, F.; Vincze, L.; Van Der Voort, P.; Van Driessche, I.; Lommens, P. *Spectrochimica Acta B* 2015, 110 (0), 45-50.
- **Highly Crystalline Nanoparticle Suspensions for Low-Temperature Processing of TiO₂ Thin Films**
Watte, J.; Lommens, P.; Pollefeyt, G.; Meire, M.; De Buysser, K.; Van Driessche, I. *Acs Applied Materials & Interfaces* 2016, 8 (20), 13027-13036.
- **Microwave-assisted synthesis of mesoporous titania with increased crystallinity, specific surface area, and photocatalytic activity**
Meire, M.; Verbruggen, S. W.; Lenaerts, S.; Lommens, P.; Van Der Voort, P.; Van Driessche, I. *Journal of Materials Science* 2016, 51 (21), 9822-9829.

- **TiO₂ functionalized nanofibrous membranes for removal of organic (micro)pollutants from water**
Geltmeyer, J.; Teixido, H.; Meire, M.; Van Acker, T.; Deventer, K.; Vanhaecke, K.; Van Hulle, S.; De Buysser, K.; De Clerck, K. *Separation and Purification Technology* 2017, 179 (2),533-541

B.2 Conference contributions: oral presentations

- **6th Forum on New Materials - Montecatini Terme, Italy - 2014**
Degradation of pesticides, dye molecules and relevant surface interactions with mesoporous titania - Mieke Meire, Isabelle Ascoop, Pascal Van Der Voort, Isabel Van Driessche and Petra Lommens
- **16th Netherlands' Catalysis and Chemistry Conference - Noordwijkerhout, The Netherlands - 2015**
Effect of microwave irradiation on the synthesis of mesoporous titania - Mieke Meire, Pascal Van Der Voort, Isabel Van Driessche and Petra Lommens

B.3 Conference contributions: poster presentations

- **14th Netherlands' Catalysis and Chemistry Conference - Noordwijkerhout, The Netherlands - 2013**
Microwave assisted synthesis of mesoporous titania functionalized with gold nanoparticles - Mieke Meire, Petra Lommens, Pascal Van Der Voort and Isabel Van Driessche
- **Advanced Complex Inorganic Nanomaterials 2013 - Namur, Belgium - 2013**
Microwave assisted synthesis of mesoporous titania functionalized with gold nanoparticles - Mieke Meire, Petra Lommens, Pascal Van Der Voort and Isabel Van Driessche
- **3rd European symposium on Photocatalysis - Portoroz, Slovenia - 2013**
Innovative synthesis routes for mesoporous titania: influence on the photocatalytic activity - Mieke Meire, Petra Lommens, Pascal Van Der Voort and Isabel Van Driessche
- **ChemCYS - Blankenberge, Belgium - 2014**
Microwave assisted syntheses of mesoporous titania: influence on structural properties - Mieke Meire, Pascal Van Der Voort, Isabel Van Driessche and Petra Lommens

- **Dutch Zeolite Association meeting - Ghent, Belgium, 2014**
Microwave assisted synthesis of mesoporous titania and relevant surface interactions with dye molecules - Mieke Meire, Pascal Van Der Voort, Isabel Van Driessche and Petra Lommens
- **Belgian Ceramic Society Annual meeting - Ghent, Belgium, 2014**
Microwave assisted synthesis of mesoporous titania and relevant surface interactions with dye molecules - Mieke Meire, Pascal Van Der Voort, Isabel Van Driessche and Petra Lommens
- **MRS Spring Meeting, Phoenix, United States of America, 2016**
Microwave assisted synthesis of mesoporous titania - Mieke Meire, Petra Lommens, Pascal Van Der Voort and Isabel Van Driessche